HELSINKI UNIVERSITY OF TECHNOLOGY
Department of Electrical and Communications Engineering

Peter Jantunen

Modelling of Nonlinear Power Amplifiers for Wireless Communications

The thesis has been submitted for official examination for the degree of Master of Science in Espoo, Finland on March 5th, 2004.

Supervisor Professor Timo Laakso

TEKNILLINEN KORKEAKOULU Diplomityön tiivistelmä

Tekijä:	Peter Jantunen
Työn nimi:	Tehovahvistimien epälineaarisuuksien mallintaminen matkaviestinjärjestelmissä
Päivämäärä:	5.3.2004 **Sivumäärä:** 123
Osasto:	Sähkö- ja tietoliikennetekniikan osasto
Professuuri:	Signaalinkäsittelytekniikka
Työn valvoja:	Professori Timo Laakso
Työn ohjaaja:	Professori Timo Laakso

Tehovahvistimen epälineaarisuus vääristää lähetettävää signaalia useilla eri tavoilla. Tämän diplomityön tavoitteena on mallintaa tehovahvistimen epälineaarisuutta, jotta vahvistimen aiheuttamaa vääristymää voidaan pienentää, esimerkiksi linearisointitekniikoiden avulla.

Aluksi diplomityössä tarkastellaan tehovahvistimen aiheuttamaa vääristymää. Seuraavaksi käsitellään tieteellisessä kirjallisuudessa esitettyjä malleja. Lopuksi kaksi kiinnostavaa mallia on valittu tarkempaa tutkimista varten; yksi taajuusriippumaton ja yksi taajuusriippuva malli.

Polynomimallia käytettiin vahvistimen taajuusriippumatonta mallintamista varten. Todettiin että matala-asteiset polynomit mallintavat tarkasti vahvistimen ominaisuuksia tietyllä taajuudella. Tyydyttäviin tuloksiin päästiin jo viidennen asteen mallilla.

Vahvistimen taajuusriippuvaa käyttäytymistä mallinnettiin Hammerstein mallilla, jossa epälineaarinen lohko toteutettiin polynomimallilla ja lineaarinen lohko toteutettiin FIR-suotimella. Saatu malli osoittautui erittäin tarkaksi halutulla taajuuskaistalla kaikilla tehotasoilla aina pohjakohinasta vahvistimen 1-dB:n kompressiopisteeseen asti. Lisäksi estimaatiovirhe halutun kaistan ulkopuolella osoittautui riittävän pieneksi.

Avainsanat: Tehovahvistin, epälineaarisuus, muistillisuus, polynomimalli, FIR approksimaatio, Hammerstein malli.

HELSINKI UNIVERSITY OF TECHNOLOGY Abstract of the Master's Thesis

Author:	Peter Jantunen
Name of the Thesis:	Modelling of Nonlinear Power Amplifiers for Wireless Communications
Date:	5.3.2004 **Pages:** 123
Department:	Department of Electrical and Communications Engineering
Professorship:	Signal Processing
Supervisor:	Professor Timo Laakso
Instructor:	Professor Timo Laakso

The nonlinearity of a power amplifier distorts the transmitted signal in several ways. The objective of this thesis is to find a model of the power amplifier that can be utilized for reducing its nonlinear distortion, e.g., by linearization techniques.

In this thesis, the distortion characteristics of the power amplifier are first discussed. Next, the models that have already been proposed in scientific literature are presented. Finally, two attractive models are chosen for more detailed study; one for frequency-independent and one for frequency-dependent modelling.

A polynomial model was used for frequency-independent modelling of a power amplifier. It was concluded that even low-order polynomials can accurately estimate the characteristics of the power amplifier at a given frequency. Sufficiently accurate results were obtained already with a fifth-order model.

The frequency-dependent behavior of the power amplifier was modelled using a Hammerstein model, where the nonlinear static block was implemented using a polynomial model and the linear dynamic block as an FIR filter. The obtained model was shown to be very accurate on the desired frequency band at all power levels from the noise floor to the 1-dB compression point. Furthermore, the estimation error outside the desired band was well behaved.

Keywords:	Power amplifier, nonlinearity, memory effect, polynomial model, FIR approximation, Hammerstein model.

Preface

The research work for this thesis was carried out in the Signal Processing Laboratory at Helsinki University of Technology during the years 2003–2004. The thesis is part of the XMIT project that was funded by Nokia.

I wish to express my gratitude to my supervisor, Professor Timo Laakso, for his continuous encouragement, guidance and support during the course of this work. I am also very grateful to Stefan Werner for his numerous advice and endless interest towards my research.

My deepest and dearest thanks go to Gilda Gámez for making the required measurements. I am especially grateful for her understanding, patience and support during the long days and nights that I have spent in the lab writing the thesis.

I would like to thank all my colleagues at the lab for creating such a nice working atmosphere. In particular, I would like to thank Mei Yen Cheong, Martin Makundi and Matti Rintamäki for many interesting discussions. The advice and help of my good friend Matias With is also very highly appreciated. Special thanks to Fabio Belloni and Eugenio Delfino for the relaxing discussions not related to signal processing. I am also grateful to Randolph Höglund and Teemu Koski for proofreading the thesis with such great accuracy.

In addition, I wish to express my appreciation to all the people at Nokia who made this work possible. In particular, I would like to thank Risto Kaunisto and Pauli Seppinen for their encouraging comments.

Finally, I would like to express my deepest gratitude towards my family and all my friends for their endless support during my studies.

Helsinki, March 5$^{\text{th}}$, 2004

Peter Jantunen

Contents

List of Acronyms

ACPR	Adjacent Channel Power Ratio
AM/AM	Amplitude Modulation/Amplitude Modulation
AM/PM	Amplitude Modulation/Phase Modulation
AWGN	Additive White Gaussian Noise
BJT	Bipolar Junction Transistor
BLB	Barankin Lower Bound
BLUE	Best Linear Unbiased Estimator
CRLB	Cramer-Rao Lower Bound
DC	Direct Current
FIR	Finite Impulse-Response
IDFT	Inverse Discrete Fourier Transform
IIR	Infinite Impulse-Response
IM	Intermodulation
IP	Internet Protocol
LLF	Log-Likelihood Function
LS	Least-Squares
LSE	Least-Squares Estimator
LTI	Linear Time-Invariant
MIMR	Multitone Intermodulation Ratio
MMSEE	Minimum Mean Square Error Estimator
MSE	Mean Square Error
MVUE	Minimum Variance Unbiased Estimator

NPR	Noise Power Ratio
OFDM	Orthogonal Frequency Division Multiplexing
PAPR	Peak-to-Average Power Ratio
PDF	Probability Density Function
RMS	Root-Mean-Square
SSPA	Solid State Power Amplifier
TWTA	Traveling-Wave Tube Amplifier
VNA	Vector Network Analyzer
WLSE	Weighted Least-Squares Estimator
WWLB	Weiss-Weinstein Lower Bound
ZZLB	Ziv-Zakai Lower Bound

List of Figures

List of Tables

List of Symbols

ξ	estimator
σ	standard deviation
τ	time delay
Φ	phase conversion function
ϕ	phase
$\phi_{d,l}$	desired output phase values
$\phi_{d_s,l}$	scaled desired output phase values
$\boldsymbol{\phi}_{out}$	output phase shift
Ψ	nonlinear conversion function
ω	angular frequency
ω_c	center frequency of the desired band
A	amplitude
$A_{d,l}$	desired output amplitude values
A_s	input amplitude level of the measured small-signal frequency response
$\mathbf{a}$	coefficient vector of gain conversion polynomial
$\mathbf{b}$	coefficient vector of phase conversion polynomial
$\mathbf{C}$	covariance matrix
D	filter delay
E	error function
e	error signal
$\mathbf{e}$	discrete-time Fourier transform vector
$\mathbf{F}$	Fisher information matrix

f	frequency
f_s	sampling frequency
G	voltage gain
g	gain conversion function
H	frequency response
H_d	desired frequency response
$H_{d,p}$	desired power-dependent frequency response
$H_{d,s}$	small-signal frequency response
H_{d,s_0}	scaled small-signal frequency response
H_p	estimated power-dependent frequency response
$\mathbf{h}$	filter coefficient vector
$\mathbf{I}$	identity matrix
K	number of measured frequency points
L	number of measured amplitude levels
M	filter order
N	order of the nonlinearity
$\mathcal{N}$	Gaussian probability density function
$\mathbf{p}_{in}$	input power values
$\mathbf{p}_{out}$	output power values
Q	amplifier operating point
$\mathbf{R}$	whitening matrix
$\mathbf{s}$	signal model
t	time
$\mathbf{U}$	observation matrix
V_{in}	input voltage
V_{out}	output voltage
$\mathbf{W}$	weighting matrix
$\mathbf{w}$	noise vector
W_f	weighting factor
x	input signal
y	output signal

Chapter 1

Introduction

1.1 Background

The major driver for future wireless broadband multimedia communication systems is the increasing demand for personal mobile communications that require increased data rates, capacity, flexibility and reliability. Users are expecting mobile Internet Protocol (IP) applications and services comparable to fixed line applications and services at home or in the office. The new radio interfaces are predicted to support data rates up to 100 Mbit/s for mobile access and up to 1 Gbit/s for wireless local area access [1]. This means that the limited bandwidth, transmit power and other resources must be used as efficiently as possible, close to the optimal theoretical limits.

Orthogonal Frequency Division Multiplexing (OFDM) is one of the most promising modulation technologies for these future systems. OFDM is a multicarrier modulation technique where a single data stream is transmitted over a number of lower rate subcarriers. Some of the key advantages of OFDM are efficient handling of multipath environments, channel capacity enhancement in slow time-varying channels, robustness against narrowband interference and high spectral efficiency. The

most notable drawbacks are the high Peak-to-Average Power Ratio (PAPR) and sensitivity to both frequency offset and phase noise.

High PAPR indicates that a highly linear power amplifier is required at the transmitter. The linearity requirement can be met by driving the power amplifier well below its saturation point. This causes poor power efficiency, which is especially bad in a mobile transmitter. Driving the power amplifier closer to its saturation point is appealing, since it would increase power efficiency and prolong battery life of a mobile transmitter. However, driving the power amplifier above the linear region results in nonlinear distortion effects. The nonlinear distortion makes it more difficult to receive the signal and generates harmonic and intermodulation signals outside of the intended frequency band. These unwanted distortion products are potential interfering sources to other users of the radio interface, especially on adjacent frequency bands. The interference must therefore be reduced to a level where both systems can operate satisfactorily.

1.2 Objective and Scope

The goal of this thesis is to find a model for the power amplifier that can be utilized by linearization techniques in order to reduce the nonlinear distortion caused by the power amplifier. Narrowband amplifiers can usually be characterized by frequency-independent models, while wideband amplifiers require frequency-dependent models. Frequency-independent models can easily be obtained using polynomials, since estimation of the coefficients of the polynomials can be done using linear parameter estimation techniques. Frequency-dependent models are much more complex to obtain, since usually nonlinear estimation techniques must be used. Therefore, simplified block models that split the nonlinearity and the dynamics of the system have been shown to be more promising.

The objective is to find both a frequency-independent and a frequency-dependent model that can be used for modelling different types of amplifiers, that are used in

various applications and environments. Preferably, it should be possible to model the nonlinearity of the frequency-dependent model using the frequency-independent model. Hence, the more simple frequency-independent model can be first evaluated, and if satisfactory results cannot be obtained, it is easy to extend it with a frequency-dependent block.

1.3 Organization of the Text

The outline of the thesis is illustrated in Figure 1.1. The thesis can be divided into two parts, where Chapters 2–5 consist of the literature study and the theoretical background and Chapters 6–7 consist of my own contribution to identification of nonlinear systems.

Chapter 2 describes how an amplifier distorts the transmitted signal, how the distortion can be measured, and what are the effects of the distortion. The difference of memoryless nonlinearities and nonlinearities with memory is also discussed. Chapter 3 provides background on the parameter estimation theory required for determining the unknown coefficients of the power amplifier models. The focus is on linear parameter estimation techniques. Chapters 4 and 5 discuss the most widely used frequency-independent and frequency-dependent power amplifier models found in the scientific literature.

In the two following chapters, the models presented in Chapters 4 and 5 are applied for modelling a practical wideband power amplifier. Chapter 6 presents the estimation results using a frequency-independent polynomial model and Chapter 7 presents the estimation results using a frequency-dependent Hammerstein model. In addition, Chapter 7 presents a simplified parameter estimation technique for separately determining the coefficients of the two blocks of the Hammerstein model. Furthermore, a design technique for Finite Impulse-Response (FIR) filters that can have arbitrary amplitude and phase response is derived. Finally, Chapter 8 presents the conclusions and some suggestions for future work.

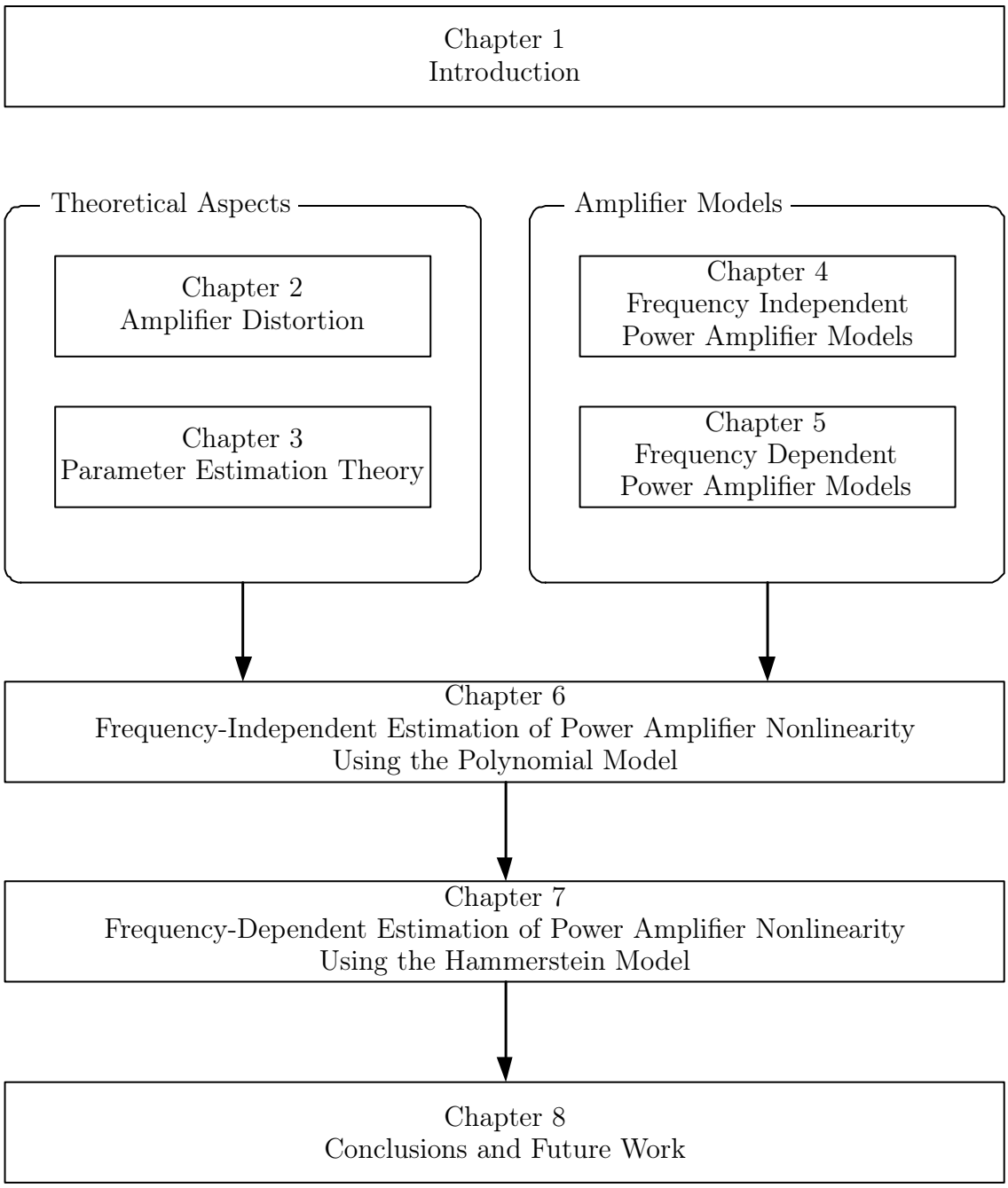

Figure 1.1: Organization of the thesis.

Chapter 2

Amplifier Distortion

All amplifiers distort the signals that they are intended to amplify. The distortion impairs the transmitted signal, which makes it more difficult to receive the transmission correctly. The distortion may not only present problems for users in the same channel but also for users in adjacent channels. This chapter defines what distortion is, what its measures are and what are the effects of the distortion.

2.1 The Ideal Amplifier

An ideal amplifier would produce as its output a perfect replica of the input multiplied by a scalar value. The linear transfer characteristics can be written as

$$V_{out}(t) = GV_{in}(t) \tag{2.1}$$

where G is the voltage gain of the amplifier. Mathematically, an operator L is said to be linear if the scaling and superposition principles

$$L(\alpha x_1) = \alpha L(x_1) \tag{2.2a}$$

$$L(x_1 + x_2) = L(x_1) + L(x_2) \tag{2.2b}$$

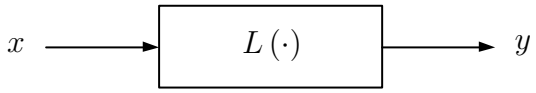

Figure 2.1: Illustration of a linear operator.

hold for every pair of functions x_1 and x_2 and scalar α [2]. The linear operator is illustrated in Figure 2.1. The linearity implies that the ideal amplifier does not affect the waveform of the transmitted signal nor does it introduce any new frequency components. The ideal amplifier is illustrated in Figure 2.2(a).

2.2 Practical Amplifiers

Real amplifiers exhibit various magnitudes of nonlinearities. These are usually described by the amplitude transfer characteristics and the phase transfer characteristics of the amplifier. The first one is often also referred to as the Amplitude Modulation/Amplitude Modulation (AM/AM) conversion and the latter one as the Amplitude Modulation/Phase Modulation (AM/PM) conversion of the amplifier.

A comparison between a real amplifier and its ideal counterpart is shown in Figure 2.2. The figure shows that there are significant differences between the two amplifiers. The real amplifier illustrated in Figure 2.2(b) has three different operating regions. When the input signal voltage is low, the amplifier is operating in the cutoff region and the input-output relationship has an exponential form. In the linear region the amplifier performs almost as its ideal counterpart until the input rises high enough, so that the output saturates to the maximum output level. The label Q is the quiescent point often also referred to as the Direct Current (DC) bias or the operating point of the amplifier. More detailed information on operation characteristics of real amplifiers can be found in [3].

The nonlinearity depicted in Figure 2.2(b) shows that the saturation of the amplifier has smoothly decreased the amplitude of the output signal's upper half. Besides the AM/AM conversion shown in the figure, real amplifiers may also cause AM/PM

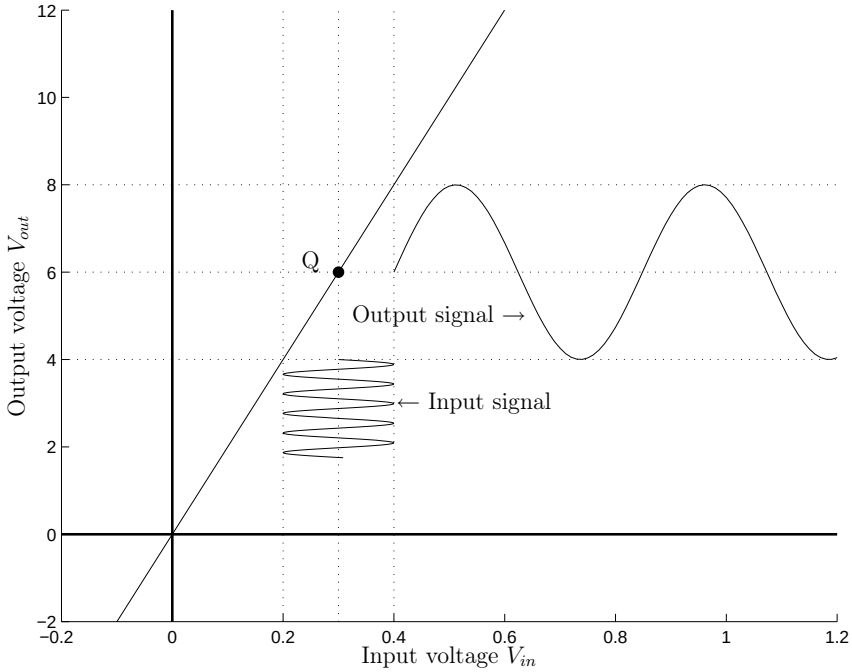

(a) Ideal amplifier with voltage gain $G = 20$.

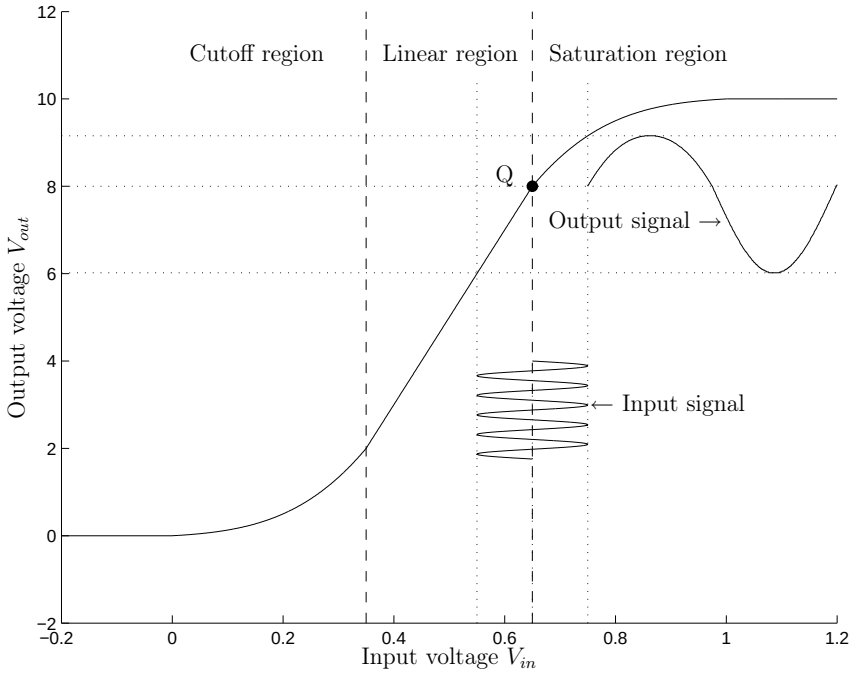

(b) Real amplifier with voltage gain $G = 20$ in the linear region.

Figure 2.2: Comparison between an ideal amplifier and a real amplifier. Q is the operating point of the amplifier.

conversion and both the AM/AM and AM/PM characteristics may also depend on the input signal frequency.

2.3 Amplitude Distortion

2.3.1 Second-order Nonlinearity

Since no physical device can act as the ideal amplifier illustrated in Figure 2.2(a), models for nonlinear amplifiers are needed. The simplest nonlinearity can be illustrated by adding a squared term to the input-output relationship of the ideal amplifier in Equation (2.1). The input-output relationship is now written as

$$V_{out}(t) = G_1 V_{in}(t) + G_2 V_{in}^2(t). \tag{2.3}$$

Using a sinusoidal input

$$V_{in}(t) = A(\omega)\cos(\omega t) \tag{2.4}$$

the output of the nonlinear amplifier can be calculated using basic trigonometric identities

$$\begin{aligned} V_{out}(t) &= G_1 A(\omega)\cos(\omega t) + G_2 A^2(\omega)\cos^2(\omega t) \\ &= G_1 A(\omega)\cos(\omega t) + G_2 A^2(\omega)\frac{1+\cos(2\omega t)}{2} \\ &= \frac{G_2 A^2(\omega)}{2} + G_1 A(\omega)\cos(\omega t) + \frac{G_2 A^2(\omega)}{2}\cos(2\omega t). \end{aligned} \tag{2.5}$$

The input-output relationship of the second-order nonlinearity is illustrated in Figure 2.3(a) using $G_1 = 10$, $G_2 = 4$ and $A = 1$. Equation (2.5) shows that the second order nonlinearity introduces a DC component and a new signal component at twice the frequency of the fundamental component. This is illustrated in Figure 2.4. Since the fundamental component is not affected by the nonlinearity, the distortion can be removed by filtering.

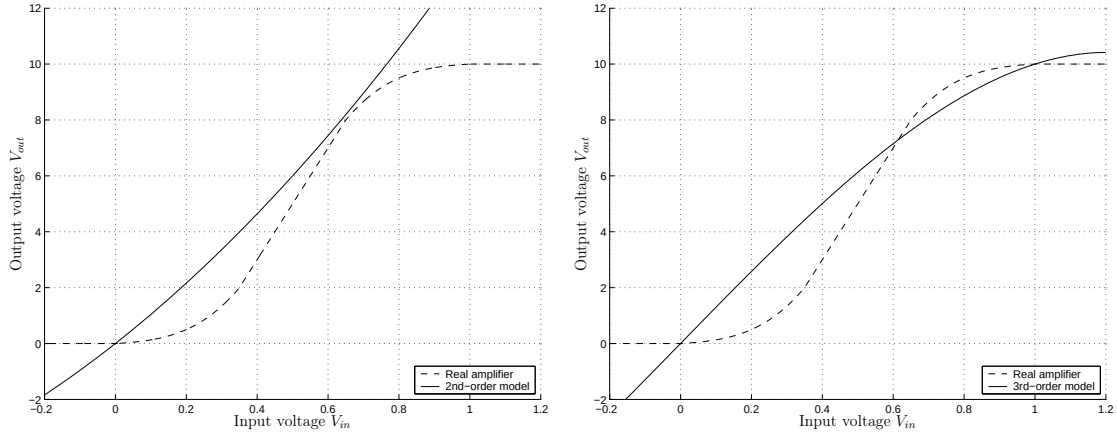

(a) $V_{out}(t) = 10V_{in}(t) + 4V_{in}^2(t)$ (b) $V_{out}(t) = 13V_{in}(t) - 3V_{in}^3(t)$

Figure 2.3: Second-order and third-order nonlinear input-output characteristics compared to the real amplifier illustrated in Figure 2.2(b). The input signal is $V_{in}(t) = \cos(\omega t)$.

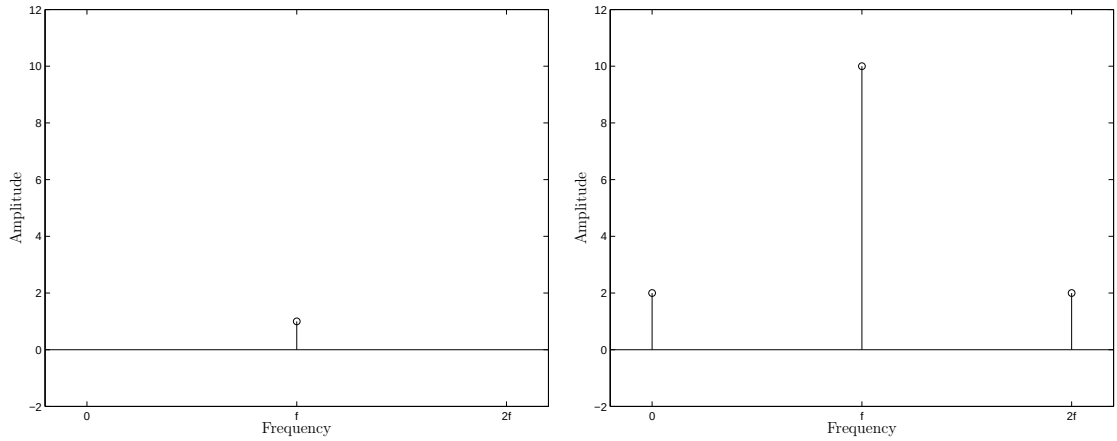

(a) Input signal (b) Output signal

Figure 2.4: Frequency domain characteristics of a second-order nonlinearity $V_{out}(t) = 10V_{in}(t) + 4V_{in}^2(t), V_{in}(t) = \cos(\omega t)$.

2.3.2 Third-order Nonlinearity

Adding a third-order term to the input-output relationship of the ideal amplifier in Equation (2.1) gives a very different set of problems compared to the second order nonlinearity. The input-output relationship of the nonlinear amplifier is now

$$V_{out}(t) = G_1 V_{in}(t) + G_3 V_{in}^3(t). \tag{2.6}$$

Using the sinusoidal input defined in Equation (2.4), it is easy to calculate the output of the amplifier

$$\begin{aligned} V_{out}(t) &= G_1 A(\omega)\cos(\omega t) + G_3 A^3(\omega)\cos^3(\omega t) \\ &= (G_1 A(\omega) + \frac{3G_3 A^3(\omega)}{4})\cos(\omega t) + \frac{G_3 A^3(\omega)}{4}\cos(3\omega t). \end{aligned} \tag{2.7}$$

The third-order input-output relationship is illustrated in Figure 2.3(b) using $G_1 = 13, G_3 = -3$ and $A = 1$. With the third-order nonlinearity, the amplifier produces a new signal component with three times the frequency of the fundamental component. There is no DC component, but instead, the fundamental component has been multiplied by a factor proportional to the cube of the input amplitude. The frequency domain transfer characteristics are illustrated in Figure 2.5.

The most notable difference between the second-order and the third-order nonlinearity is that the latter produces in-band distortion which cannot be filtered away. This can be verified by looking at the example plotted in Figure 2.5. The transfer function indicates that the fundamental component should have an output amplitude of 13 times the input signal amplitude, but from Figure 2.5(b) it can be seen that the output signal only has an amplitude of 10.75 V. This is because the third order nonlinearity produces a component at the fundamental frequency with an amplitude of -2.25 V, so that the final output amplitude becomes only 10.75 V instead of 13 V.

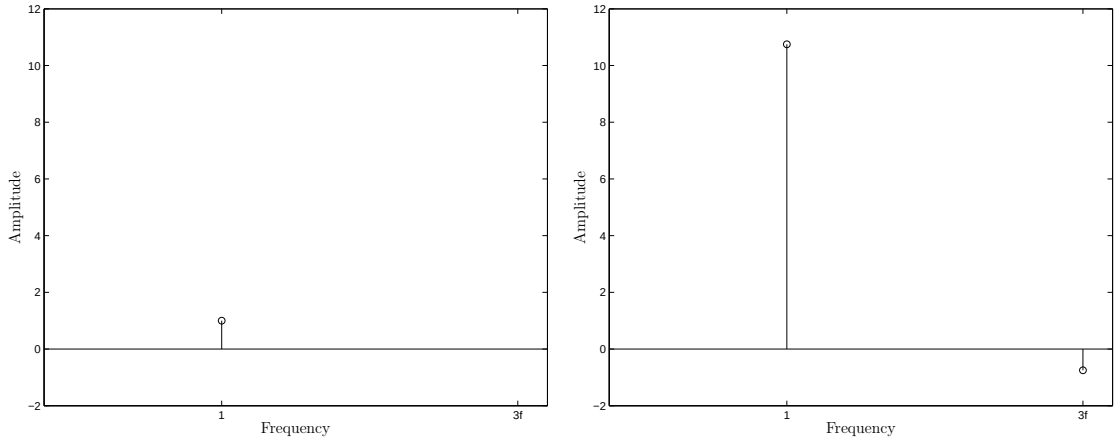

(a) Input signal (b) Output signal

Figure 2.5: Frequency domain characteristics of a third-order nonlinearity $V_{out}(t) = 13V_{in}(t) - 3V_{in}^3(t), V_{in}(t) = \cos(\omega t)$.

2.3.3 Higher-order Nonlinearities

Sections 2.3.1 and 2.3.2 showed that the characteristics of the nonlinearity are very different depending on the order of the nonlinearity. The results of these sections can be generalized for even-order and odd-order nonlinearities.

Even-order Nonlinearities

An Nth-order even-order nonlinearity can be characterized by the relationship

$$V_{out}(t) = \sum_{n=0}^{N/2} G_{2n} V_{in}^{2n}. \tag{2.8}$$

Using the input defined in Equation (2.4) the output of the amplifier is

$$V_{out}(t) = G_0 + \sum_{n=1}^{N/2} G_{2n} A^{2n}(\omega) \cos^{2n}(\omega t). \tag{2.9}$$

Expanding the cosine term at the output using (Id. 8, Sec. 5.4 in [4])

$$\cos^{2n}(\omega t) = \binom{2n}{n}\frac{1}{2^{2n}} + \frac{1}{2^{2n-1}}\sum_{k=1}^{n}\binom{2n}{n-k}\cos(2k\omega t) \tag{2.10}$$

the output of the even-order nonlinearity can be evaluated as

$$\begin{aligned} V_{out}(t) = G_0 &+ \sum_{n=1}^{N/2}\binom{2n}{n}\frac{G_{2n}A^{2n}(\omega)}{2^{2n}} \\ &+ \sum_{n=1}^{N/2}\frac{G_{2n}A^{2n}(\omega)}{2^{2n-1}}\sum_{k=1}^{n}\binom{2n}{n-k}\cos(2k\omega t). \end{aligned} \tag{2.11}$$

Equation (2.11) shows that an even-order nonlinearity leaves the fundamental component unchanged, but produces harmonic components at even multiples of the fundamental frequency up to the order of the nonlinearity. It also adds a DC component to the output. This means that all even-order nonlinearities can be mitigated by filtering.

The frequency domain characteristics of an even-order nonlinearity can be illustrated using the 4th-order input-output relationship

$$V_{out}(t) = G_0 + G_1 V_{in}(t) + G_2 V_{in}^2(t) + G_4 V_{in}^4(t). \tag{2.12}$$

Using the input from Equation (2.4) and expanding the output using Equation (2.11), the result is

$$\begin{aligned} V_{out}(t) = &\frac{8G_0 + 4G_2A^2(\omega) + 3G_4A^4(\omega)}{8} \\ &+ G_1A(\omega)\cos(\omega t) \\ &+ \frac{G_2A^2(\omega) + G_4A^4(\omega)}{2}\cos(2\omega t) \\ &+ \frac{G_4A^4(\omega)}{8}\cos(4\omega t). \end{aligned} \tag{2.13}$$

The different frequency components in Equation (2.13) have been plotted in Figure 2.6(a), using $G_0 = 0$, $G_1 = 1$, $G_2 = G_4 = 1$ and $A = 1$.

Odd-order Nonlinearities

The Nth-order odd-order nonlinearity can be written as

$$V_{out}(t) = \sum_{n=1}^{(N+1)/2} G_{2n-1} V_{in}^{2n-1}. \tag{2.14}$$

Using the input defined in Equation (2.4) the output of the amplifier is

$$V_{out}(t) = \sum_{n=1}^{(N+1)/2} G_{2n-1} A^{2n-1}(\omega) \cos^{2n-1}(\omega t). \tag{2.15}$$

The cosine term can be expanded using (Id. 8, Sec 5.4 in [4])

$$\cos^{2n-1}(\omega t) = \frac{1}{2^{2n-2}} \sum_{k=1}^{n} \binom{2n-1}{n-k} \cos[(2k-1)\omega t] \tag{2.16}$$

and therefore the output can be evaluated as

$$V_{out}(t) = \sum_{n=1}^{(N+1)/2} \frac{G_{2n-1} A^{2n-1}(\omega)}{2^{2n-2}} \sum_{k=1}^{n} \binom{2n-1}{n-k} \cos[(2k-1)\omega t]. \tag{2.17}$$

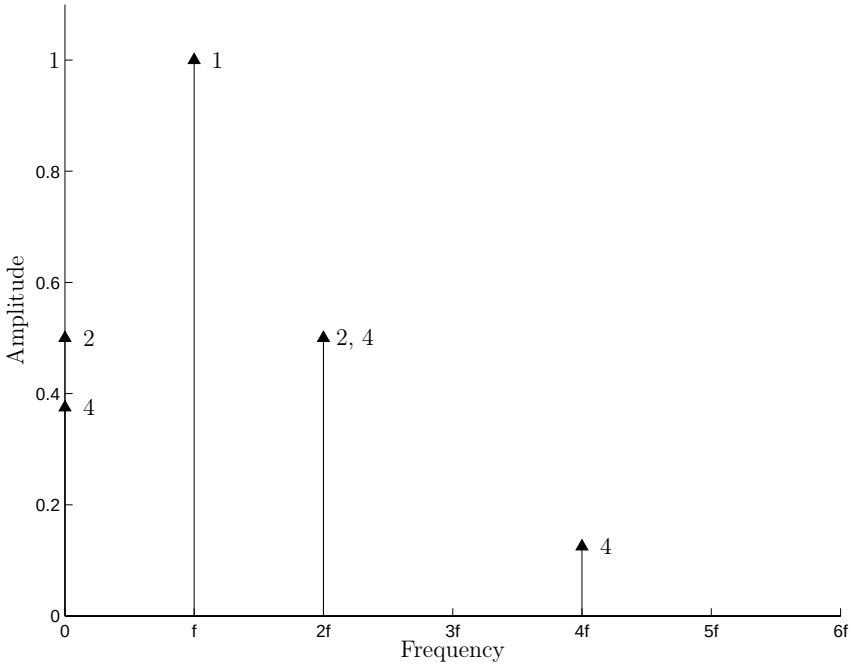

(a) $V_{out}(t) = V_{in}(t) + V_{in}^2(t) + V_{in}^4(t)$

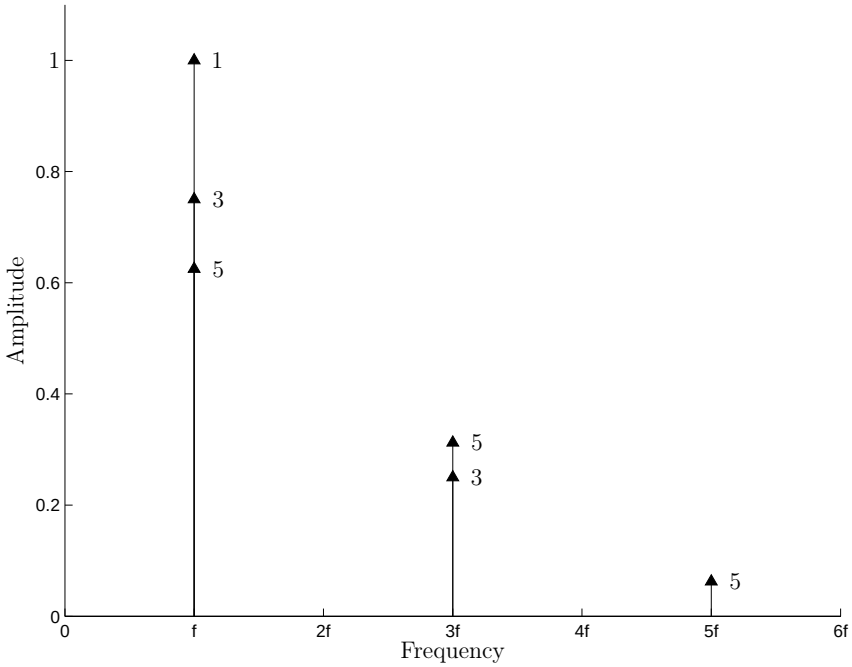

(b) $V_{out}(t) = V_{in}(t) + V_{in}^3(t) + V_{in}^5(t)$

Figure 2.6: Frequency responses of 4th- and 5th-order nonlinearities, showing separate components from different degrees of nonlinearity.

Equation (2.17) shows that the odd-order nonlinearity produces harmonic components at odd multiples of the fundamental frequency up to the order of the nonlinearity. A major difference to the even-order nonlinearity is that the amplitude of the fundamental frequency has been changed. This can be illustrated by considering a 5th-order nonlinearity

$$V_{out}(t) = G_1 V_{in}(t) + G_3 V_{in}^3(t) + G_5 V_{in}^5(t). \tag{2.18}$$

Using the input from Equation (2.4) and expanding the output using Equation (2.17) yields

$$\begin{aligned} V_{out}(t) =& \frac{16G_1A(\omega) + 12G_3A^3(\omega) + 10G_5A^5(\omega)}{16}\cos(\omega t) \\ &+ \frac{4G_3A^3(\omega) + 5G_5A^5(\omega)}{16}\cos(3\omega t) \\ &+ \frac{G_5A^5(\omega)}{16}\cos(5\omega t). \end{aligned} \tag{2.19}$$

This result verifies that an odd-order nonlinearity produces odd-order harmonics and that the amplitude of the fundamental frequency has been multiplied by coefficients from the higher-order components of the transfer function. The result is illustrated in Figure 2.6(b), using $G_1 = G_2 = G_3 = 1$ and $A = 1$.

2.4 Phase Distortion

Phase distortion occurs when an amplifier does not delay all frequency components by the same amount. Different time delays distort a waveform consisting of several sinusoids. The relationship between the time delay and phase shift can be written as

$$\tau = \frac{\phi}{2\pi f} \tag{2.20}$$

where τ is the time delay, ϕ is the phase shift and f is the fundamental frequency of the waveform [5]. The equation clearly shows that if the phase does not increase linearly with the frequency the time delay will vary between different frequencies.

2.5 Memoryless Nonlinearities and Nonlinearities with Memory

The output of a memoryless system is a function of the input at a given time instant or after a fixed time delay. Any change in the input occurs instantaneously at the output. This means that the system cannot include any energy storing components which implies that the output is in-phase with the input. In frequency domain the zero-memory nonlinearity implies that the transfer characteristics are frequency independent.

In systems with memory the output of the system also depends on the previous input values. This means that the system includes energy storing components. Besides gain distortion, a nonlinear system with memory may also cause phase distortion. Furthermore, both the gain and phase distortion may be frequency-dependent. A detailed discussion of nonlinearities with and without memory can be found in [6,7].

Memoryless amplifiers are an idealization since practical amplifiers include energy storing components. Therefore the memory of a system is not a good criterion for classifying amplifiers. A more natural approach is to denote amplifiers as frequency-independent or frequency-dependent systems. A frequency-independent system can be either a memoryless system or a system with memory. Frequency-dependent systems on the other hand are always systems with memory. The distortion effects generated by frequency-independent and frequency-dependent nonlinear amplifiers are summarized in Table 2.1.

2.6 Two-Tone Characterization

Two-tone characterization can illustrate both amplitude and phase distortions present in an amplifier. In a two-tone test the amplifier is fed by a signal of the form

$$V_{in} = A_1 \cos(\omega_1 t) + A_2 \cos(\omega_2 t). \tag{2.21}$$

Table 2.1: Distortion effects generated by frequency-independent and frequency-dependent nonlinear amplifiers.

Frequency-Independent Systems	Frequency-Dependent Systems
Memoryless Systems:	Systems with Memory:
• Gain Distortion	• Frequency-Dependent Gain Distortion
Systems with Memory:	• Frequency-Dependent Phase Distortion
• Gain Distortion	
• Phase Distortion	

Figure 2.7 illustrates the signal in both frequency and time domain. The frequency domain plot is an idealization, since it only shows two sinusoids. In practice there would be small frequency components caused by the nonlinearities of the signal generator. The time domain plot reveals that the input signal can be set to vary throughout the whole dynamic range of the amplifier.

2.6.1 Frequency Generation

The two-tone input to a nonlinear device produces new frequency components at the output of the device. The new components occur at linear combinations of the two excitation frequencies. The generated frequencies are of the form

$$\omega_{m,n} = m\omega_1 + n\omega_2 \tag{2.22}$$

where m and n are positive or negative integers and $|m| + |n| \leq N$ where N is the order of the nonlinearity. [8]

2.6.2 A Third-order System

A third-order system $V_{out} = G_0 + G_1 V_{in} + G_2 V_{in}^2 + G_3 V_{in}^3$ generates frequency components illustrated in Table 2.2. The linear term G_1 amplifies the fundamental components ω_1 and ω_2. The quadratic term G_2 converts the signal down to the DC

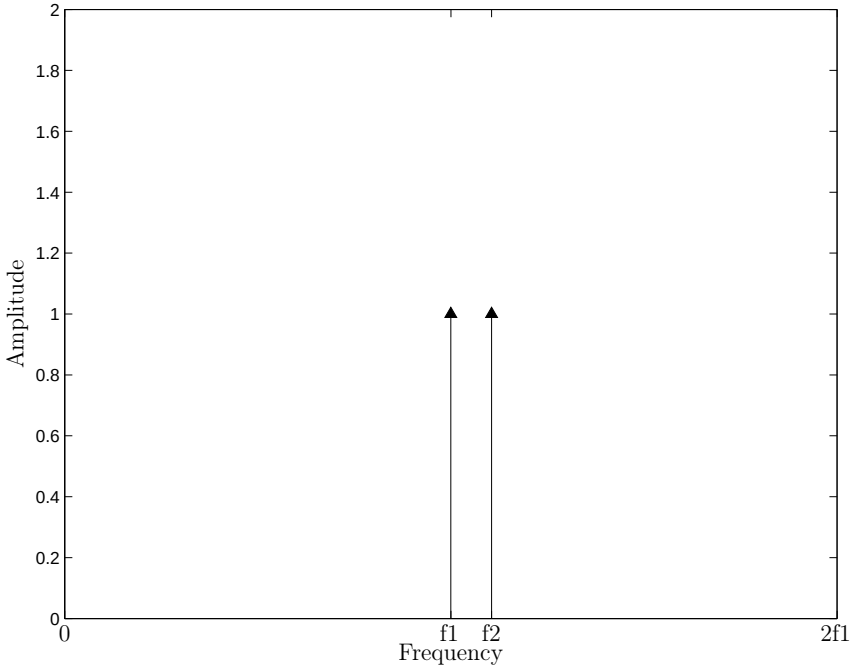

(a) Two-tone excitation in the frequency domain.

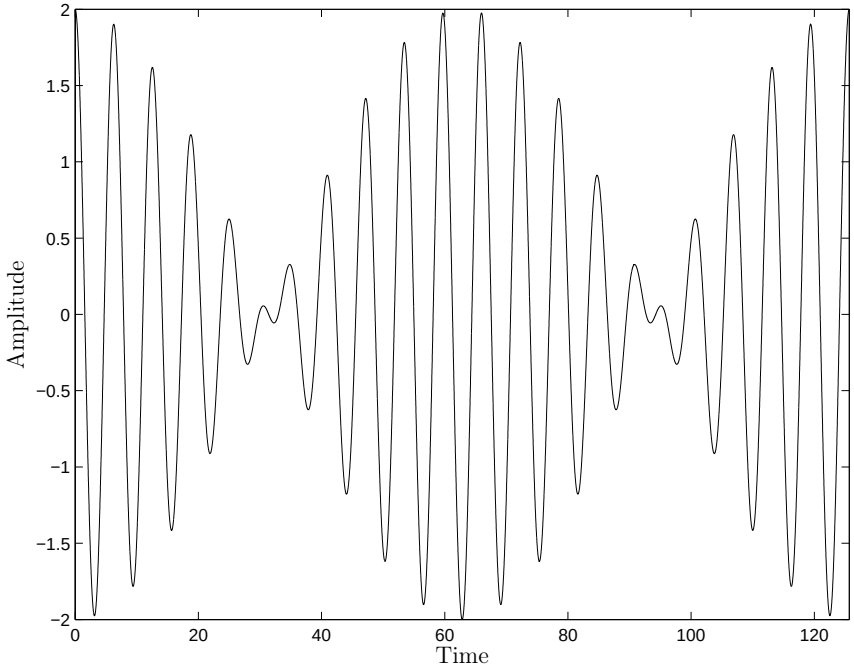

(b) Two-tone excitation in the time domain.

Figure 2.7: Illustration of a two-tone excitation.

Table 2.2: Frequency components generated by the nonlinear input-output relationship $V_{out} = G_0 + G_1 V_{in} + G_2 V_{in}^2 + G_3 V_{in}^3$, where V_{in} is a two tone excitation.

Frequency	Amplitude	Frequency	Amplitude
0	$G_0 + G_2 A^2$	$\omega_1 + \omega_2$	$G_2 A^2$
$\omega_2 - \omega_1$	$G_2 A^2$	$2\omega_2$	$\frac{G_2 A^2}{2}$
$2\omega_1 - \omega_2$	$\frac{3G_3 A^3}{4}$	$3\omega_1$	$\frac{G_3 A^3}{4}$
ω_1	$\frac{4G_1 A + 9G_3 A^3}{4}$	$2\omega_1 + \omega_2$	$\frac{3G_3 A^3}{4}$
ω_2	$\frac{4G_1 A + 9G_3 A^3}{4}$	$2\omega_2 + \omega_1$	$\frac{3G_3 A^3}{4}$
$2\omega_2 - \omega_1$	$\frac{3G_3 A^3}{4}$	$3\omega_2$	$\frac{G_3 A^3}{4}$
$2\omega_1$	$\frac{G_2 A^2}{2}$		

band to the frequencies 0 Hz and $\omega_2 - \omega_1$. It also creates the second harmonic band with components $2\omega_1$, $2\omega_2$ and $\omega_1 + \omega_2$. The cubic term G_3 creates the third-order intermodulation components $2\omega_1 - \omega_2$ and $2\omega_2 - \omega_1$, the compression or expansion terms on top of the fundamental tones ω_1 and ω_2, and also the third harmonic band with components $3\omega_1$, $2\omega_1 + \omega_2$, $2\omega_2 + \omega_1$ and $3\omega_2$.

The third-order system is further illustrated in Figure 2.8, where the output of the transfer function $V_{out} = 2 + 10V_{in} + V_{in}^2 - 3V_{in}^3$ is plotted in both time and frequency domain. The input signal is $V_{in} = 0.5\cos(0.95t) + 0.5\cos(1.05t)$. The frequency domain plot clearly shows the different frequency bands created by the nonlinearity. The output amplitude values of the frequency plot are listed in Table 2.3.

2.6.3 Nonlinear Phenomena

The generated frequency components can be roughly grouped into two categories, namely the harmonic components and the intermodulation (IM) components. In communication systems the harmonics may interfere with other systems and must therefore be reduced by filters or by other means. This is not a major problem since the harmonics occur at frequencies high above the desired frequency, so that the filtering can be quite easily performed.

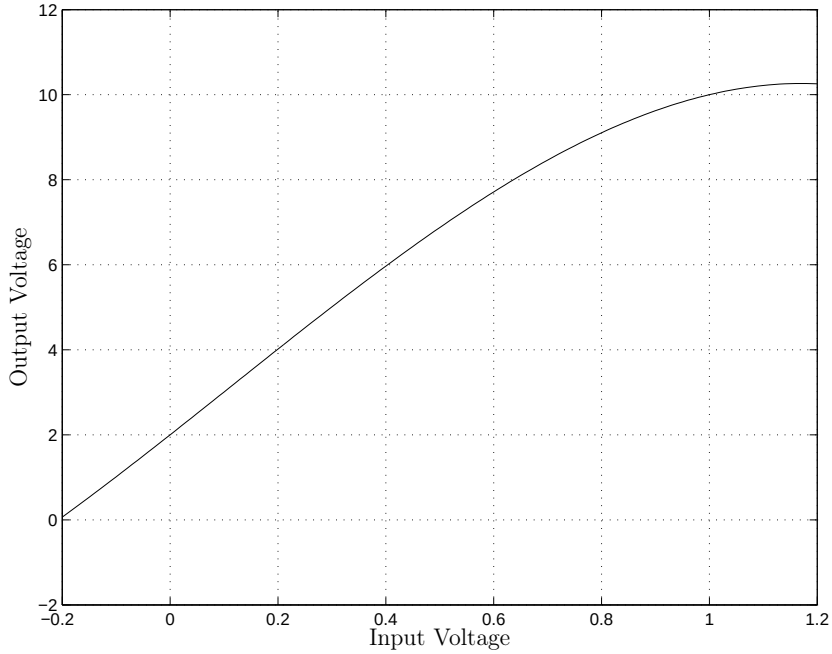

(a)

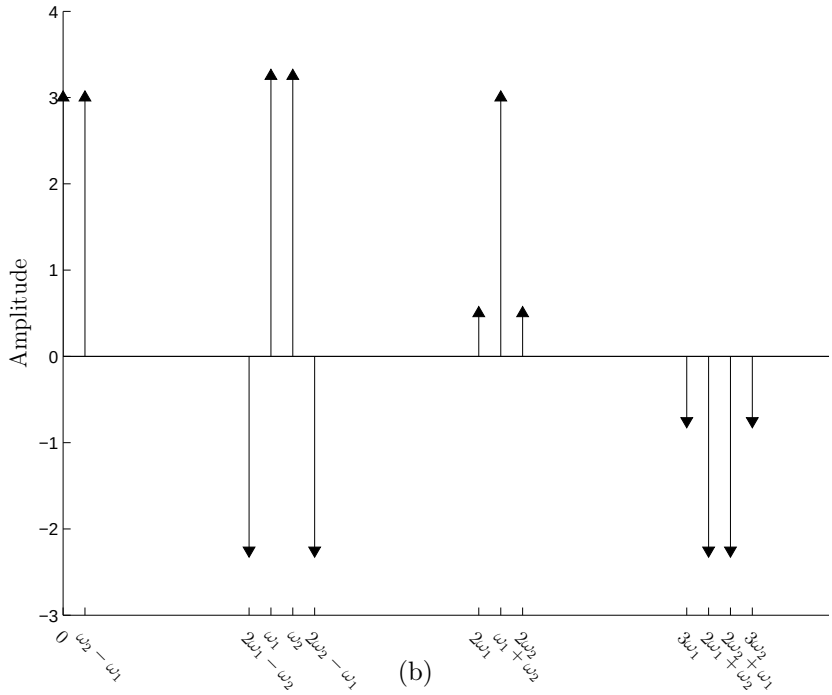

(b)

Figure 2.8: Time and frequency domain plots of the output of a third-order nonlinear system $V_{out} = 2 + 10V_{in} + V_{in}^2 - 3V_{in}^3$ *using a two-tone input* $V_{in} = \cos(0.95t) + \cos(1.05t)$*. The amplitude values are listed in Table 2.3.*

Table 2.3: List of frequency components generated by the nonlinear input-output relationship $V_{out} = 2 + 10V_{in} + V_{in}^2 - 3V_{in}^3$, where $V_{in} = \cos(0.95t) + \cos(1.05t)$.

Frequency	Amplitude	Frequency	Amplitude
0	3.00	$\omega_1 + \omega_2$	3.00
$\omega_2 - \omega_1$	3.00	$2\omega_2$	0.50
$2\omega_1 - \omega_2$	−2.25	$3\omega_1$	−0.75
ω_1	3.25	$2\omega_1 + \omega_2$	−2.25
ω_2	3.25	$2\omega_2 + \omega_1$	−2.25
$2\omega_2 - \omega_1$	−2.25	$3\omega_2$	−0.75
$2\omega_1$	0.50		

The intermodulation components on the other hand often pose a more serious problem, because some of them appear in-band and can be mistaken for desired signals. The even-order IM products are not a problem since they appear at frequencies well below or above the signals that created them. However, the odd-order IM products present a problem, since they appear in-band. The third-order products present the greatest problems because they are the strongest and the closest to the signals that generated them and thus are often impossible to reject with the use of filters [8].

2.7 Measures of Nonlinearity

2.7.1 The 1-dB Compression Point

The 1-dB compression point refers to the output power level where the transfer characteristics of the amplifier have dropped by 1 dB from the ideal linear characteristics [5]. The 1-dB compression point of an amplifier with a third-order nonlinearity is illustrated in Figure 2.9.

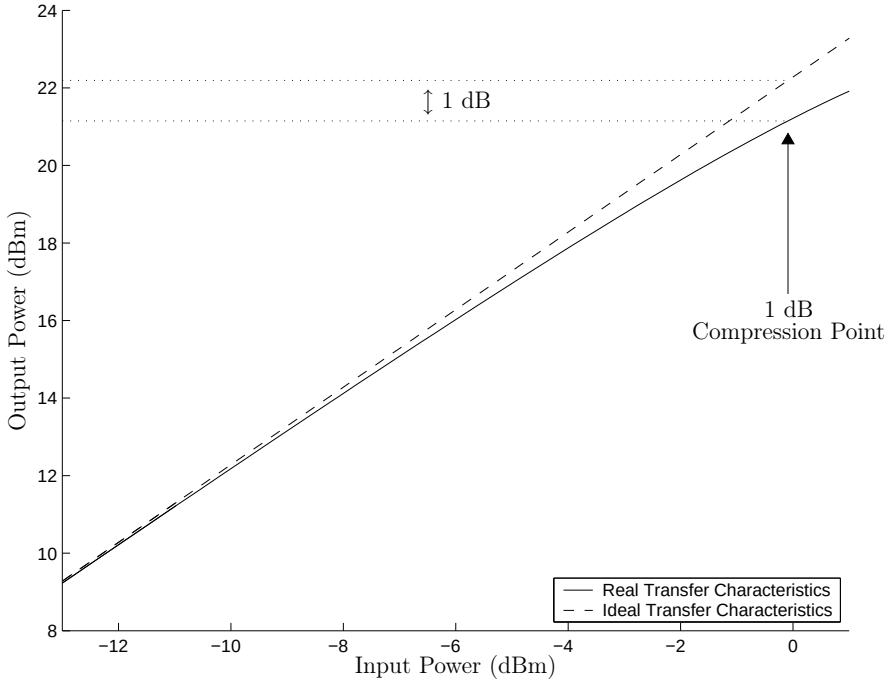

Figure 2.9: Illustration of the 1 dB compression point.

2.7.2 Intercept Points

Intercept points provide a simple method for predicting the amount of nonlinear distortion of an amplifier at a particular operating point. If the input-output relationship of a device is plotted on a log-log scale, the slope of the linear component will be 1. If the second-order distortion products are shown on the same scale, they will have a slope of 2, the third order distortion products will have a slope of 3, etc. [7]

The intercept point is the point where the linear extrapolation of the harmonic component intersects with the linear extrapolation of the fundamental component. The second-order and third-order intercept points of the nonlinear transfer functions in Equations (2.3) and (2.6) are illustrated in Figure 2.10.

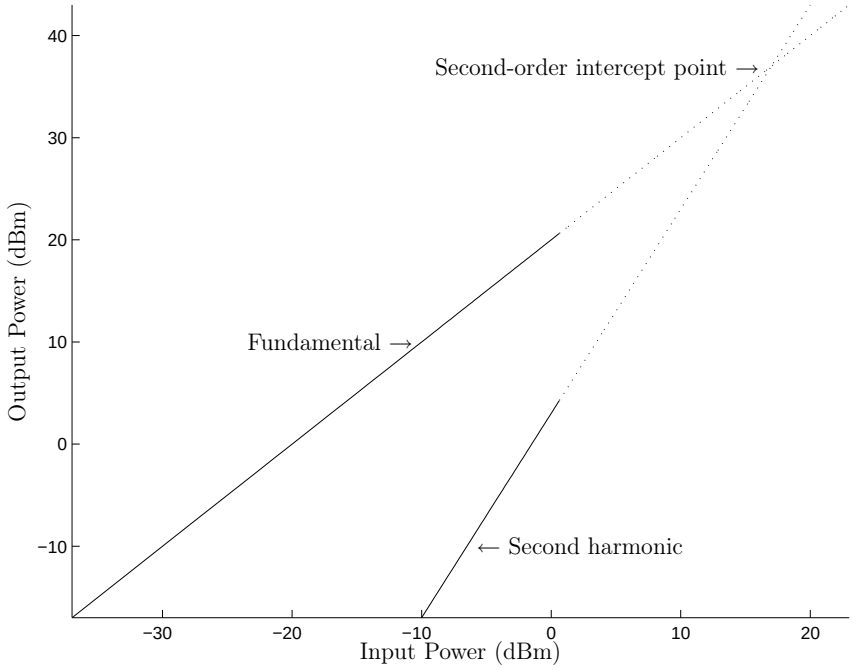

(a) $V_{out}(t) = 10V_{in}(t) + 4V_{in}^2(t)$

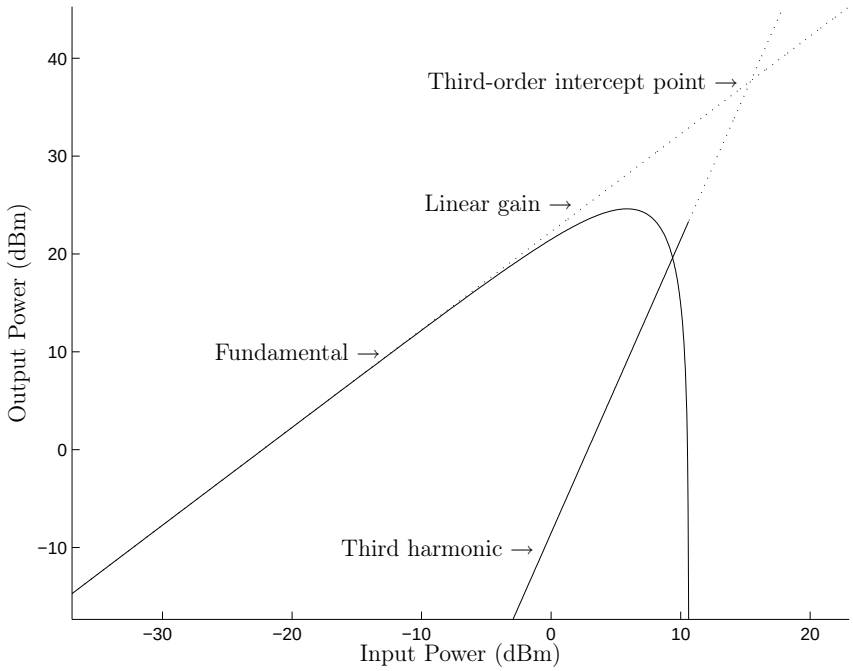

(b) $V_{out}(t) = 13V_{in}(t) - 3V_{in}^3(t)$

Figure 2.10: Illustration of the second-order and third-order intercept points.

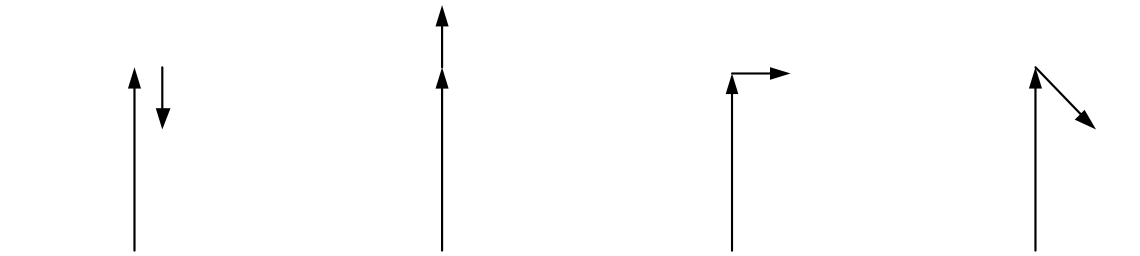

(a) AM-AM compression (b) AM-AM expansion (c) AM-PM conversion (d) AM-AM and AM-PM conversion

Figure 2.11: Amplitude and phase distortion caused by a third-order nonlinearity.

2.7.3 AM-AM and AM-PM Conversion

Another widely used measure is to show the fundamental and third-order spectral components as vectors. This is done by showing the third-order vector on top of the fundamental vector. This is illustrated in Figure 2.11, where the vectors of the system $V_{out} = G_1 V_{in} + G_3 V_{in}^3$ are shown at a certain input amplitude value. The length of the third-order vectors will grow as the input amplitude is increased.

Figure 2.11(a) shows the situation where the output signal is compressed due to the third-order term. In this case both G_1 and G_3 are real and have opposite signs. If the signs are equal, amplitude expansion will occur. This is illustrated in Figure 2.11(b). Figure 2.11(c) illustrates a 90° phase conversion. The third-order vector is now pointing to the right and therefore the third-order term G_3 must be a complex number to model the phase shift. Figure 2.11(d) shows the situation where the nonlinearity causes both amplitude and phase conversion. [7]

2.7.4 Adjacent Channel Power Ratio

Adjacent Channel Power Ratio (ACPR) is a measure of the degree of signal spreading into adjacent channels, caused by nonlinearities in a power amplifier. It is defined as the power contained in a defined bandwidth (B_1) at a defined offset (f_0) from the channel center frequency (f_c), divided by the power in a defined bandwidth (B_2) placed around the channel center frequency. This is illustrated in Figure 2.12(a). [5]

2.7.5 Noise Power Ratio

Noise Power Ratio (NPR) is a measure of the unwanted in-channel distortion power caused by the nonlinearity of the power amplifier. It can be measured by applying a notch filter at the center frequency of the transmission channel and examining the level of distortion that fills the notch. NPR is defined as the ratio between the noise power spectral density passing through the amplifier measured at the center of the notch compared to the noise power spectral density without the notch filter. The concept is illustrated in Figure 2.12(b). [5]

2.7.6 Multitone Intermodulation Ratio

Multitone Intermodulation Ratio (MIMR) is a measure of the effect of nonlinearity on a multicarrier signal. It is defined as the ratio between the wanted tone power and the highest intermodulation tone power just outside of the wanted band. This is illustrated in Figure 2.12(c). [5]

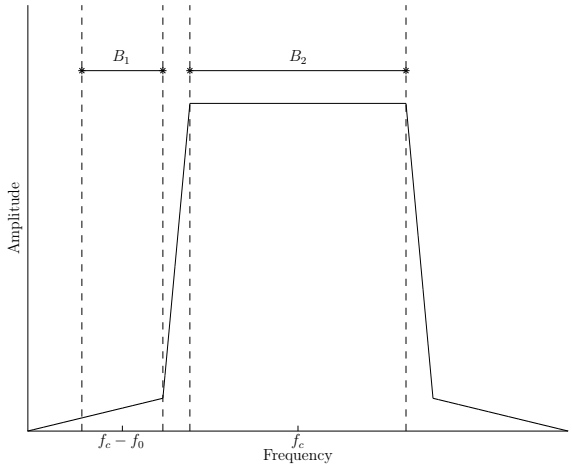

(a) Adjacent power ratio

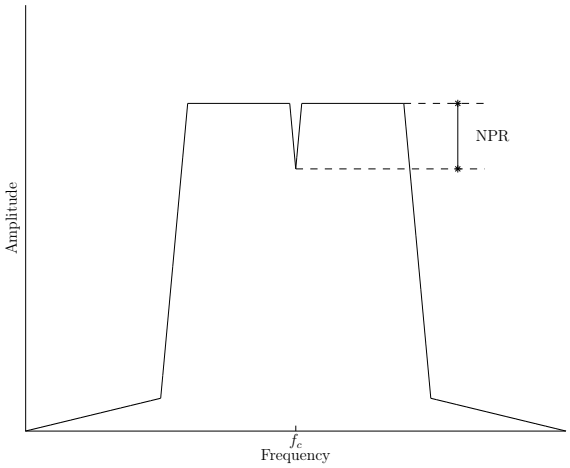

(b) Noise power ratio

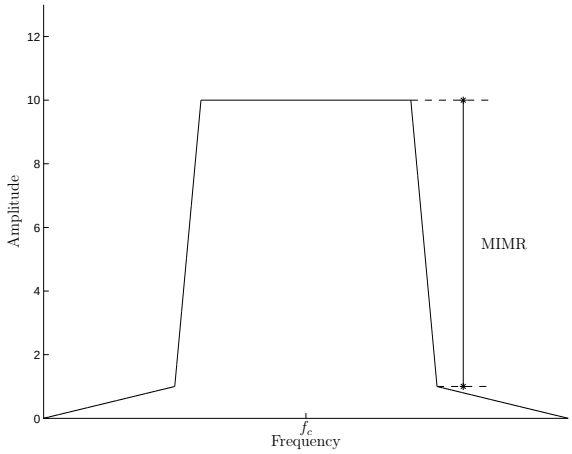

(c) Multitone intermodulation ratio

Figure 2.12: Illustration of nonlinearity measures for multitone and modulated signals [5].

2.8 Effects of Amplifier Distortion

The nonlinearities of the amplifier degrade the transmitted signal in several ways. The following lists some of the most significant adverse effects.

- Additional nonlinear interference in the receiver [9]
- Spectral spreading of the transmitted signal, which can cause adjacent channel interference [9]
- Signal constellation deformation and spreading [10, 11]
- Interference between the in-phase and quadrature components due to AM/PM conversion [9]
- Intermodulation effects, which occur, when several channels are amplified in a single amplifier [9]
- Degradation in the antenna amplitude and phase weightings due to intermodulation in adaptive antenna systems. This causes degradation to the antenna beam pattern and null depth [5]

2.9 Summary

This chapter introduced some definitions of amplifier nonlinearities as well as categorized the nonlinearities. Measures of nonlinearities for single-tone and multitone inputs were also illustrated. Finally some effects of the distortion were listed.

A linear system does not alter the signal waveform that passes through it. Nonlinear systems on the other hand distort the signal due to amplitude and phase conversion. The nonlinear system can be characterized as a memoryless system or as a system with memory. In a memoryless system the output of the system is an instantaneous function of the input and therefore the system cannot present any phase conversion.

If the system has memory, then also the previous input values affect the output. The memory is caused by energy storing components inside the system that cannot alter their state instantaneously.

Two-tone measurements can be used to verify the transfer characteristics of an amplifier. A two-tone excitation fed to a nonlinear system generates harmonic bands as well as in-band intermodulation distortion. The most serious problems are faced due to the third-order intermodulation components, because these are the strongest components and also the ones that are closest to the signals that generated them and are thus often impossible to reject by filtering.

Chapter 3

Parameter Estimation Theory

3.1 Introduction

The subsequent chapters present models for the adverse nonlinear effects discussed in the previous chapter. These models include unknown parameters that need to be determined. Mathematically this can be formulated as follows. Given a set of data $x[0], x[1], \cdots, x[L-1]$ that depends on an unknown parameter ξ, we wish to determine ξ based on the data or in other words to define an *estimator*

$$\hat{\xi} = \gamma(x[0], x[1], \cdots, x[L-1]) \tag{3.1}$$

where γ is some function [12]. This is the problem of parameter estimation that is addressed in this chapter.

The estimation process begins by assuming an appropriate model for the input. Since the data is inherently random, it is usually described by its Probability Density Function (PDF) denoted by $p(x[0], x[1], \cdots, x[L-1]; \xi)$. The PDF is parameterized by the unknown parameter ξ, so that changing the value of ξ yields different PDFs. To illustrate the situation let us assume only one measurement data point, i.e., $L = 1$

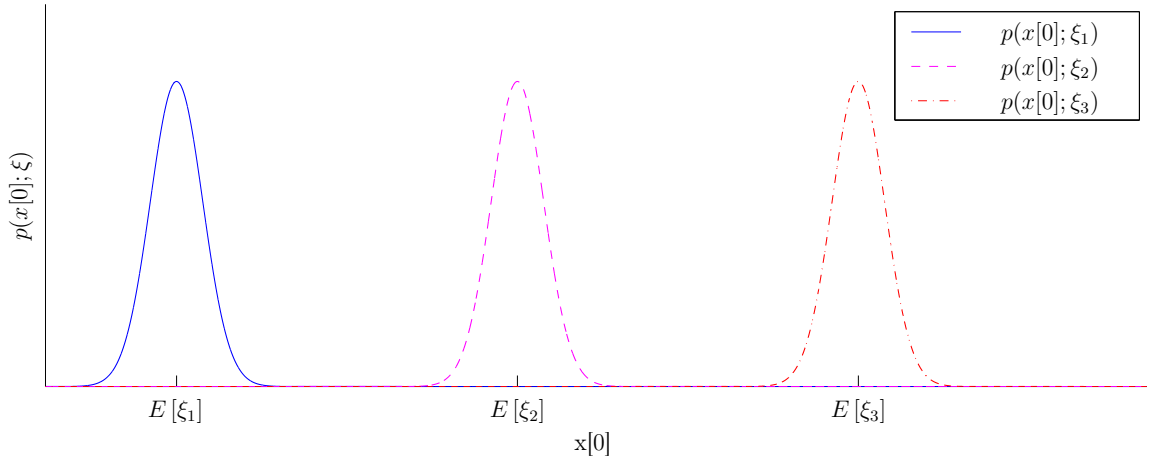

Figure 3.1: Probability density function dependency of the estimator value ξ.

and that the data $x[k]$ can be modelled by the Gaussian probability density function

$$p(x[0];\xi) = \frac{1}{\sqrt{2\pi\sigma^2}} \exp\left(-\frac{1}{2\sigma^2}(x[0]-\xi)^2\right) \tag{3.2}$$

where σ is the standard deviation. Changing ξ in Equation (3.2) gives different PDFs as shown in Figure 3.1.

In practice the PDF is not given but instead one should be chosen that is assumed to model the given observations as well as possible in some sense. Besides being consistent with the problem and any other available information, it should also be mathematically tractable. Once the PDF has been chosen the next thing to do is to find the optimal estimator of the data as formulated in Equation (3.1).

A brief outline of the rest of the chapter follows. The chapter begins by defining criteria on which optimal estimators are based and how good they can be. Next some principles which estimators are commonly derived from are discussed. Based on these principles, estimators for the linear data model are derived. The chapter ends with a summary of the derived estimators and a comparison of their performance.

3.2 Optimality of an Estimator

Any estimate based on a finite number of observations is expected to contain some error. Therefore, a criterion for the optimality of the estimator is needed. Obviously it is desirable that the estimator should produce correct values. An estimator that produces correct values on the average is called an *unbiased estimator*. Mathematically such an estimator is defined as

$$E(\hat{\xi}) = \xi. \tag{3.3}$$

The fact that the estimator is unbiased does not necessarily make it a good one. It only guarantees that the estimator will produce correct values on the average. Generally it is not even guaranteed that an estimation problem has an unbiased estimator or it might exist but it may be very difficult to compute.

Another criterion for the optimality is the variance of the estimator. Figure 3.2(a) shows two unbiased estimators with different variances. Naturally the estimator that has smaller variance produces more accurate results than the one that has larger variance. Thus, an optimal estimator should be unbiased and have minimum variance. In order to find the optimal estimator some measure is required to define the goodness of an estimator. An obvious choice for the measure is to use the Mean Square Error (MSE) which is a measure of the average mean squared deviation of the estimator from the correct value. The MSE can also be expressed by the bias and the variance of the estimator as follows

$$MSE(\xi) = bias^2(\xi) + var(\xi). \tag{3.4}$$

This equation shows that the accuracy of an estimator is always a trade-off between the bias and the variance. The importance of the unbiasedness is illustrated in Figure 3.2(b). The figure shows that even though the unbiased estimator has greater variance, it still produces more accurate results than the biased one.

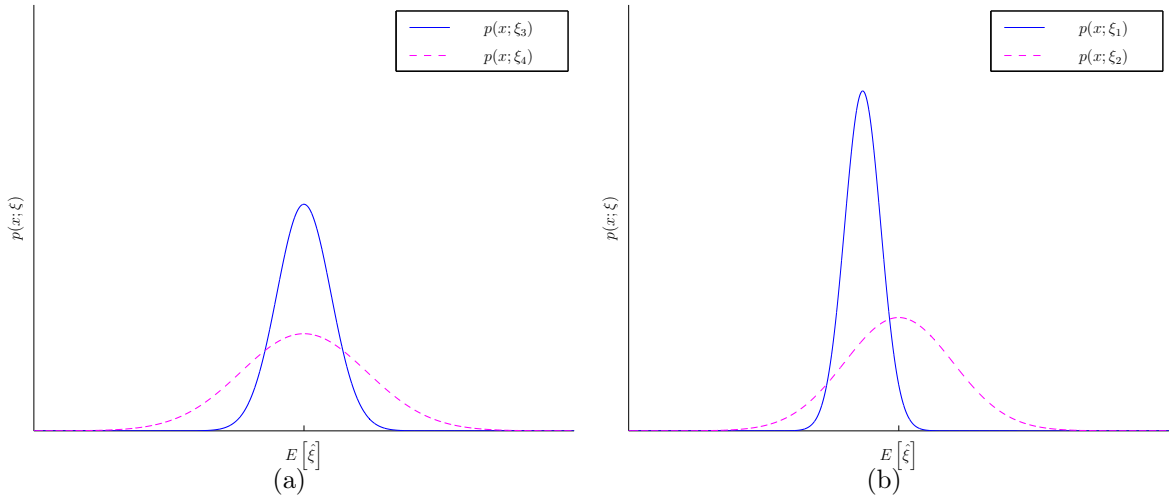

Figure 3.2: Illustration of the optimality criterions of estimators. a) The effect of the variance on the accuracy of an unbiased estimator and b) the effect of the bias on the accuracy of an estimator.

Unfortunately, the MSE criterion generally leads to unrealizable estimators, although for some problems realizable Minimum Mean Square Error Estimators (MMSEE) can be found [12]. Consequently, some other measure than the MSE must be used. A more practical approach is to require the estimator to be unbiased and then minimize the variance. The resulting estimator named the Minimum Variance Unbiased Estimator (MVUE) is discussed in Section 3.4.

3.3 Cramer-Rao Lower Bound

In practical problems it is often impossible or untractable to find the MMSEE or the MVUE. Therefore it proves to be highly useful to be able to set a lower bound on the MSE. For an unbiased estimator this is the same as setting a lower bound on the variance as can be easily seen from Equation (3.4). The lower bound can be used to investigate the fundamental limits of a parameter estimation problem, it can be used as a benchmark for a specific estimator or it can be used to prove that the derived estimator is the MVUE.

Several lower bounds have been presented in the literature. Probably the most well known are the Cramer-Rao Lower Bound (CRLB) [12], the Barankin Lower Bound (BLB) [13,14], the Ziv-Zakai Lower Bound (ZZLB) [15–18] and the Weiss-Weinstein Lower Bound (WWLB) [19]. Generally the CRLB is by far the easiest to evaluate and, therefore, it will be used in this text.

Before describing the CRLB it is necessary to clarify some concepts used to express the bound. Firstly, the estimation accuracy depends directly on the PDF, since all the information that is available of the estimation problem is embedded in the PDF. As already mentioned the PDF is parameterized by the estimator ξ, and hence the more the PDF depends on ξ, the more accurate results can be obtained. Therefore, it is not surprising that the CRLB is also derived from the PDF. Secondly, viewing the PDF as a function of the unknown parameter, i.e., $\mathbf{x}$ assumed fixed, is denoted as the *likelihood function*. The *curvature* of the likelihood function depicts how accurate the estimator is. Larger curvature indicates a sharper form of the PDF and hence a more accurate estimator. The average curvature of the Log-Likelihood Function (LLF) is defined as

$$\kappa_{ave} = -E\left[\frac{\partial^2 \ln p(\mathbf{x};\xi)}{\partial \xi^2}\right]. \tag{3.5}$$

The CRLB states the minimum variance of an unbiased estimator as a function of the average curvature of the LLF. For a *scalar parameter* the CRLB can be stated as follows [12].

Theorem 1. *Cramer-Rao Lower Bound – Scalar Parameter*

Assume that the PDF $p(\mathbf{x};\xi)$ satisfies the regularity condition

$$E\left[\frac{\partial \ln p(\mathbf{x};\xi)}{\partial \xi}\right] = 0 \qquad \textit{for all } \xi \tag{3.6}$$

then the variance of any unbiased estimator $\hat{\xi}$ must satisfy

$$var\left(\hat{\xi}\right) \geq \frac{1}{-E\left[\frac{\partial^2 \ln p(\mathbf{x};\xi)}{\partial \xi^2}\right]}. \tag{3.7}$$

In addition an unbiased estimator may be found that attains the bound for all ξ if and only if

$$\frac{\partial \ln p(\mathbf{x};\xi)}{\partial \xi} = F(\xi)\left(\gamma(\mathbf{x}) - \xi\right) \tag{3.8}$$

for some functions F and γ. The estimator $\hat{\xi} = \gamma(\mathbf{x})$ is the MVUE and the minimum variance is $1/F(\xi)$.

The CRLB can also be extended to express a lower bound for a *vector parameter* estimation problem. Given a vector parameter estimator

$$\boldsymbol{\xi} = \begin{bmatrix} \xi_1 & \xi_1 \cdots \xi_n \end{bmatrix}^{\mathrm{T}} \tag{3.9}$$

the vector parameter CRLB gives a lower bound for the variance of each element of $\boldsymbol{\xi}$. A derivation of both the scalar and vector parameter CRLB can be found in [12]. The vector parameter CRLB is stated as follows [12].

Theorem 2. *Cramer-Rao Lower Bound – Vector Parameter*

Assume that the PDF $p(\mathbf{x};\boldsymbol{\xi})$ satisfies the regularity conditions

$$E\left[\frac{\partial \ln p(\mathbf{x};\boldsymbol{\xi})}{\partial \boldsymbol{\xi}}\right] = \mathbf{0} \qquad \text{for all } \boldsymbol{\xi} \tag{3.10}$$

then the covariance matrix of any unbiased estimator $\hat{\xi}$ satisfies

$$\mathbf{C}_{\hat{\xi}} - \mathbf{F}^{-1} \geq \mathbf{0} \tag{3.11}$$

where $\geq \mathbf{0}$ is interpreted as positive semidefinite and $\mathbf{F}$ is the Fisher information matrix

$$\left[\mathbf{F}(\boldsymbol{\xi})\right]_{ij} = -E\left[\frac{\partial^2 \ln p(\mathbf{x};\boldsymbol{\xi})}{\partial \boldsymbol{\xi}_i \partial \boldsymbol{\xi}_j}\right]. \tag{3.12}$$

Furthermore an unbiased estimator may be found that attains the bound in that $\mathbf{C}_{\hat{\xi}} = \mathbf{F}^{-1}$ *if and only if*

$$\frac{\partial \ln p(\mathbf{x};\boldsymbol{\xi})}{\partial \boldsymbol{\xi}} = \mathbf{F}(\boldsymbol{\xi})\left(\boldsymbol{\gamma}(\mathbf{x}) - \boldsymbol{\xi}\right) \tag{3.13}$$

for some $n \times n$ *matrix* $\mathbf{F}$ *and some n-dimensional function* $\boldsymbol{\gamma}$*. The estimator* $\hat{\boldsymbol{\xi}} = \boldsymbol{\gamma}(\mathbf{x})$ *is the MVUE estimator and its covariance matrix is* $\mathbf{F}^{-1}(\boldsymbol{\xi})$*.*

The lower bound for the variance of each element in the vector parameter estimator $\boldsymbol{\xi}$ defined in Equation (3.9) can be found by noting that the diagonal elements of a positive semidefinite matrix are nonnegative. Therefore,

$$\left[\mathbf{C}_{\hat{\xi}} - \mathbf{F}^{-1}(\boldsymbol{\xi})\right]_{ii} \geq 0 \tag{3.14}$$

and hence

$$var\left(\hat{\xi}_i\right) = \left[\mathbf{C}_{\hat{\xi}}\right]_{ii} \tag{3.15}$$

$$\geq \left[\mathbf{F}^{-1}(\boldsymbol{\xi})\right]_{ii} \tag{3.16}$$

which is the needed result.

3.4 Minimum Variance Unbiased Estimation

The MVUE is extensively used in classical parameter estimation. Generally the determination of the MVUE estimator is a difficult task since there is no universally applicable method for determining it. Fortunately many estimation problems can be represented by linear models where the MVUE estimator is easy to find. In the following a derivation of the MVUE estimator for the linear data model embedded in both white and colored noise is derived.

3.4.1 MVUE for the Linear Model Embedded in White Noise

A linear model can be compactly written in vector notation as

$$\mathbf{x} = \mathbf{U}\boldsymbol{\xi} + \mathbf{w} \tag{3.17}$$

where $\mathbf{x}$ is a $L \times 1$ vector of observations, $\mathbf{U}$ is a $L \times n$ *observation matrix*, $\boldsymbol{\xi}$ is a $n \times 1$ vector of parameters to be estimated and $\mathbf{w}$ is a $L \times 1$ noise vector with PDF $\mathcal{N}(\mathbf{0}, \sigma^2\mathbf{I})$.

Now that the data model has been defined, the MVUE for this case can be derived using the CRLB. Theorem 2 states that the estimator $\hat{\boldsymbol{\xi}} = \boldsymbol{\gamma}(\mathbf{x})$ will be the MVUE if and only if

$$\frac{\partial \ln p(\mathbf{x}; \boldsymbol{\xi})}{\partial \boldsymbol{\xi}} = \mathbf{F}(\boldsymbol{\xi})\left(\boldsymbol{\gamma}(\mathbf{x}) - \boldsymbol{\xi}\right) \tag{3.18}$$

for some function $\boldsymbol{\gamma}$ and that the covariance matrix of $\hat{\boldsymbol{\xi}}$ will be $\mathbf{F}^{-1}(\boldsymbol{\xi})$.

The PDF of the linear model is

$$p(\mathbf{x}; \boldsymbol{\xi}) = \frac{1}{(2\pi\sigma^2)^{N/2}} \exp\left(-\frac{1}{2\sigma^2}\left(\mathbf{x} - \mathbf{U}\boldsymbol{\xi}\right)^2\right) \tag{3.19}$$

and the LLF is thus

$$\ln p(\mathbf{x}; \boldsymbol{\xi}) = -\frac{N}{2}\ln\left(2\pi\sigma^2\right) - \frac{1}{2\sigma^2}\left(\mathbf{x} - \mathbf{U}\boldsymbol{\xi}\right)^{\mathrm{T}}\left(\mathbf{x} - \mathbf{U}\boldsymbol{\xi}\right). \tag{3.20}$$

Differentiating the LLF with respect to $\boldsymbol{\xi}$ using the product differentiation rule yields

$$\frac{\partial \ln p(\mathbf{x}; \boldsymbol{\xi})}{\partial \boldsymbol{\xi}} = -\frac{1}{2\sigma^2}\left[-\mathbf{U}^{\mathrm{T}}\left(\mathbf{x} - \mathbf{U}\boldsymbol{\xi}\right) - \left(\mathbf{x} - \mathbf{U}\boldsymbol{\xi}\right)^{\mathrm{T}}\mathbf{U}\right] \tag{3.21a}$$

$$= -\frac{1}{\sigma^2}\left[-\mathbf{U}^{\mathrm{T}}\mathbf{x} + \mathbf{U}^{\mathrm{T}}\mathbf{U}\boldsymbol{\xi}\right] \tag{3.21b}$$

$$= \frac{\mathbf{U}^{\mathrm{T}}\mathbf{U}}{\sigma^2}\left[\left(\mathbf{U}^{\mathrm{T}}\mathbf{U}\right)^{-1}\mathbf{U}^{\mathrm{T}}\mathbf{x} - \boldsymbol{\xi}\right] \tag{3.21c}$$

where Equation (3.21c) is exactly as stated in (3.18) with

$$\hat{\boldsymbol{\xi}} = \left(\mathbf{U}^{\mathrm{T}}\mathbf{U}\right)^{-1}\mathbf{U}^{\mathrm{T}}\mathbf{x} \tag{3.22}$$

$$\mathbf{F}\left(\boldsymbol{\xi}\right) = \frac{\mathbf{U}^{\mathrm{T}}\mathbf{U}}{\sigma^2} \tag{3.23}$$

and hence the MVUE is given by (3.22) and its covariance matrix is

$$\mathbf{C}_{\hat{\boldsymbol{\xi}}} = \mathbf{F}^{-1} \tag{3.24}$$

$$= \sigma^2\left(\mathbf{U}^{\mathrm{T}}\mathbf{U}\right)^{-1}. \tag{3.25}$$

3.4.2 MVUE for the Linear Model Embedded in Colored Noise

This section extends the results of the previous section for linear models embedded in colored noise. The noise is now statistically characterized as

$$\mathbf{w} \sim \mathcal{N}\left(\mathbf{0}, \mathbf{C}\right). \tag{3.26}$$

The covariance matrix $\mathbf{C}$ is assumed to be positive definite, which means that $\mathbf{C}^{-1}$ is also positive semidefinite and can therefore factorized as

$$\mathbf{C}^{-1} = \mathbf{R}^{\mathrm{T}}\mathbf{R} \tag{3.27}$$

for some $L \times L$ nonsingular matrix $\mathbf{R}$ [20]. The matrix $\mathbf{R}$ is a transformation matrix that whitens the noise $\mathbf{w}$ since

$$\begin{aligned} E\left[\left(\mathbf{Rw}\right)\left(\mathbf{Rw}\right)^{\mathrm{T}}\right] &= \mathbf{RCR}^{\mathrm{T}} \\ &= \mathbf{RR}^{-1}\left(\mathbf{R}^{\mathrm{T}}\right)^{-1}\mathbf{R} \\ &= \mathbf{I}. \end{aligned} \tag{3.28}$$

Applying the transformation $\mathbf{R}$ to the extended linear model with colored noise

$$\mathbf{x} = \mathbf{U}\boldsymbol{\xi} + \mathbf{w} \tag{3.29}$$

gives

$$\begin{aligned} \tilde{\mathbf{x}} &= \mathbf{R}\mathbf{x} \\ &= \mathbf{R}\mathbf{U}\boldsymbol{\xi} + \mathbf{R}\mathbf{w} \\ &= \tilde{\mathbf{U}}\boldsymbol{\xi} + \tilde{\mathbf{w}} \end{aligned} \tag{3.30}$$

which is exactly the linear model with whitened noise $\tilde{\mathbf{w}} = \mathbf{R}\mathbf{w} \sim \mathcal{N}(\mathbf{0}, \mathbf{I})$.

The MVUE for the linear model with colored noise can now be solved using the estimator for white noise defined in Equation (3.22)

$$\hat{\boldsymbol{\xi}} = \left(\tilde{\mathbf{U}}^{\mathrm{T}}\tilde{\mathbf{U}}\right)^{-1}\tilde{\mathbf{U}}^{\mathrm{T}}\tilde{\mathbf{x}} \tag{3.31a}$$

$$= \left(\mathbf{U}^{\mathrm{T}}\mathbf{R}^{\mathrm{T}}\mathbf{R}\mathbf{U}\right)^{-1}\mathbf{U}^{\mathrm{T}}\mathbf{R}^{\mathrm{T}}\mathbf{R}\mathbf{x} \tag{3.31b}$$

$$= \left(\mathbf{U}^{\mathrm{T}}\mathbf{C}^{-1}\mathbf{U}\right)^{-1}\mathbf{U}^{\mathrm{T}}\mathbf{C}^{-1}\mathbf{x}. \tag{3.31c}$$

The covariance matrix can be found in a similar fashion:

$$\mathbf{C}_{\hat{\xi}} = \left(\tilde{\mathbf{U}}^{\mathrm{T}}\tilde{\mathbf{U}}\right)^{-1} \tag{3.32a}$$

$$= \left(\mathbf{U}^{\mathrm{T}}\mathbf{C}^{-1}\mathbf{U}\right)^{-1}. \tag{3.32b}$$

Hence the MVUE for the linear model with colored noise is given by Equation (3.31c) and its covariance matrix is given by Equation (3.32b).

3.5 Best Linear Unbiased Estimation

As already mentioned in the previous section, finding the MVUE might not be practical or even possible. An attractive approach is to restrict the estimator to be

unbiased with the constraint that it is linear and then finding the estimator with the smallest variance. This results in the Best Linear Unbiased Estimator (BLUE). If the noise embedded in the data model has Gaussian characteristics, i.e., $\mathbf{w} \sim \mathcal{N}(\mathbf{0}, \mathbf{C})$, then the BLUE is also the MVUE.

The BLUE for the general linear model is defined by the Gauss-Markov theorem which is stated as follows. A proof of the theorem can be found in [12].

Theorem 3. *Gauss-Markov Theorem*

If the data has the form of the general linear model

$$\mathbf{x} = \mathbf{U}\boldsymbol{\xi} + \mathbf{w} \tag{3.33}$$

where $\mathbf{x}$ *is a* $L \times 1$ *vector of observations,* $\mathbf{U}$ *is a known* $L \times n$ *observation matrix,* $\boldsymbol{\xi}$ *is a* $n \times 1$ *vector of the unknown parameters and* $\mathbf{w}$ *is a* $L \times 1$ *noise vector with zero mean and covariance matrix* $\mathbf{C}$*, then the BLUE is*

$$\hat{\boldsymbol{\xi}} = \left(\mathbf{U}^{\mathrm{T}}\mathbf{C}^{-1}\mathbf{U}\right)^{-1}\mathbf{U}^{\mathrm{T}}\mathbf{C}^{-1}\mathbf{x} \tag{3.34}$$

and its covariance matrix is

$$\mathbf{C}_{\hat{\boldsymbol{\xi}}} = \left(\mathbf{U}^{\mathrm{T}}\mathbf{C}^{-1}\mathbf{U}\right)^{-1}. \tag{3.35}$$

The minimum variance of $\hat{\xi}_i$ *is*

$$var\left(\hat{\xi}_i\right) = \left[\left(\mathbf{U}^{\mathrm{T}}\mathbf{C}^{-1}\mathbf{U}\right)^{-1}\right]_{ii}. \tag{3.36}$$

3.6 Least-Squares Estimation

Least-Squares (LS) estimation dates back to 1795 when Carl Friedrich Gauss (1777-1855) used it to study planetary motion [21]. It differs significantly from the previously discussed MVUE and BLUE, since it is purely deterministic in nature. In

LS estimation only a data model where the estimated data depend explicitly on the unknown parameters is assumed. Mathematically this can be written as

$$x[k] = s[k; \boldsymbol{\xi}] + w[k] \tag{3.37}$$

or in vector notation as

$$\mathbf{x} = \mathbf{s}(\boldsymbol{\xi}) + \mathbf{w} \tag{3.38}$$

where $\mathbf{x}$ is the observed data, $\mathbf{s}$ is the estimated data and the noise $\mathbf{w}$ has zero mean. The Least-Squares Estimator (LSE) minimizes the squared distance between the observed data and the estimated data. The cost function E of the LSE is defined as

$$E(\xi) = \sum_{k=0}^{L-1} (x[k] - s[k])^2 \tag{3.39}$$

where L is the number of samples, x is the observed data and s is the estimated data.

The key advantage of the LSE is that no assumptions of the observed data x are required. A drawback is that no guarantee of the derived estimator's performance can be made. A typical application of the LSE is an estimation problem where accurate statistical characterization can not be made or where optimal estimators are difficult to implement.

The derivation of the LSE for a given problem might not be straightforward, but as with the MVUE the derivation of the linear LSE is quite straightforward. In the following text both the linear and the weighted linear LSE are derived.

3.6.1 Linear Least-Squares Estimator

For the linear case the estimated signal model is simply

$$\mathbf{s} = \mathbf{U}\boldsymbol{\xi} \tag{3.40}$$

where $\mathbf{U}$ is an $L \times n$ observation matrix and $\boldsymbol{\xi}$ is an $n \times 1$ vector of the unknown parameters. Inserting Equation (3.40) into Equation (3.39) and writing the cost function in vector notation yields

$$E(\boldsymbol{\xi}) = (\mathbf{x} - \mathbf{U}\boldsymbol{\xi})^{\mathrm{T}}(\mathbf{x} - \mathbf{U}\boldsymbol{\xi}). \tag{3.41}$$

The LSE can be found by minimizing Equation (3.41) which is easy since E is a quadratic function of $\boldsymbol{\xi}$. The minimum is found by differentiating with respect to $\boldsymbol{\xi}$ which has already been calculated in Equation (3.21). The gradient is

$$\frac{\partial E(\boldsymbol{\xi})}{\partial \boldsymbol{\xi}} = -2\mathbf{U}^{\mathrm{T}}\mathbf{x} + 2\mathbf{U}^{\mathrm{T}}\mathbf{U}\xi. \tag{3.42}$$

Setting the gradient to zero and solving for $\boldsymbol{\xi}$ yields the LS estimator

$$\hat{\boldsymbol{\xi}} = \left(\mathbf{U}^{\mathrm{T}}\mathbf{U}\right)^{-1}\mathbf{U}^{\mathrm{T}}\mathbf{x}. \tag{3.43}$$

As can be seen from (3.43) the linear model LSE has exactly the same form as the MVUE defined in Equation (3.22). This does not mean that the derived LSE is the MVUE. For it to be the MVUE the noise embedded in the model must be statistically characterized by $\mathbf{w} \sim \mathcal{N}(\mathbf{0}, \sigma^2\mathbf{I})$.

3.6.2 Weighted Linear Least-Squares Estimator

Adding a $L \times L$ positive definite *weighting matrix* $\mathbf{W}$ to the cost function in Equation (3.39) produces the weighted linear LSE. The idea of the weighting matrix is to emphasize the importance of those observations that are more reliable. The cost function can now be written as

$$\begin{aligned} E(\boldsymbol{\xi}) &= (\mathbf{x} - \mathbf{U}\boldsymbol{\xi})^{\mathrm{T}}\mathbf{W}(\mathbf{x} - \mathbf{U}\boldsymbol{\xi}) \\ &= \mathbf{x}^{\mathrm{T}}\mathbf{W}\mathbf{x} - 2\boldsymbol{\xi}^{\mathrm{T}}\mathbf{U}^{\mathrm{T}}\mathbf{W}\mathbf{x} + \boldsymbol{\xi}^{\mathrm{T}}\mathbf{U}^{\mathrm{T}}\mathbf{W}\mathbf{U}\boldsymbol{\xi}. \end{aligned} \tag{3.44}$$

Differentiating with respect to $\boldsymbol{\xi}$ gives

$$\frac{\partial E(\boldsymbol{\xi})}{\partial \boldsymbol{\xi}} = -2\mathbf{U}^{\mathrm{T}}\mathbf{W}\mathbf{x} + 2\mathbf{U}^{\mathrm{T}}\mathbf{W}\mathbf{U}\boldsymbol{\xi}. \tag{3.45}$$

Setting the gradient to zero and solving for $\boldsymbol{\xi}$ yields the weighted LSE

$$\hat{\boldsymbol{\xi}} = \left(\mathbf{U}^{\mathrm{T}}\mathbf{W}\mathbf{U}\right)^{-1}\mathbf{U}^{\mathrm{T}}\mathbf{W}\mathbf{x}. \tag{3.46}$$

This is also the MVUE for the linear model with colored noise $\mathbf{w} \sim \mathcal{N}(\mathbf{0}, \mathbf{C})$ if the weighting matrix is chosen as $\mathbf{W} = \mathbf{C}^{-1}$. If the noise has an arbitrary zero mean PDF with covariance $\mathbf{C}$, instead of Gaussian PDF, but the weighting matrix is chosen as before, then the weighted linear LSE is the BLUE.

3.7 Summary

This chapter discussed the problem of parameter estimation. First the optimality of an estimator was defined and the evaluation of the estimator's performance was discussed. Thereafter optimal estimators were introduced and their use in linear estimation problems was highlighted. Finally the widely used least-squares estimator was introduced and compared to the optimal estimators.

An optimal estimator is unbiased and has as small variance as possible. An estimator that fulfils these criteria will on the average produce correct results. Means to measure the goodness of a derived estimator is provided by the Cramer-Rao Lower Bound (CRLB). It sets a lower bound for the variance of an unbiased estimator and can therefore be used to check if the derived estimator really is the (Minimum Variance Unbiased Estimator) MVUE. Besides being a benchmark for estimators it can also be used to investigate the fundamental limits of an estimation problem.

MVUE estimators are generally difficult to find. Fortunately, many estimation problems can be represented by linear models for which the MVUE is easy to find. In situations where the MVUE cannot be found, an attractive approach is to try to

find the Best Linear Unbiased Estimator (BLUE). If no information of the statistical characteristics is available, then the obvious solution is to use the Least-Squares Estimator (LSE). The LSE is very different from the MVUE and BLUE in that it has no optimality properties associated with it. A drawback of this is that no guarantee of the estimator's performance can be made. On the other hand, if the statistical characterization of the data is available, then the LSE can be shown to be the MVUE or the BLUE.

Generally parameter estimation is a complex problem and obtaining good results in it depends on many factors. The first task is to find a good model for the data. It should be complex enough to describe all the principal features of the data and at the same time it should be mathematically tractable. After this obstacle has been passed, the quest for the estimator can begin. Preferably it should be optimal or at least suboptimal in some sense, but this might lead to implementation problems. To summarize, there is no straightforward method for solving a parameter estimation problem and the different approaches must be weighted separately for a given estimation problem.

Chapter 4

Frequency-Independent Power Amplifier Models

This chapter begins by introducing the polynomial model, which can be universally applied for any curve fitting problem. It is followed with a discussion of models that are specifically designed for amplifier modelling based on measurements and engineering intuition. Finally the use of these models in simulations is illustrated.

A common descriptor of these models is that they are unable to model frequency dependent distortion. The strength of a model of this type lies in the fact that its parameters are quite easy to estimate and the required measurements for the parameter estimation are quite simple to perform. The estimation requires only a single sine-wave, swept-tone measurement of both amplitude and phase. If the model is also linearly parameterized, then the parameter estimation is straightforward to do.

4.1 Polynomial Model

Fitting a polynomial both to the AM/AM and AM/PM measurements seems to be an obvious starting point for amplifier modelling. The model can be written as

$$g(A) = \sum_{p=0}^{N_g} a_p A^p = a_0 + a_1 A + a_2 A^2 + \cdots + a_{N_g} A^{N_g} \tag{4.1a}$$

$$\Phi(A) = \sum_{q=0}^{N_\Phi} b_q A^q = b_0 + b_1 A + b_2 A^2 + \cdots + b_{N_\Phi} A^{N_\Phi} \tag{4.1b}$$

where $g(A)$ is the amplitude conversion function and $\Phi(A)$ is the phase conversion function. The coefficients a_p and b_p can be easily found by applying linear least-squares approximation. Least-squares estimation theory was presented in Chapter 3.6 and results of the fitting procedure are presented in Section 6.2.

The polynomial model has been applied as a nonlinearity estimator in various problems: in references [22, 23] it is used as part of a predistorter, in reference [24] it is used in the context of spectral regrowth approximation and in reference [25] it is used for modelling and identification of Wiener systems.

4.2 Saleh Model

This model was presented by Adel A. M. Saleh in 1983 for modelling Traveling-Wave Tube Amplifiers (TWTA) [26]. The two-parameter gain and phase conversion functions are

$$g(A) = \frac{a_0 A}{1 + a_1 A^2} \tag{4.2a}$$

$$\Phi(A) = \frac{b_0 A^2}{1 + b_1 A^2}. \tag{4.2b}$$

The model has also a quadrature representation

$$S_I(A) = \frac{a_0 A}{1 + a_1 A^2} \tag{4.3a}$$

$$S_Q(A) = \frac{a_2 A^3}{(1 + a_3 A^2)^2} \tag{4.3b}$$

where S_I is the conversion of the in-phase component and S_Q is the conversion of the quadrature component. The quadrature form model can be extended to also model frequency dependent systems. The frequency dependent Saleh model is introduced in Section 5.4.

Saleh verified his model against several sets of measurement data in the article where he presented the model [26]. Figure 4.1(a) shows the amplitude and phase conversion characteristics of this model with parameters obtained from the same article. This model has been well adopted for modelling power amplifiers. It has been extensively applied in the context of predistortion[1] and characterization of amplifier nonlinearities. The most recent and notable references include [10, 22, 27–31].

4.3 Ghorbani Model

Although the Saleh model fits very well for TWTA amplifiers, its characteristics are not suitable for Solid State Power Amplifiers (SSPA). Typically SSPAs do not have as large roll-off at saturation as TWTAs and their phase distortion is much smaller. The Ghorbani model [32] has a very similar approach as Saleh's model, but it is designed to model especially SSPAs. The four-parameter equations for amplitude

[1] A predistorter approximates distortion characteristics complementary to the distortion characteristics of the amplifier in order to ensure that the output of the cascade of the predistorter and the amplifier has little or no distortion.

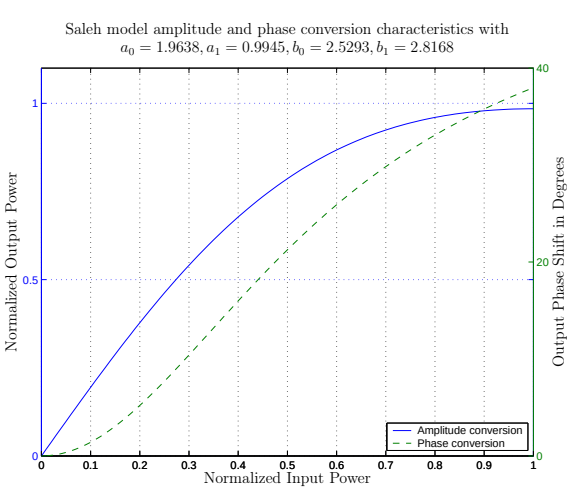

(a) Saleh model

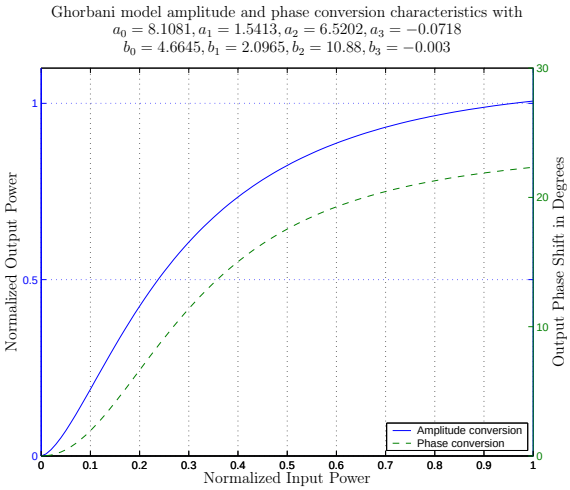

(b) Ghorbani model

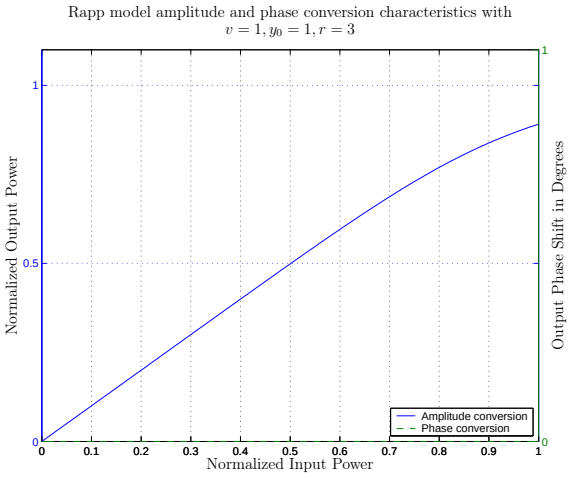

(c) Rapp model

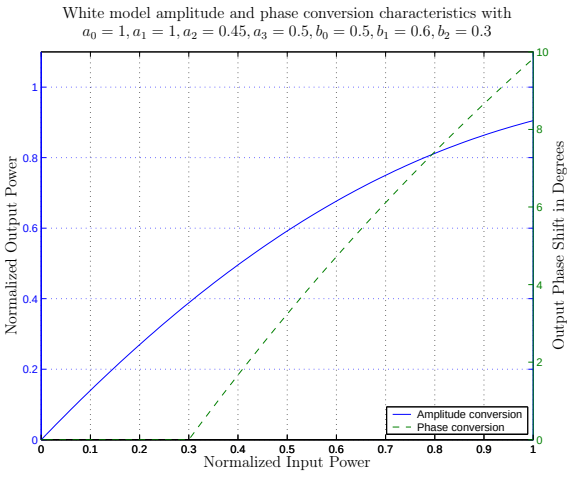

(d) White model

Figure 4.1: Illustration of amplitude and phase conversion characteristics of frequency independent amplifier models.

and phase conversion can be written as

$$g(A) = \frac{a_0 A^{a_1}}{1 + a_2 A^{a_1}} + a_3 A \tag{4.4a}$$

$$\Phi(A) = \frac{b_0 A^{b_1}}{1 + b_2 A^{b_1}} + b_3 A. \tag{4.4b}$$

The characteristics of this model are illustrated in Figure 4.1(b). The parameters are obtained from the publication where Ghorbani originally presented his model [32]. The figure shows that the amplitude conversion curve has less roll-off at saturation and the small-signal amplification has an exponential form instead of a linear as in the Saleh model. The output phase distortion has a logarithmic shape instead of being linearly increasing as in the Saleh model. This means that the output phase shift is almost constant at high input amplitude values.

4.4 Rapp Model

Christopher Rapp published his model in 1991 [9]. His approach is very different from the approach Saleh and Ghorbani had. First of all the phase distortion is assumed to be small enough, so that it can be neglected. Secondly the analytical expression for the amplitude conversion curve has a clearly different form than the two previously presented models. The amplitude and phase conversion expressions are

$$g(A) = v \frac{A}{\left[1 + \left(\frac{vA}{y_0}\right)^{2r}\right]^{\frac{1}{2r}}} \tag{4.5a}$$

$$\Phi(A) = 0, \tag{4.5b}$$

where v is the small signal gain, y_0 is the limiting output amplitude and r controls the smoothness of the transition from linear operation to saturated operation.

Figure 4.1(c) illustrates the amplitude and phase conversion characteristics of the Rapp model. The amplitude conversion has a perfectly linear form for small-signal inputs. For high input values the amplitude begins to saturate until it reaches the saturated output level. In this figure the value of the smoothness factor r was 3. According to Rapp, this should well match a 1-Watt SSPA.

As the Saleh model, also the Rapp model is quite commonly referenced in scientific publications. Applications of the Rapp model can be found in references [10, 22, 28, 31]. A derivative of the Rapp model was presented by Mauri Honkanen in 1997. He modified the small signal region of the Rapp model for better approximation of amplifiers built using Bipolar Junction Transistors (BJT). More detailed information of the derived model can be found in references [33, 34].

4.5 White Model

This model was published in 2003 by George White for accurate modelling of Ka-band (26–40 GHz) SSPAs [35]. He has suggested the following equations for modelling amplitude and phase conversion

$$g(A) = a_0(1 - e^{-a_1 A}) + a_2 A e^{-a_3 A^2} \tag{4.6a}$$

$$\Phi(A) = \begin{cases} b_0 \left(1 - e^{-b_1(A-b_2)}\right), & A \geq b_2 \\ 0, & A < b_2. \end{cases} \tag{4.6b}$$

The parameter a_0 represents the amplitude saturation level, a_1 is the linear region gain and parameters a_2 and a_3 are used to match the nonlinearity of the amplitude conversion. The output phase shift is controlled by three parameters. Magnification is controlled by b_0, the steepness by b_1 and b_2 controls the shift along the input power level axis. Figure 4.1(d) illustrates the amplitude and phase conversion characteristics. The parameter values are chosen to obtain normalized characteristics.

4.6 Simulation Model for Memoryless Bandpass Amplifiers

This section shows how the models presented in the previous sections can be used in simulations. The bandpass simulation model refers to devices where only bandpass inputs produce any measurable output. Experiments have shown that an amplitude and phase modulated carrier

$$x(t) = A(t)\cos(\omega_0 t + \phi(t)) \tag{4.7}$$

produces the output

$$y(t) = g[A(t)]\cos(\omega_0 t + \phi(t) + \Phi[A(t)]) \tag{4.8}$$

in a bandpass amplifier [6]. In the above equations ω_0 is the carrier angular frequency, $A(t)$ is the amplitude modulation and $\phi(t)$ is the phase modulation. The distortion of the output signal is shown by the amplitude and phase conversion functions g and Φ.

The Equations (4.7) and (4.8) form a block model that is illustrated in Figure 4.2(a). Implementation of the model in code from the symbolic block diagram is not completely straightforward. The first thing to do is to express the input and output signal as complex envelopes

$$\tilde{x}(t) = A(t)e^{j\phi(t)} \tag{4.9}$$

$$\tilde{y}(t) = g[A(t)]e^{j(\phi(t)+\Phi[A(t)])}. \tag{4.10}$$

Now that the carrier has been suppressed from the equations the simulation is much easier to perform. Figure 4.2(b) explicitly shows what must be done to implement the model in code.

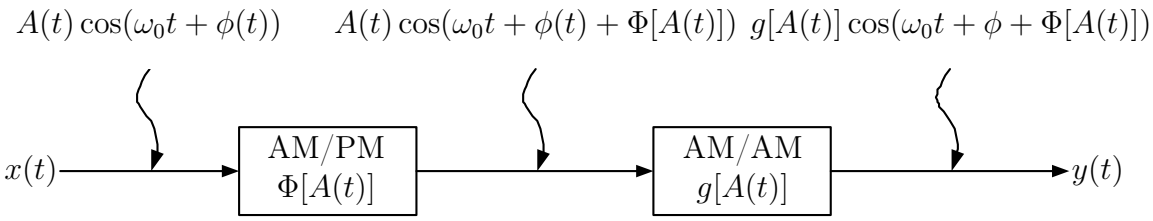

(a) Block model for AM/AM and AM/PM bandpass nonlinearity.

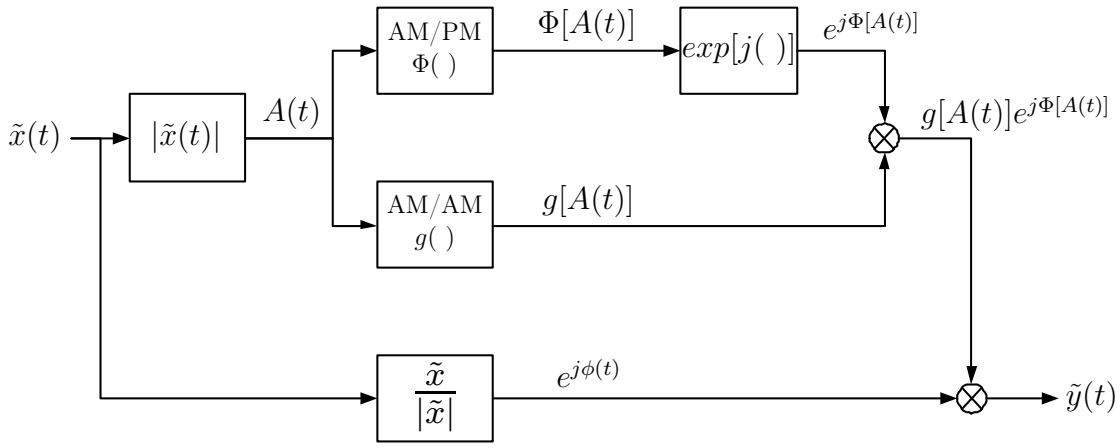

(b) Simulation model for AM/AM and AM/PM bandpass nonlinearity at the complex envelope level.

Figure 4.2: Simulation model for bandpass nonlinearities.

The simulation model for the in-phase and quadrature form signal conversion functions can be derived from Equation (4.8) using basic trigonometric identities. The output of the system in quadrature form for the input defined in Equation (4.7) is

$$y(t) = S_I(t)\cos\left[\omega_0 t + \phi(t)\right] - S_Q(t)\cos\left[\omega_0 t + \phi(t)\right] \tag{4.11}$$

where the in-phase S_I and the quadrature S_Q signal conversion components are defined as

$$S_I(t) = g\left[A(t)\right]\cos\Phi\left[A(t)\right] \tag{4.12}$$

$$S_Q(t) = g\left[A(t)\right]\sin\Phi\left[A(t)\right]. \tag{4.13}$$

The quadrature form simulation model is illustrated in Figure 4.3.

4.7 Summary

This chapter introduced the most well-known frequency independent amplifier models and illustrated how they can be used in simulations. The use of these models is justified when the input signal's bandwidth is small compared to the amplifier's bandwidth. A drawback with most of these models is that the authors, except for Saleh, have not included a solution for parameter estimation. This makes the verification of the models difficult, because the models are not linearly parameterized and thus the parameter estimation can be very tedious.

The recommended model for frequency independent modelling and simulation is the polynomial model. It is linearly parameterized, so the estimation is very straightforward to do and the accuracy is also good as will be shown in Chapter 6.2. Another option to start with is the Saleh model, since the fitting solution is available and the model can be expanded to include also frequency dependent distortion as will be illustrated in the next chapter. A drawback of the Saleh model is that it does not work very well with SSPAs. The other models are not recommended because they do not include a solution for parameter estimation.

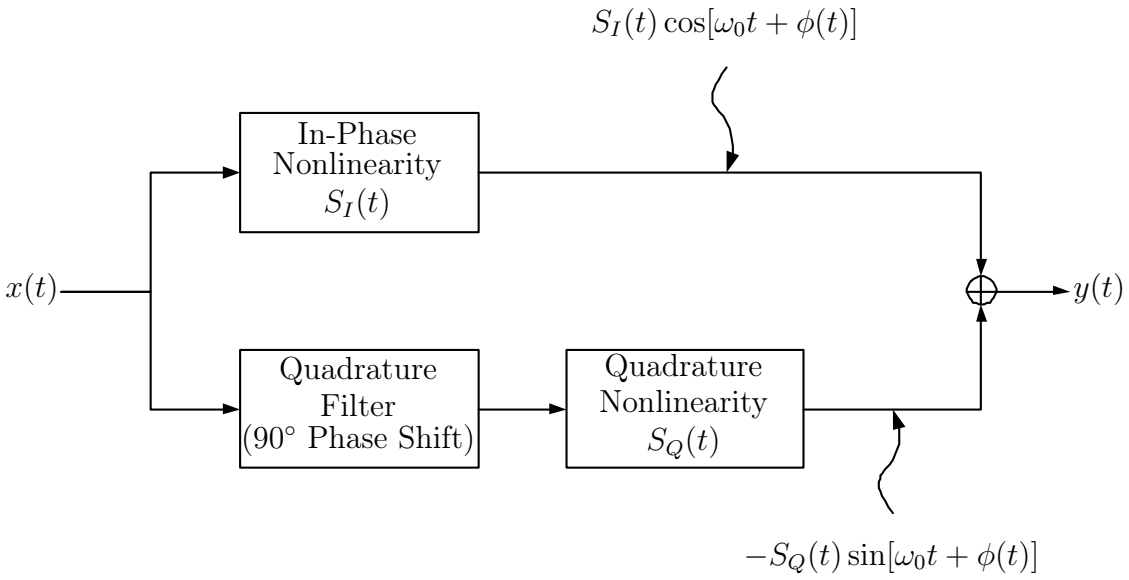

(a) Quadrature form block model for bandpass nonlinearities.

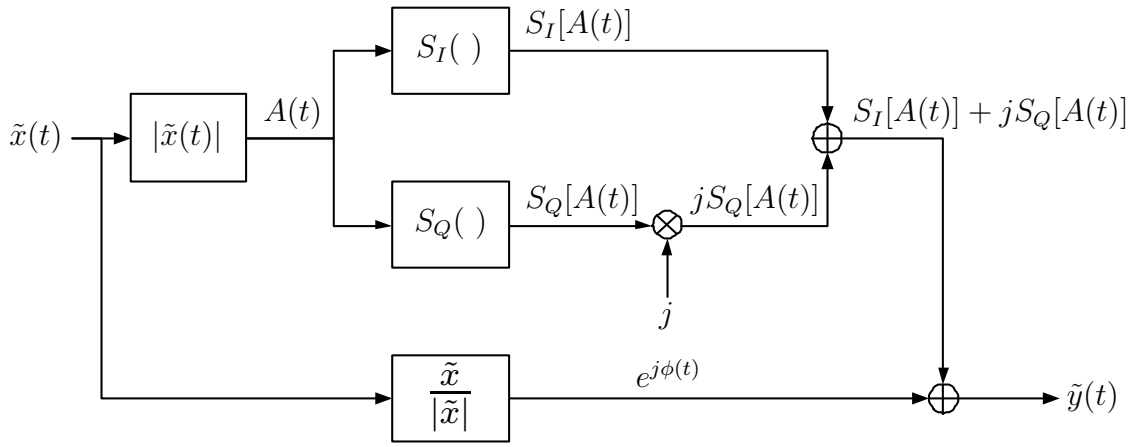

(b) Quadrature form simulation model for bandpass nonlinearities at the complex envelope level.

Figure 4.3: Quadrature form simulation model for bandpass nonlinearities.

Chapter 5

Frequency-Dependent Power Amplifier Models

This chapter discusses power amplifier models that are able to characterize the frequency dependent behavior of an amplifier. An amplifier exhibits frequency dependent behavior when the bandwidth of the input signal is comparable to the bandwidth of the amplifier. Therefore, these models are required when an amplifier is fed by a wideband input signal.

The chapter begins by introducing the Volterra series expansion which is the analytical approach to modelling nonlinear systems with memory. In the the two subsequent sections the block-oriented Hammerstein and Wiener models are discussed. After that, the frequency dependent Saleh model is presented, which is an extension to the frequency independent Saleh model discussed in Section 4.2. The chapter ends with a summary of the discussed models.

5.1 Volterra Series

Nonlinear systems with memory can be characterized by the *Volterra series expansion* named after the Italian mathematician Vito Volterra (1860–1940). It relates the input signal $x(k)$ and output signal $y(k)$ of the modelled system as [36]

$$\begin{aligned} y(k) = {} & w_0 \\ & + \sum_{\tau_1=0}^{\infty} w_1(\tau_1)x(k-\tau_1) \\ & + \sum_{\tau_1=0}^{\infty}\sum_{\tau_2=0}^{\infty} w_2(\tau_1,\tau_2)x(k-\tau_1)x(k-\tau_2) \\ & + \sum_{\tau_1=0}^{\infty}\sum_{\tau_2=0}^{\infty}\cdots\sum_{\tau_p=0}^{\infty} w_p(\tau_1,\tau_2,\ldots\tau_p)x(k-\tau_1)x(k-\tau_2)\cdots x(k-\tau_p) \\ & + \cdots \end{aligned} \tag{5.1}$$

where the functions $w_p(\tau_1, \tau_2, \ldots, \tau_p)$ are called the *Volterra kernels*. The zeroth-order kernel w_0 is a constant, the first-order kernel w_1 is a linear filter and the rest of the kernels are higher order convolutions. The kernels are symmetric, which means that all permutations of the indices $\tau_1, \tau_2, \ldots, \tau_p$ define the same kernel [37].

The Volterra series expansion can be written more compactly by defining the pth-order *Volterra operator* $w_p[x(k)]$ as

$$w_p[x(k)] = \sum_{\tau_1=0}^{\infty}\sum_{\tau_2=0}^{\infty}\cdots\sum_{\tau_p=0}^{\infty} w_p(\tau_1,\tau_2,\ldots\tau_p)x(k-\tau_1)x(k-\tau_2)\cdots x(k-\tau_p). \tag{5.2}$$

Substituting Equation (5.2) into Equation (5.1) yields

$$y(k) = w_0 + \sum_{p=1}^{\infty} w_p[x(k)]. \tag{5.3}$$

The structure of the Volterra series expansion is illustrated by the block diagram in Figure 5.1.

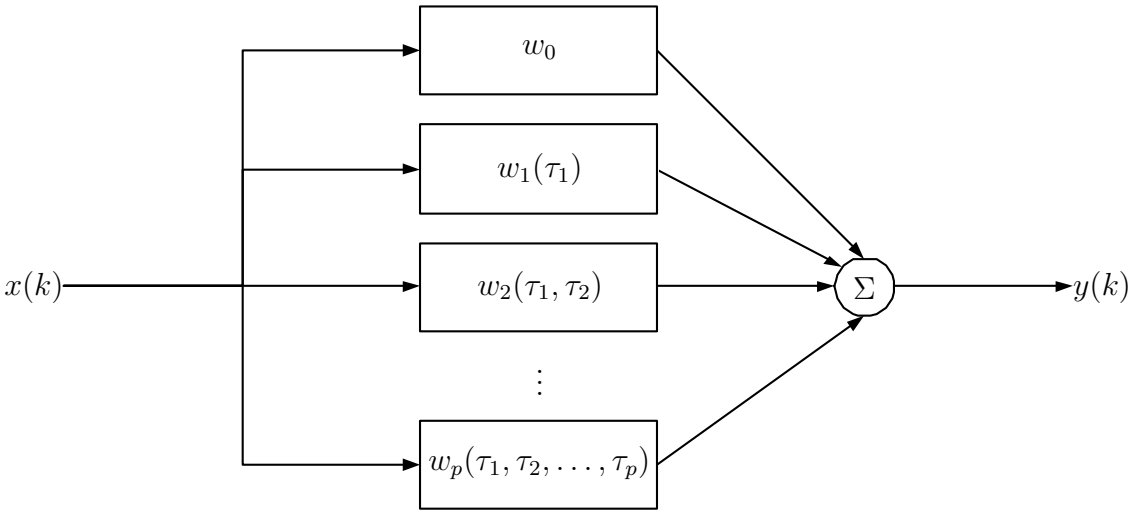

Figure 5.1: Block diagram interpretation of the Volterra series expansion. The functions $w_0, w_1, w_2, \ldots, w_p$ are called the Volterra kernels.

The infinite series in Equation (5.3) is not applicable for practical modelling. Therefore, the series expansion must be truncated at some point. The truncated Volterra series can be written as

$$\begin{aligned} y(k) &= w_0 + \sum_{p=1}^{P} w_p\left[x(k)\right] \\ &= w_0 \\ &+ \sum_{\tau_1=0}^{K-1} w_1(\tau_1)x(k-\tau_1) \\ &+ \sum_{\tau_1=0}^{K-1}\sum_{\tau_2=0}^{K-1} w_2(\tau_1,\tau_2)x(k-\tau_1)x(k-\tau_2) \\ &+ \sum_{\tau_1=0}^{K-1}\sum_{\tau_2=0}^{K-1}\cdots\sum_{\tau_p=0}^{K-1} w_p(\tau_1,\tau_2,\ldots\tau_p)x(k-\tau_1)x(k-\tau_2)\cdots x(k-\tau_p) \end{aligned} \tag{5.4}$$

where P is the *order* or the *degree* of the Volterra series expansion, K is referred to as its *length* and $K-1$ as its *memory*. As can be observed from Equation (5.4) the number of coefficients is proportional to K^P, i.e., the Volterra series has computational complexity $O\left(K^P\right)$. This means that even models of moderate order and

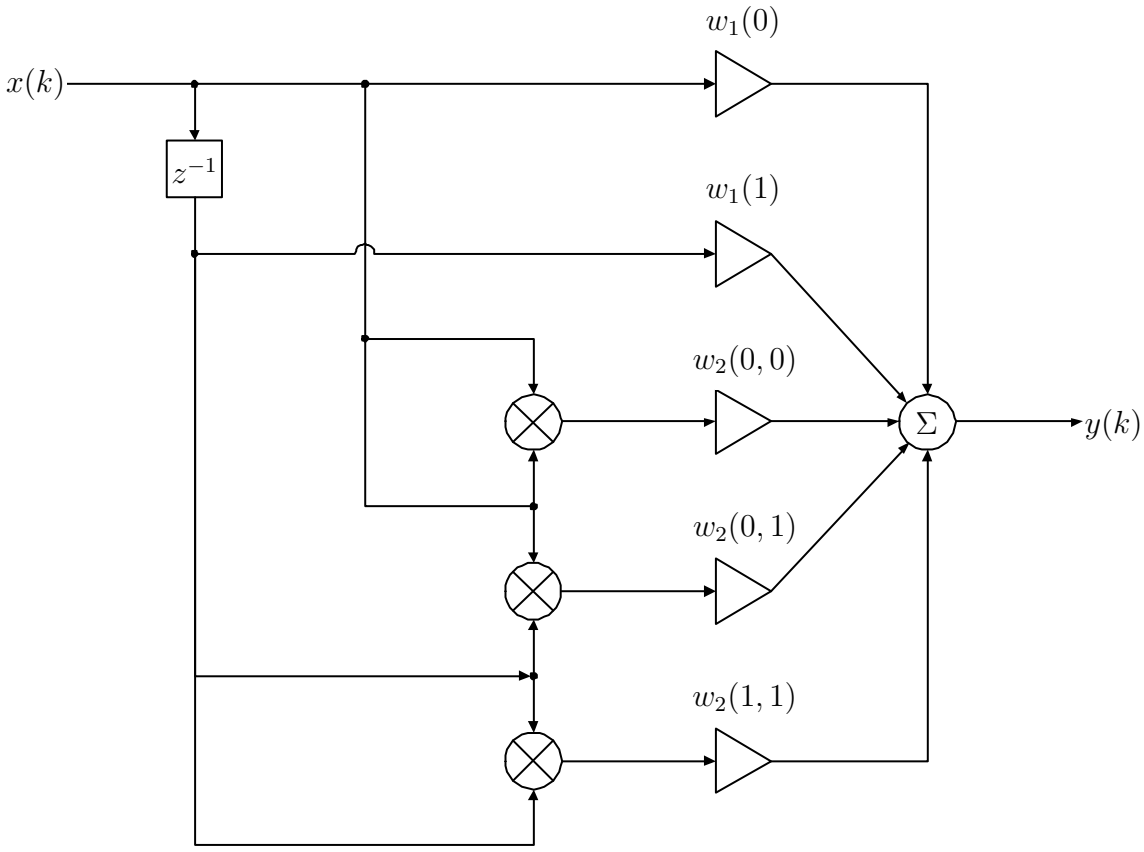

Figure 5.2: Illustration of a 2nd-order Volterra filter of length 2.

length are highly complex to implement. Consequently, practical implementations of Volterra series usually involve low-order models.

An example of a 2nd-order Volterra filter of length 2 is shown in Figure 5.2. Writing out Equation (5.4) with $P = 2$ and $K = 2$ yields

$$\begin{aligned} y(k) = {} & w_1(0)x(k) + w_1(1)x(k-1) + w_2(0,0)x(k)x(k) + w_2(0,1)x(k)x(k-1) \\ & + w_2(1,0)x(k-1)x(k) + w_2(1,1)x(k-1)x(k-1). \end{aligned} \tag{5.5}$$

From this equation it is easy to derive the filter structure shown in Figure 5.2. Note that in the figure the kernels $w_2(0,1)$ and $w_2(1,0)$ have been combined to a single kernel $w_2(0,1)$. This simplification can be done since all permutations of

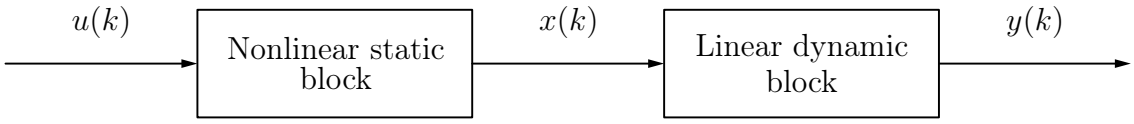

Figure 5.3: Hammerstein model.

the kernel indices produce the same kernel as already mentioned. Furthermore, the zeroth-order kernel ω_0 has been assumed zero. This can be done without any loss of generality.

The Volterra series expansion can also be thought of as a Taylor series with memory. This closeness to power series poses some limitations on the applications where it can be used. It is not possible to find a convergent Volterra series for a system that includes strong nonlinearities such as discontinuities or functions that are not differentiable in the domain of interest. Detailed studies of convergence and applicability of Volterra series for different types of problems can be found in references [38–41]. The limitations of the Volterra series due to convergence problems do not restrict it from being an attractive alternative for modelling nonlinear systems. It has been successfully applied in a wide variety of applications. A nice cross-section of the various applications can be found in [36]. Applications of the Volterra series expansion within the context of this text can be found in references [42–49].

5.2 Hammerstein Model

The Hammerstein model represents a block-oriented approach where the nonlinearity and the dynamics of the system are assumed to be separable [50]. It is a cascade of a static nonlinear block and a dynamic linear block as illustrated in Figure 5.3. The static nonlinear block is simply described as

$$x(k) = \Psi\left(u(k)\right) \tag{5.6}$$

where Ψ is the unknown nonlinear conversion function. Typically it is implemented as a polynomial. The input-output characteristics of the linear dynamic system are

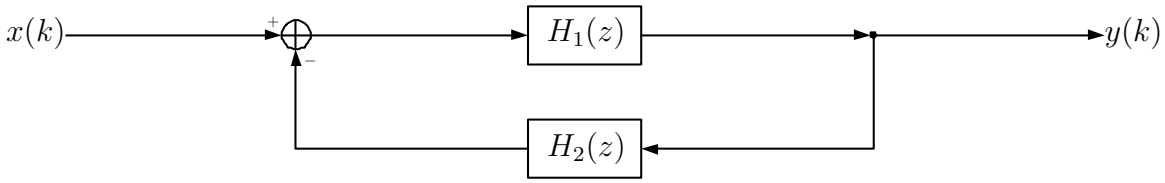

Figure 5.4: Block diagram of a linear dynamic system.

more difficult to represent. A Linear Time-Invariant (LTI) system is described by the difference equation [51]

$$\sum_{\tau=0}^{M_2} b_\tau x(k-\tau) = \sum_{\tau=0}^{M_1} a_\tau y(k-\tau). \tag{5.7}$$

where time-invariance refers to that the coefficients $a_0, \ldots, a_{M_1}$ and $b_0, \ldots, b_{M_2}$ are constant. Choosing $a_0 = 1$ the difference equation can be rewritten to explicitly define $y(k)$ as a function of $x(k)$

$$y(k) = \sum_{\tau=0}^{M_2} b_\tau x(k-\tau) - \sum_{\tau=1}^{M_1} a_\tau y(k-\tau), \qquad a_0 = 1. \tag{5.8}$$

The LTI system described by Equation (5.8) is illustrated in Figure 5.4 where H_1 corresponds to the first term and H_2 to the second term of the equation . This type of system is also often referred to as an Infinite Impulse-Response (IIR) filter with filter coefficients $a_0, \ldots, a_{M_1}, b_0, \ldots, b_{M_2}$. Removing the feedback loop, i.e., setting $a_1, \ldots, a_{M_1}$ to zero, results in a Finite Impulse-Response (FIR) filter. To summarize, the Hammerstein system can be described by the equations

$$x(k) = \Psi\left(u(k)\right) \tag{5.9a}$$

$$y(k) = \sum_{\tau=0}^{M_2} b_\tau x(k-\tau) - \sum_{\tau=1}^{M_1} a_\tau y(k-\tau), \qquad a_0 = 1. \tag{5.9b}$$

Table 5.1: Mapping between the original parameters and the linearized parameters of the Hammerstein system described in Equations (5.11) *and* (5.12).

$a_0 = 1$	$b_1 = \frac{d_2}{d_0}$
$a_1 = d_6$	$b_2 = \frac{d_4}{d_0}$
$a_2 = d_7$	$c_1 = d_0$
$b_0 = 1$	$c_3 = d_1$

To illustrate the model let us look at an example where the static nonlinear block is implemented as a third-order polynomial

$$x(k) = c_1 u(k) + c_3 u^3(k) \tag{5.10}$$

and the dynamic system has order $M_1 = M_2 = 2$. The output of this system is

$$\begin{aligned} y(k) = {} & b_0 c_1 u(k) + b_0 c_3 u^3(k) + b_1 c_1 u(k-1) + b_1 c_3 u^3(k-1) \\ & + b_2 c_1 u(k-2) + b_2 c_3 u^3(k-2) - a_1 y(k-1) - a_2 y(k-2). \end{aligned} \tag{5.11}$$

As can be seen from Equation (5.11) the Hammerstein model is nonlinear in parameters, even though the individual blocks are linearly parameterized. This makes the estimation of the coefficients difficult, since nonlinear estimation techniques must be applied. The estimation process can be simplified by re-parameterizing the model in a manner that results in linear parameters. Linearizing the previously presented example by re-parametrization yields

$$\begin{aligned} y(k) = {} & d_0 u(k) + d_1 u^3(k) + d_2 u(k-1) + d_3 u^3(k-1) \\ & + d_4 u(k-2) + d_5 u^3(k-2) - d_6 y(k-1) - d_7 y(k-2). \end{aligned} \tag{5.12}$$

where the parameters $d_0, \ldots, d_7$ can be found using linear estimation methods. Obviously no one-to-one mapping between the original parameters and the linearized parameters can be found, but setting for instance $b_0 = 1$ the original parameters may be found as shown in Table 5.1

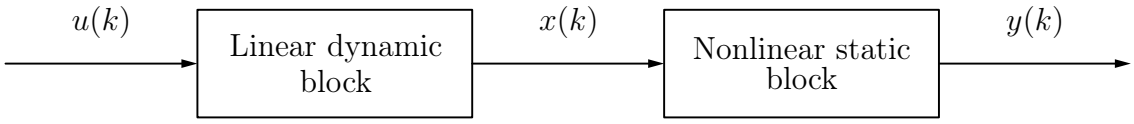

Figure 5.5: Wiener model.

The Hammerstein model has been extensively used within control theory and numerous different identification methods have been proposed [52]. The Hammerstein system has been commonly used as a predistorter in Wiener systems that will be presented in the next section [23, 27, 53–57].

5.3 Wiener Model

In the Wiener model a linear dynamic block is followed by a nonlinear static block as shown in Figure 5.5 [50]. It can be described by the following equations

$$x(k) = \sum_{\tau=0}^{M_2} b_\tau u(k-\tau) - \sum_{\tau=1}^{M_1} a_\tau x(k-\tau), \qquad a_0 = 1. \tag{5.13a}$$

$$y(k) = \Psi\left(x(k)\right) \tag{5.13b}$$

where the linear dynamic block is typically implemented as an FIR or an IIR filter and the nonlinear static block by a polynomial.

A drawback of the Wiener model is that it may not be possible to write the output $y(k)$ explicitly as a function of the input $u(k)$. Substituting (5.13a) into (5.13b) yields

$$y(k) = \Psi\left[\sum_{\tau=0}^{M_2} b_\tau u(k-\tau) - \sum_{\tau=1}^{M_1} a_\tau x(k-\tau)\right]. \tag{5.14}$$

To eliminate the unresolvable intermediate signal $x(k)$ from Equation (5.14), the inverse of Ψ must be determined from Equation (5.13b) in order to express $x(k)$ as a function of the output $y(k)$. If the inverse of Ψ exists and can be determined, then

the input-output characteristics can be written as

$$y(k) = \Psi\left[\sum_{\tau=0}^{M_2} b_\tau u(k-\tau) - \sum_{\tau=1}^{M_1} a_\tau \Psi^{-1}\Big(y(k-\tau)\Big)\right]. \tag{5.15}$$

Another drawback of the Wiener model is that it cannot be linearized as can be observed from Equation (5.15). This means that nonlinear parameter estimation methods must be used for determining the parameters of the model.

Despite the difficulties related to parameter estimation of the Wiener model, different alternatives for identification of the model parameters have been proposed [25,58,59]. Applications with respect to amplifier modelling can be found in [23, 27, 53–57].

5.4 Saleh Model

The frequency dependent Saleh model stems from the assumption that the quadrature form functions of the frequency independent Saleh model in Equation (4.3) hold for any given frequency. The frequency dependent in-phase and quadrature signal conversion functions can be written as [26]

$$S_I(A,\omega) = \frac{a_0(f)A}{1 + a_1(f)A^2} \tag{5.16a}$$

$$S_Q(A,\omega) = \frac{a_2(f)A^3}{[1 + a_3(f)A^2]^2} \tag{5.16b}$$

where S_I is the conversion of the in-phase component and S_Q is the conversion of the quadrature component.

The Equations (5.16) can be represented as a block diagram as shown in Figure 5.6. The in-phase and quadrature signal conversion functions can be simplified into dynamic linear blocks and static nonlinear blocks. In both branches the input signal amplitude is first scaled by the filter $H(\omega)$, then the signal passes through the frequency independent nonlinearity $S(A)$ and finally the output signal amplitude is

scaled by the filter $G(\omega)$. Next the branches are combined and passed through an allpass filter with unit amplitude response and phase response corresponding to the measured small-signal phase response.

A drawback of the frequency dependent Saleh model is that it has been constructed using single-tone inputs and is thus strictly valid only for those. For use with arbitrary inputs the model must therefore be experimentally verified. Another issue that can be noted from Figure 5.6 is that the model assumes that the in-phase and quadrature signal conversion functions have similar shape for all frequencies. This is quite obvious since the only frequency-dependent components in the model are the filters that merely scale the signal.

5.5 Summary

In this chapter frequency dependent amplifier models were discussed. Unlike the frequency independent models presented in the previous chapter, these models can be used to model wideband systems.

First, the analytical approach of the Volterra series expansion was discussed. Its drawback is that it suffers from very high computational complexity. Therefore, it is not very tractable for modelling systems where power consumption is a key issue, since high complexity requires more processing power which indicates increased power consumption. The complexity of the Volterra series stems from the fact that its number of coefficients grows exponentially as the order of the model increases. Thus, practical implementations of Volterra series involve only low-order models. Its resemblance to power series poses some limitations on the applications it is used for. Converging Volterra series can only be found for systems that merely exhibit weak nonlinearities, i.e., where the nonlinearity can be represented by an analytic function[1]. Despite these drawbacks, it has been successfully applied for a wide variety of applications.

[1] A function is analytic in a domain Ω if it is differentiable at every point of Ω [4].

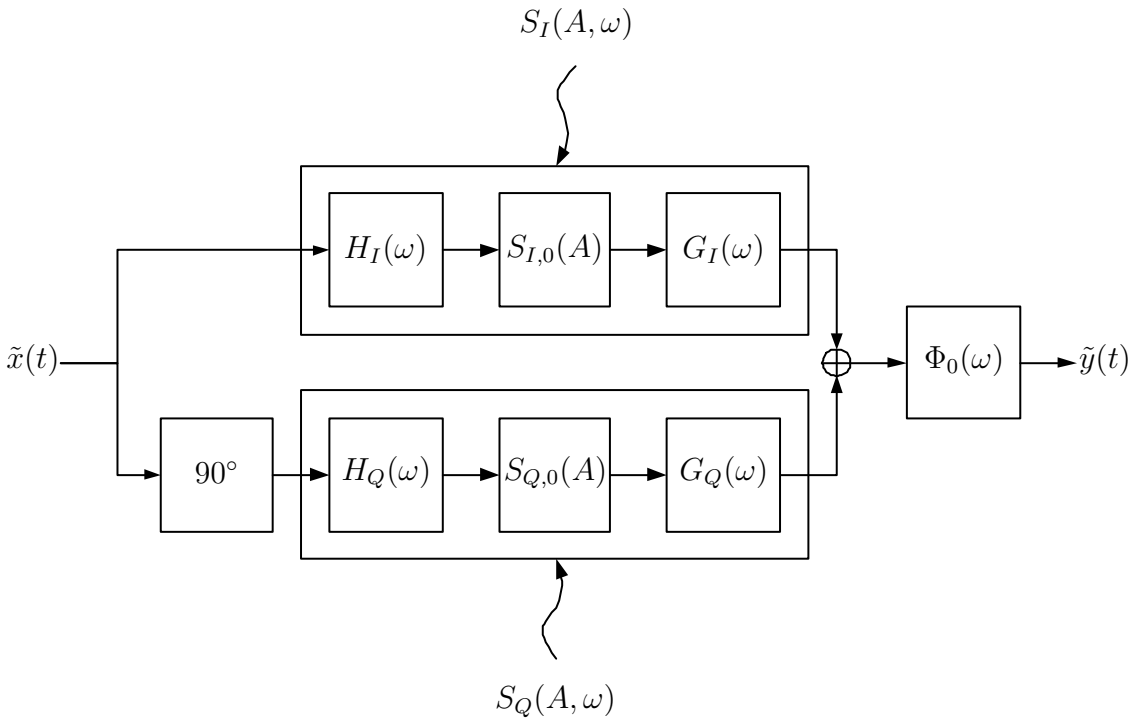

Legend	
$\Phi_0(\omega)$ = small signal phase response	
$H_I(\omega) = \sqrt{a_1(\omega)}$	$G_I(\omega) = \frac{a_0(\omega)}{\sqrt{a_1(\omega)}}$
$H_Q(\omega) = \sqrt{a_3(\omega)}$	$G_Q(\omega) = \frac{a_2(\omega)}{\sqrt{a_3^{3/2}(\omega)}}$
$S_{I,0}(A) = \frac{A}{1+A^2}$	$S_{Q,0}(A) = \frac{A^3}{(1+A^2)^2}$

Figure 5.6: The frequency-dependent Saleh model.

Lower computational complexity can be achieved using the models discussed in the two subsequent sections namely, the Hammerstein model and the Wiener model. Both of these represent a block-oriented approach, where the nonlinearity and the dynamics of the system are assumed separable. The Hammerstein model is a cascade of a nonlinear static block followed by linear dynamic block. Reversing the blocks results in a Wiener model. Typically the nonlinear static block is implemented as a polynomial and the linear dynamic block as an Infinite Impulse-Response (IIR) or a Finite Impulse-Response (FIR) filter. Even though the blocks would be linearly parameterized the cascade of the blocks is nonlinear in its parameters. This means that nonlinear parameter estimation techniques must be used to estimate the parameters of the blocks. The parameters of the Hammerstein model can be linearized and hence linear estimation methods can be used, but the same is not true for the Wiener model. This is quite unfortunate since in scientific literature the Wiener model is usually considered more suitable for modelling of the amplifier nonlinearity than the Hammerstein model.

Finally the frequency dependent Saleh model was discussed. It models the in-phase and quadrature signal components separately using a Wiener-Hammerstein model. The in-phase and quadrature branch nonlinearities are assumed to have similar form for all frequencies. The Saleh model also differs from the previous models in that its parameters are obtained from the measured frequency response instead of the relationship between the detected output samples and the input samples fed into the system. Furthermore, the model has only been validated for single-tone inputs and hence its accuracy with other inputs needs to be verified.

Chapter 6

Frequency-Independent Estimation of Power Amplifier Nonlinearity Using the Polynomial Model

In this chapter, the polynomial model discussed in Chapter 4.1 is applied for modelling a nonlinear power amplifier. The polynomial model was chosen because it is suitable for modelling both SSPAs and TWTAs. In addition, it is linearly parameterized and thus the coefficients of the polynomials can be estimated using linear parameter estimation techniques.

A brief outline of this chapter follows. First the AM/AM and AM/PM measurements made to verify the feasibility of both frequency-independent and frequency-dependent amplifier models are presented. The following section shows how the coefficients of the polynomials can be efficiently determined using least-squares estimation. After that the obtained results are presented and the estimation errors are analyzed. The chapter ends with a summary of the results.

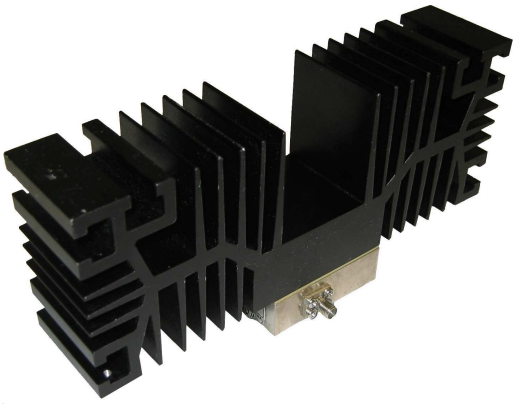

Figure 6.1: Mini-Circuits ZVE-8G power amplifier with standard heat sink attached.

Table 6.1: Mini-Circuits ZVE-8G specifications.

Frequency range	2–8 GHz
Gain	$\geq$ 30 dB
Gain flatness	$\pm$2.0 dB
Max. output power[1]	$\geq$ 30 dBm
IP3[2]	40 dBm
Width[3]	54.1/190.5 mm
Height[3]	19.1/91.4 mm
Depth	42.7 mm
Weight	755 g
Price	$1095

6.1 Measurement Results

AM/AM and AM/PM measurements of a Mini-Circuits ZVE-8G wideband power amplifier were made in order to get a realistic set of measurement data that can be used for verifying the feasibility of the amplifier models. The measurements were made in collaboration with B.Sc. Gilda Gámez and are presented in more detail in [60]. The measured Mini-Circuits ZVE-8G amplifier is shown in Figure 6.1 and its specifications can be found in Table 6.1. An Agilent Technologies PNA Series Vector Network Analyzer (VNA) was used to make the measurements using the setup shown in Figure 6.2. The attenuators shown in Figure 6.2 were used to ensure that the input of the VNA is not saturated when the amplifier is driven close to saturation.

The amplifier's amplitude and phase response for single-tone input from 1.5 GHz to 8.5 GHz was measured at power levels ranging from -27 dBm to 5 dBm with 0.5 dBm spacing. The spacing between the frequency samples was 5 MHz. In other words, the obtained data consists of measurements at 65 different power levels with 1401

[1] Output 1-dB compression point.
[2] Third-order intercept point.
[3] Heat sink excluded/included.

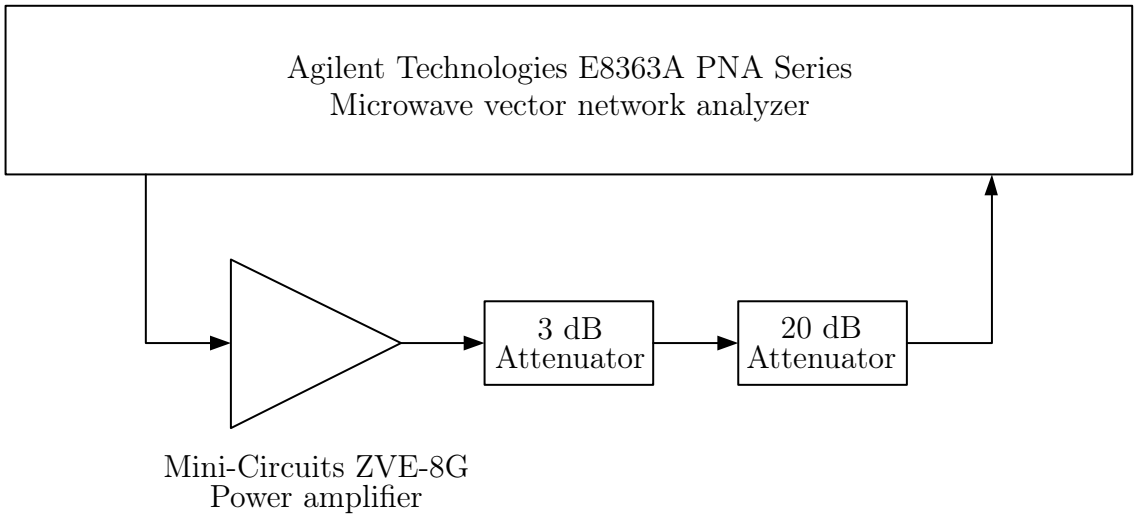

Figure 6.2: Single-tone measurement setup for AM/AM and AM/PM measurements.

frequency samples at each power level. Thus, the measurements can be considered to be comprehensive enough to model the characteristics of the amplifier for single-tone inputs.

The measured amplitude and phase response of the amplifier is shown in Figure 6.3. As can be seen from the figure, the specifications given by the manufacturer shown in Table 6.1 are a bit too optimistic at least for this individual amplifier. The output gain of the amplifier at the center frequency of the claimed operating frequency band, i.e., at 5 GHz was only 28.2 dB and the 1-dB input compression point was calculated to be 0 dBm corresponding to a maximum output power of 27.2 dBm at 5 GHz. On the other hand, the claimed gain flatness was reached for the whole operating frequency band with a maximum in-band peak-to-peak ripple of 3.6 dB. Nevertheless, the measurements correspond to the specifications given by the manufacturer quite well and hence there is no reason to doubt that they would contain any significant errors.

The AM/AM characteristics are obtained from the measurement results shown in Figure 6.3 by plotting the output power as a function of the input power. Similarly, the AM/PM characteristics are obtained by plotting the output phase shift as a

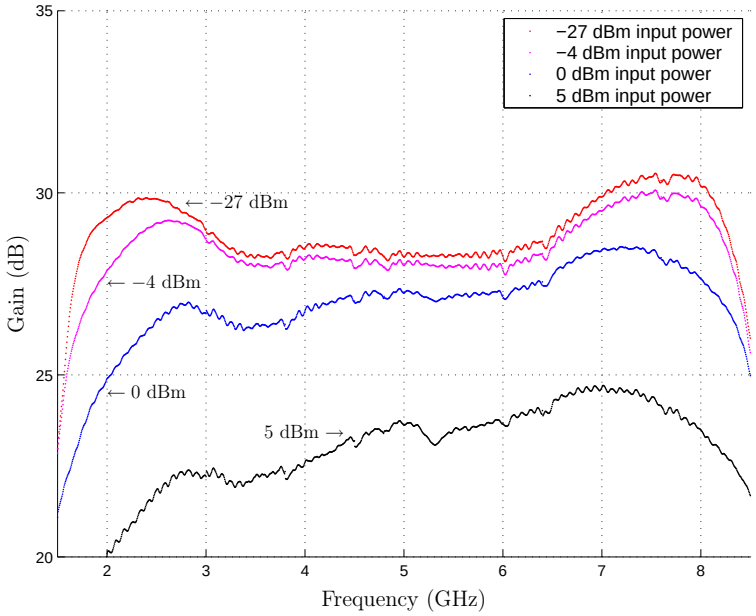

(a) Amplitude response.

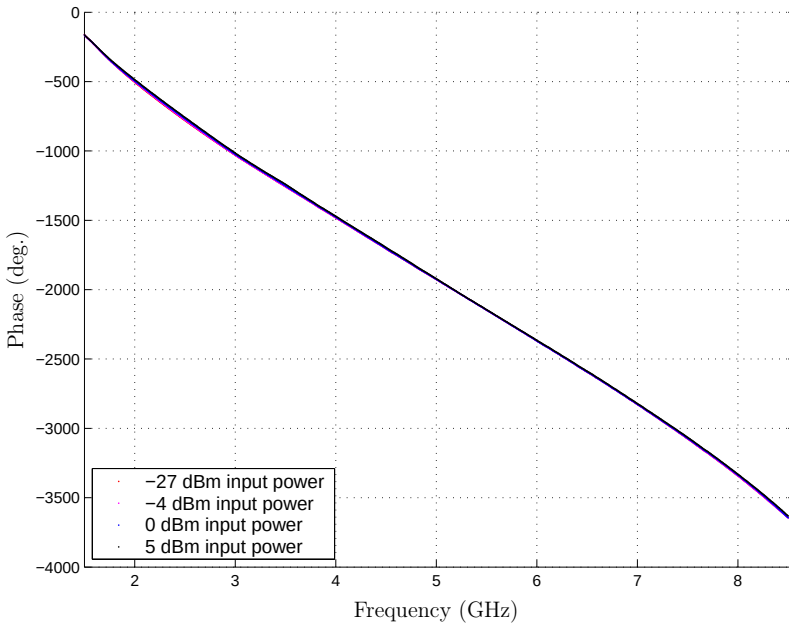

(b) Phase response

Figure 6.3: Measured amplitude and phase response of the Mini-Circuits ZVE-8G power amplifier at selected power levels. Attained gain at 5 GHz was 28.2 dB and the 1-dB input compression point was 0 dBm. The maximum peak-to-peak ripple was 3.6 dB within 2–8 GHz at 0 dBm input power.

function of the input power. The obtained AM/AM and AM/PM characteristics at selected frequencies are shown in Figure 6.4. From the AM/AM characteristics shown in Figure 6.4(a) it is easy to observe that the claimed 30 dBm maximum output power was not reached. The AM/PM characteristics on the other hand show that the phase distortion is within the typical 10 degree maximum phase shift of SSPAs at the 1-dB compression point. Note that in order to make the evaluation of the phase distortion at different frequencies easier, the phase characteristics in Figure 6.4(b) are normalized to zero degree phase shift at the smallest measured input power level (-27 dBm).

6.2 Least-Squares Estimation of the Polynomial Model Coefficients

This section presents a least-squares solution for solving the coefficients of the polynomials in Equation (4.1). An outline of the steps for finding the solution is as follows. To present the solution in a clear and compact form, both the measurement data and the polynomial model are first formulated in vector notation. After that, the least-squares estimation problem for the vector parameter polynomial model is formulated and its Least-Squares Estimator (LSE) is derived. Finally, some aspects of how to improve the accuracy and efficiency of the estimation are presented as well as conclusions of the efficiency of the derived LSE.

The obtained AM/AM and AM/PM measurement results at a given frequency can be presented by three vectors

$$\mathbf{p}_{in} = \Big[p_{in}(0) \quad p_{in}(1) \quad \cdots \quad p_{in}(L-1) \Big]^{\mathrm{T}} \tag{6.1a}$$

$$\mathbf{p}_{out} = \Big[p_{out}(0) \quad p_{out}(1) \quad \cdots \quad p_{out}(L-1) \Big]^{\mathrm{T}} \tag{6.1b}$$

$$\boldsymbol{\phi}_{out} = \Big[\phi_{out}(0) \quad \phi_{out}(1) \quad \cdots \quad \phi_{out}(L-1) \Big]^{\mathrm{T}} \tag{6.1c}$$

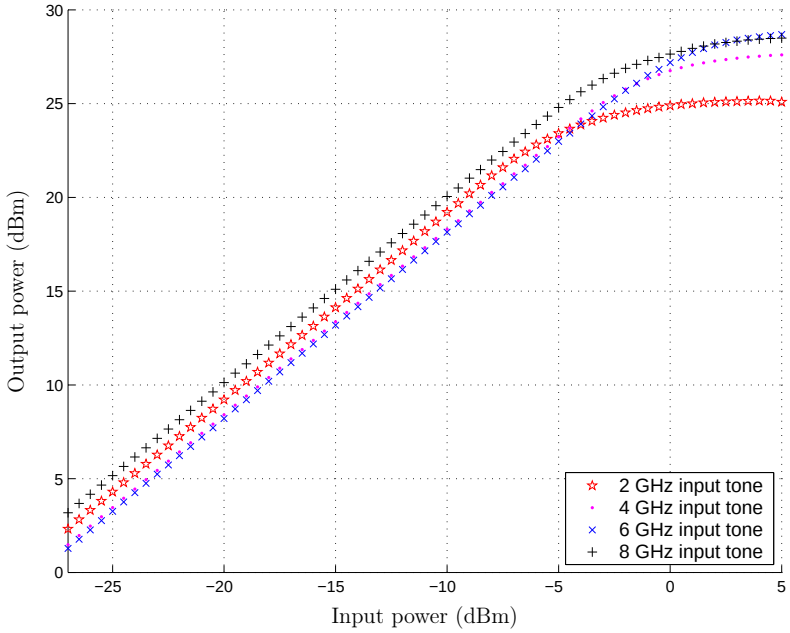

(a) AM/AM characteristics.

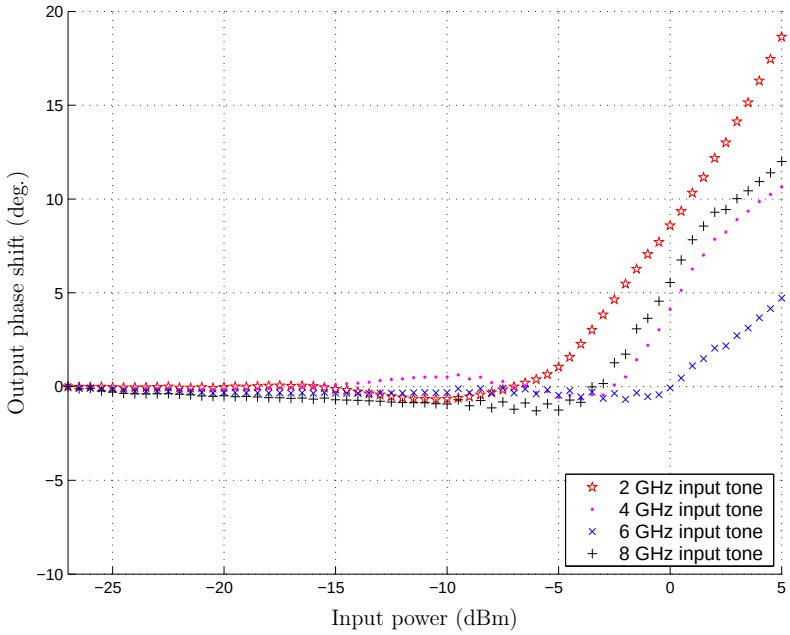

(b) AM/PM characteristics.

Figure 6.4: Measured amplitude and phase conversion characteristics of the Mini-Circuits ZVE-8G power amplifier at selected frequencies. The phase characteristics have been normalized to yield a zero degree phase shift at -27 dBm in order to make the evaluation of phase distortion at different frequencies easier.

where $\mathbf{p}_{in}$ contains the input power values, $\mathbf{p}_{out}$ contains the measured output power values, $\boldsymbol{\phi}_{out}$ contains the measured output phase shift values and L is the number of measured frequency points. The polynomial model, on the other hand, can be expressed in vector notation by defining the coefficient vectors $\mathbf{a}$ and $\mathbf{b}$

$$\mathbf{a} = \begin{bmatrix} a_0 & a_1 & \cdots & a_N \end{bmatrix}^{\mathrm{T}} \tag{6.2a}$$

$$\mathbf{b} = \begin{bmatrix} b_0 & b_1 & \cdots & b_N \end{bmatrix}^{\mathrm{T}} \tag{6.2b}$$

and the observation matrix $\mathbf{U}$

$$\mathbf{U} = \begin{bmatrix} 1 & p_{in}(0) & p_{in}^2(0) & \cdots & p_{in}^N(0) \\ 1 & p_{in}(1) & p_{in}^2(1) & \cdots & p_{in}^N(1) \\ \vdots & \vdots & \vdots & \ddots & \vdots \\ 1 & p_{in}(L-1) & p_{in}^2(L-1) & \cdots & p_{in}^N(L-1) \end{bmatrix} \tag{6.3}$$

where $\mathbf{U}$ has the special form of a Vandermonde matrix [61]. Using Equations (6.1a), (6.2) and (6.3), the polynomial model described by Equations (4.1a) and (4.1b) can be expressed in vector notation as

$$g(\mathbf{p}_{in}) = \mathbf{U}\mathbf{a} \tag{6.4a}$$

$$\Phi(\mathbf{p}_{in}) = \mathbf{U}\mathbf{b}. \tag{6.4b}$$

As can be seen from Equation (6.4), the polynomial model is linear in coefficients and hence linear least-squares estimation that was presented in Chapter 3.6.1 can be directly applied to solve it. Remembering that the LSE minimizes the squared distance between the measured data and the estimated data, the estimation problem can be written as

$$E(\mathbf{a}) = (\mathbf{p}_{out} - \mathbf{U}\mathbf{a})^{\mathrm{T}}(\mathbf{p}_{out} - \mathbf{U}\mathbf{a}) \tag{6.5a}$$

$$E(\mathbf{b}) = (\boldsymbol{\phi}_{out} - \mathbf{U}\mathbf{b})^{\mathrm{T}}(\boldsymbol{\phi}_{out} - \mathbf{U}\mathbf{b}). \tag{6.5b}$$

The LSE for the polynomial model in Equation (6.5) is defined in Equation (3.43) and hence the LSEs of $\mathbf{a}$ and $\mathbf{b}$ are

$$\hat{\mathbf{a}} = \left(\mathbf{U}^{\mathrm{T}}\mathbf{U}\right)^{-1}\mathbf{U}^{\mathrm{T}}\mathbf{p}_{out} \tag{6.6a}$$

$$\hat{\mathbf{b}} = \left(\mathbf{U}^{\mathrm{T}}\mathbf{U}\right)^{-1}\mathbf{U}^{\mathrm{T}}\boldsymbol{\phi}_{out}. \tag{6.6b}$$

The accuracy of the estimators $\hat{\mathbf{a}}$ and $\hat{\mathbf{b}}$ is affected by two types of errors. First, experimental errors arise from the measurements since no instrument is able to provide completely accurate measurements. Second, solving the estimators in Equation (6.6) using a computer introduces roundoff errors. Naturally, it is desirable that these errors affect the obtained estimator as little as possible. If small relative changes in the data due to, e.g., roundoff errors cause small relative changes in the estimator, the system is called *well-conditioned*; otherwise the system is called *ill-conditioned*.

The inaccuracy of an estimator can be examined by the *relative change* defined as

$$\Delta(\boldsymbol{\xi}) = \frac{\|\boldsymbol{\xi} - \tilde{\boldsymbol{\xi}}\|}{\|\boldsymbol{\xi}\|} \tag{6.7}$$

where $\|\cdot\|$ denotes the norm[1], $\boldsymbol{\xi}$ is the original estimator and $\tilde{\boldsymbol{\xi}}$ is the estimator of the modified system. Using the *condition number* defined as

$$\mathrm{cond}(\mathbf{A}) = \sqrt{\frac{\lambda_{min}}{\lambda_{max}}} \tag{6.8}$$

where λ_{min} and λ_{max} are the smallest and largest eigenvalues, respectively, of $\mathbf{A}^{\mathrm{H}}\mathbf{A}$, then an upper bound for the relative change of the estimators in Equation (6.6) can be written as [2]

$$\Delta(\hat{\mathbf{a}}) \leq \mathrm{cond}(\mathbf{U}^{\mathrm{T}}\mathbf{U})\Delta(\mathbf{U}^{\mathrm{T}}\mathbf{p}_{out}) \tag{6.9a}$$

$$\Delta(\hat{\mathbf{b}}) \leq \mathrm{cond}(\mathbf{U}^{\mathrm{T}}\mathbf{U})\Delta(\mathbf{U}^{\mathrm{T}}\boldsymbol{\phi}_{out}). \tag{6.9b}$$

[1] $\|\boldsymbol{\xi}\|^2 = \boldsymbol{\xi}^{\mathrm{H}}\boldsymbol{\xi}$ where $\boldsymbol{\xi}$ is a vector in $\mathbf{C}^n$ and H denotes the Hermitian operation, i.e, transposition with conjugation.

Equation (6.9) shows that if the condition number of $\mathbf{U}^{\mathrm{T}}\mathbf{U}$ is small, then a small relative change of $\mathbf{U}^{\mathrm{T}}\mathbf{p}_{out}$ and $\mathbf{U}^{\mathrm{T}}\boldsymbol{\phi}_{out}$ force a small relative change of $\hat{\mathbf{a}}$ and $\hat{\mathbf{b}}$. On the other hand, if the condition number of $\mathbf{U}^{\mathrm{T}}\mathbf{U}$ is large then the relative change of $\hat{\mathbf{a}}$ and $\hat{\mathbf{b}}$ might still be small, even if the relative change of $\mathbf{U}^{\mathrm{T}}\mathbf{p}_{out}$ and $\mathbf{U}^{\mathrm{T}}\boldsymbol{\phi}_{out}$ is large. In short, a large condition number of $\mathbf{U}^{\mathrm{T}}\mathbf{U}$ indicates possibility for large relative errors.

In order to make sure that $\mathbf{U}^{\mathrm{T}}\mathbf{U}$ is well-conditioned, its condition number can be reduced by normalizing the input vector $\mathbf{p}_{in}$. This is especially important if the order of the model is high which indicates that the spread of the eigenvalues of $\mathbf{U}^{\mathrm{T}}\mathbf{U}$ is large. In such a situation, improved estimates of $\hat{\mathbf{a}}$ and $\hat{\mathbf{b}}$ can be obtained by centering $\mathbf{p}_{in}$ to zero mean and scaling it to unit standard deviation

$$\mathbf{p}_{in,normalized} = \frac{\mathbf{p}_{in} - \mathrm{mean}(\mathbf{p}_{in})}{\mathrm{std}(\mathbf{p}_{in})}. \tag{6.10}$$

Further improvement of accuracy can be obtained by using weighted least-squares estimation discussed in Chapter 3.6.2. The weighted least-squares estimation problem can be formulated as

$$E(\mathbf{a}) = (\mathbf{p}_{out} - \mathbf{U}\mathbf{a})^{\mathrm{T}}\mathbf{W}_{\mathbf{a}}(\mathbf{p}_{out} - \mathbf{U}\mathbf{a}) \tag{6.11a}$$

$$E(\mathbf{b}) = (\boldsymbol{\phi}_{out} - \mathbf{U}\mathbf{b})^{\mathrm{T}}\mathbf{W}_{\mathbf{b}}(\boldsymbol{\phi}_{out} - \mathbf{U}\mathbf{b}). \tag{6.11b}$$

where $\mathbf{W}_{\mathbf{a}}$ and $\mathbf{W}_{\mathbf{b}}$ are weighting matrices of the measured output power values and the measured output phase shift values, respectively. The estimation problem in Equation (6.11a) can be solved using Equation (3.46) and thus the Weighted Least-Squares Estimators (WLSE) of $\mathbf{a}$ and $\mathbf{b}$ are

$$\hat{\mathbf{a}} = \left(\mathbf{U}^{\mathrm{T}}\mathbf{W}_{\mathbf{a}}\mathbf{U}\right)^{-1}\mathbf{U}^{\mathrm{T}}\mathbf{W}_{\mathbf{a}}\mathbf{p}_{out} \tag{6.12a}$$

$$\hat{\mathbf{b}} = \left(\mathbf{U}^{\mathrm{T}}\mathbf{W}_{\mathbf{b}}\mathbf{U}\right)^{-1}\mathbf{U}^{\mathrm{T}}\mathbf{W}_{\mathbf{b}}\boldsymbol{\phi}_{out}. \tag{6.12b}$$

The WLSE can be used to improve the accuracy of the estimation by emphasizing a desired power range. Furthermore, it can be used to improve the accuracy of

the estimation when some of the measured data values are less reliable than others. Giving more weight to the more reliable values will give more accurate results.

As discussed in Chapter 3.6, the performance of neither the LSE nor the WLSE can be guaranteed unless some assumptions can be made about the noise embedded in the model. If the noise can be assumed to be white then the derived LSE for the polynomial model is equivalent to the Minimum Variance Unbiased Estimator (MVUE). On the other hand, if the noise is colored, then the weighting matrix of the WLSE should be chosen as the inverse of the noise covariance matrix in order for it to be the MVUE. Generally, the noise produced by the power amplifier and the measurement equipment can be assumed Additive White Gaussian Noise (AWGN). Therefore, the derived LSE is an optimal estimator for the polynomial model, in the sense that it produces the MVUE.

6.3 Estimation Results

This section presents the estimation results obtained using the polynomial model. The polynomial model was fitted to the 6 GHz AM/AM and AM/PM measurement results shown in Figure 6.4 using the LSE stated in Equation (6.6). The result is shown in Figure 6.5 where a fifth-order polynomial is fitted to both the AM/AM and AM/PM conversion characteristics. Results similar to those shown in Figure 6.5 are obtained for any given frequency.

In order to evaluate the accuracy of the AM/AM estimation, the relative Root-Mean-Square (RMS) error was calculated. Using the error function defined in Equation (6.5a), the relative RMS error for the AM/AM estimation can be written as

$$E_{RMS,relative}(\hat{\mathbf{a}}) = 10\lg\left(\frac{\|\mathbf{p}_{out} - \mathbf{U}\hat{\mathbf{a}}\|}{\|\mathbf{p}_{out}\|}\right). \tag{6.13}$$

The relative RMS error of the AM/AM estimation is plotted as a function of the order of the polynomial in Figure 6.6(a). The AM/PM estimation accuracy was

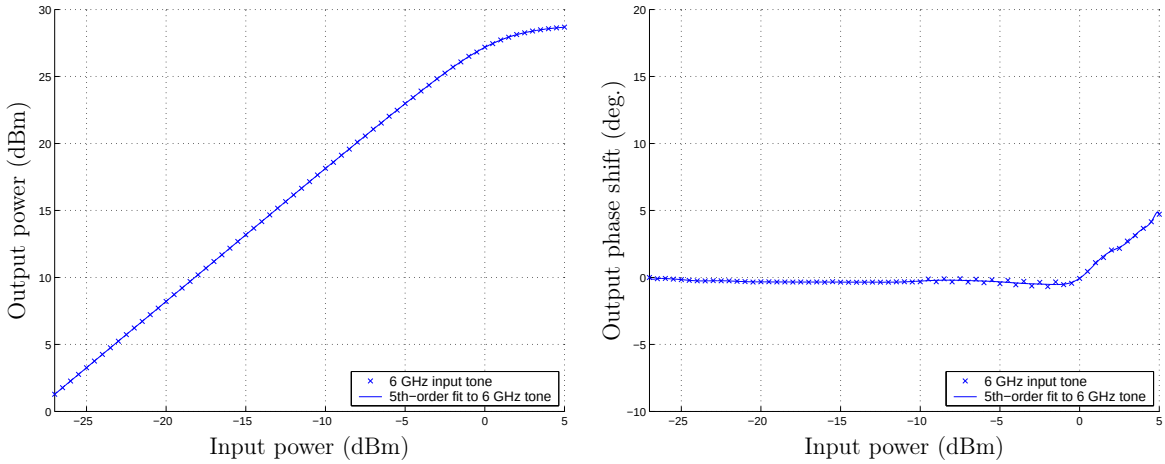

(a) AM/AM estimation.

(b) AM/PM estimation.

Figure 6.5: A 5th-order least-squares polynomial fit of the measured AM/AM and the AM/PM characteristics at 6 GHz. The relative RMS error of the AM/AM estimation is –18.18 dB and the RMS error of the AM/PM estimation is 0.19 degrees.

evaluated using the Root-Mean-Square error defined as

$$E_{RMS}(\hat{\mathbf{b}}) = \frac{\left\| \boldsymbol{\phi}_{out} - \mathbf{U}\hat{\mathbf{b}} \right\|}{\sqrt{L}} \tag{6.14}$$

where L is the number of the measured frequency points. The RMS error describes how much the estimated data values differ from the measured data values on the average. The RMS error of the AM/PM estimation is plotted as function of the order of the polynomial in Figure 6.6(b).

The relative RMS error of the fifth-order AM/AM estimation shown in Figure 6.5(a) was -18.18 dB and the RMS error of AM/PM estimation shown in Figure 6.4(b) was 0.19 degrees. Increasing the order of the polynomial from 5 to 11 reduces the error of both the AM/AM and AM/PM estimation significantly but increasing the order further does not yield substantial improvement of the estimation result as can be seen from Figure 6.6.

Since the polynomial model is fitted to the measurements at a single frequency, its capabilities to model AM/AM and AM/PM characteristics at other frequencies

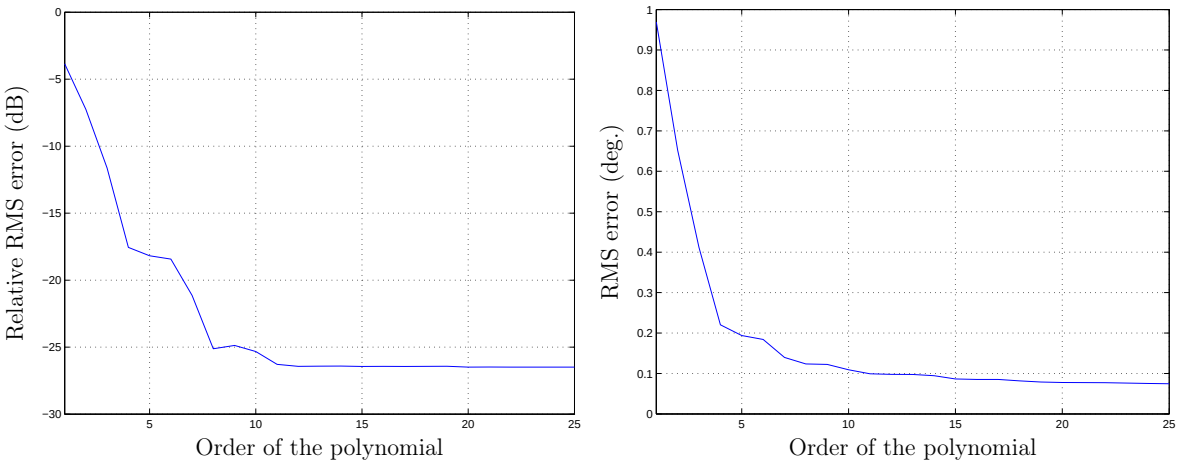

(a) AM/AM estimation error.

(b) AM/PM estimation error.

Figure 6.6: Error of the estimated AM/AM conversion and the estimated AM/PM conversion at 6 GHz as a function of the order of the polynomial. The relative RMS error of the AM/AM estimation plotted in (a) is defined in Equation (6.13) *and the RMS error of the AM/PM estimation plotted in (b) is defined in Equation* (6.14)*.*

must be verified separately. This is illustrated in Figure 6.7 where the measured AM/AM and AM/PM characteristics are compared to the estimated AM/AM and AM/PM characteristics at selected frequencies. In the figure the estimation error of two 5th-order polynomials are shown. The first polynomial is fitted to the measured 2 GHz AM/AM and AM/PM characteristics and the second polynomial is fitted to the 6 GHz AM/AM and AM/PM characteristics.

Naturally the estimation error has a minimum at the estimated frequency, but it is interesting to see how well the model estimates the AM/AM and AM/PM characteristics of other frequencies. The polynomial fitted to the 2 GHz characteristics models poorly the AM/AM and AM/PM characteristics of other frequencies, whilst the polynomial fitted to the 6 GHz measurements can be considered quite accurate between 5 GHz and 6.5 GHz.

The AM/AM characteristics estimation error behavior is an obvious consequence of the amplifier's amplitude response plotted in Figure 6.3(a), which shows that the amplitude response has a peak at 2 GHz, but is almost flat around 6 GHz.

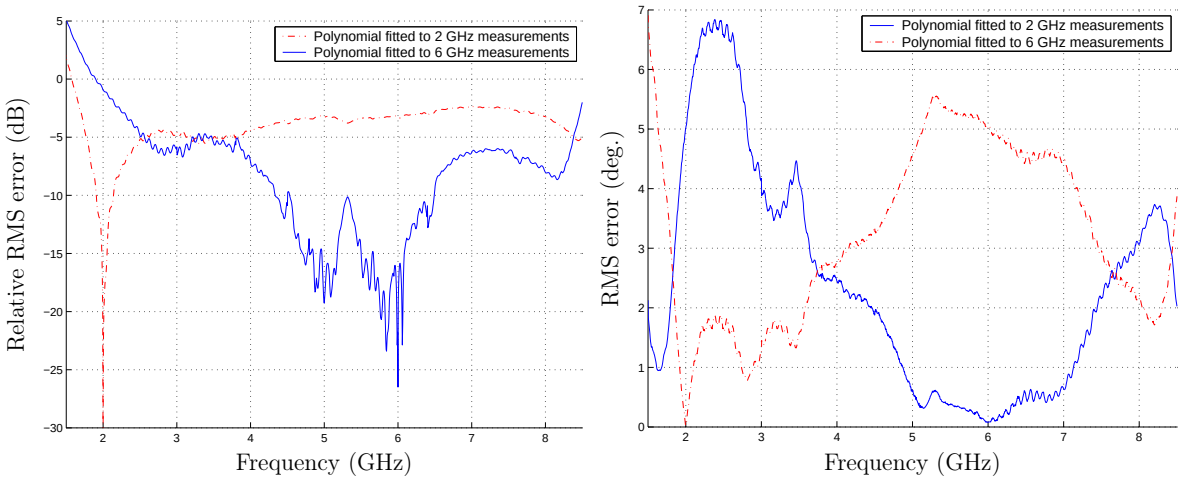

(a) AM/AM estimation error (b) AM/PM estimation error

Figure 6.7: Difference between the measured AM/AM & AM/PM and the estimated AM/AM & AM/PM characteristics of 5th-order polynomials fitted to selected frequencies. The relative RMS error of the AM/AM estimation plotted in (a) is defined in Equation (6.13) *and the RMS error of the AM/PM estimation plotted in (b) is defined in Equation* (6.14)*.*

The phase response has similar characteristics, but it is more difficult to observe it from Figure 6.3(b) since the phase shift is very small compared to the group delay of the amplifier. In order to use frequency-independent modelling techniques, the frequency response of the amplifier should be constant on the desired frequency band.

6.4 Summary

In this chapter the polynomial model discussed in Chapter 4.1 was applied for frequency-independent estimation of a Mini-Circuits ZVE-8G power amplifier. First, the measurement setup was introduced and the obtained measurement data were presented. Next, the measurement data and the polynomial model were formulated in vector notation and thereafter an optimal least-squares estimator was derived for estimation of the coefficients of the polynomials. Finally the estimation results were

presented and the error behavior of the polynomial model was analyzed.

The estimation accuracy of the polynomial model for a single frequency is very good even for models of low order. Accurate results were obtained using a fifth-order polynomial model. The relative RMS error of the AM/AM estimation was -18.18 dB and the RMS error of the AM/PM estimation was 0.19 degrees. The estimation accuracy can be improved using a higher-order model, but increasing the order above 11 does not yield substantial improvement of the estimation. The polynomial model's capability to estimate other frequencies than the fitting frequency was also studied.

The AM/AM and AM/PM characteristics play a crucial role in this since the polynomial is not able to model the frequency dependent behavior of the amplifier. Quite good estimation performance can be obtained if the amplifier is designed to have nearly flat gain and phase characteristics. However, if the amplifier is fed by wideband signals and has non-flat characteristics, a frequency-dependent model is required.

Chapter 7

Frequency-Dependent Estimation of Power Amplifier Nonlinearity Using the Hammerstein Model

The objective of this chapter is to model the measured frequency-dependent nonlinear behavior of the Mini-Circuits ZVE-8G power amplifier using a Hammerstein model as discussed in Chapter 5.2. The estimation problem is to minimize the difference between the output of the power amplifier and the Hammerstein model as illustrated in Figure 7.1.

The required measurements were discussed in Chapter 6.1 and the measured amplitude and phase response of the Mini-Circuits ZVE-8G power amplifier were plotted in Figures 6.3 and 6.4. A picture of the Mini-Circuits ZVE-8G power amplifier was shown in Figure 6.1 and its specifications were presented in Table 6.1.

A brief outline of this chapter follows. First, the chosen implementation of the Hammerstein model is discussed. As shown in Figure 7.1, the nonlinear static block is implemented by the polynomial model discussed in Chapter 4.1 and the linear dynamic block is implemented as an FIR filter. The following section presents a

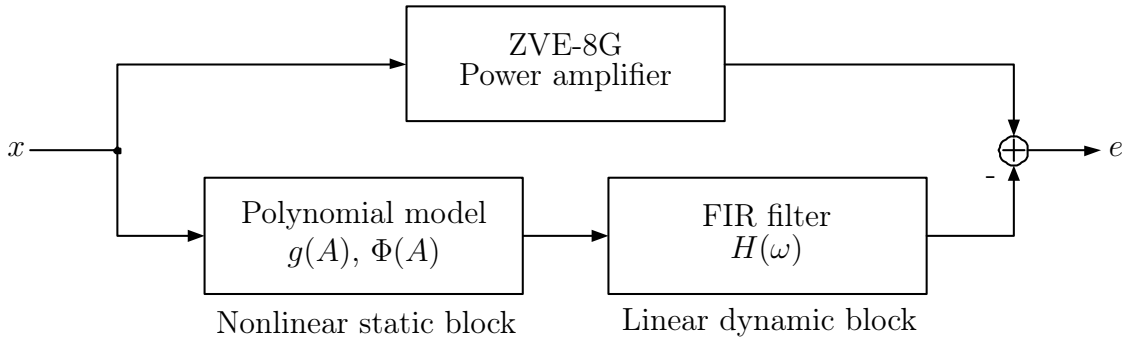

Figure 7.1: Block diagram of the frequency-dependent estimation problem for the Hammerstein model where x is the input that is fed to both the power amplifier and the model and e is the error of the estimation. The nonlinear static block is implemented by the polynomial model discussed in Chapter 4.1 and the linear dynamic block is implemented as an FIR filter.

simple estimation method for determining the parameters of the two blocks separately. After that a solution for estimating the coefficients of the FIR filter that implements the linear dynamic block of the Hammerstein model is derived. Finally, the estimation results of both the FIR design and the Hammerstein model are presented and the estimation error is analyzed. The chapter ends with a summary of the obtained results.

7.1 Implementation of the Hammerstein Model

This section presents the implementation of the Hammerstein model for estimation of the Mini-Circuits ZVE-8G power amplifier. As earlier mentioned in Chapter 5.2 the Hammerstein model is a cascade of a nonlinear static block and a linear dynamic block. Typically the static nonlinearity is implemented as a polynomial and the linear dynamic block as an IIR or an FIR filter [50].

Chapter 6 showed that the polynomial model can estimate the nonlinearity of the amplifier quite well at a single frequency and therefore, it is chosen to implement the nonlinear static block. For simplicity, an FIR filter was chosen to implement

the linear dynamic block. Besides simplicity of design and implementation, FIR filters are also superior to IIR filters in that they are always stable, exhibit less quantization noise when implemented in fixed-point arithmetic, and have smoother phase characteristics [62].

7.2 Simplified Parameter Estimation of the Hammerstein Model

This section defines the estimation problem for the Hammerstein model and proposes a solution for separately determining the parameters of the two cascaded blocks. The estimation problem for the chosen implementation of the Hammerstein model is illustrated in Figure 7.1. The objective is to minimize the difference between the output of the power amplifier and the output of the Hammerstein model based on the measured frequency response.

The frequency response of the Mini-Circuits ZVE-8G power amplifier that was plotted in Figure 6.3 clearly shows that both the amplitude and phase response of the power amplifier depend on the input power level. Therefore the explicit estimation problem is to minimize the difference between the desired complex-valued power-dependent frequency response $H_{d,p}(A_l, \omega_k)$ and the estimated complex-valued power-dependent frequency response $H_p(A_l, \omega_k)$. Mathematically this can be formulated as

$$E = \left| H_{d,p}(A_l, \omega_k) - H_p(A_l, \omega_k) \right|^2 \tag{7.1}$$

where A_l and ω_k are the discrete amplitude and frequency points at which both $H_{d,p}$ and H_p are evaluated. Direct minimization of the error function defined in Equation (7.1) is very difficult and hence the estimation problem must be further simplified. Note that the error measure in Equation (7.1) is chosen so that the required measurements can be done with the available equipment.

Denoting the frequency response of the FIR filter as $H(\omega_k)$, the estimated power-dependent frequency response $H_p(A_l, \omega_k)$ can be written as

$$\left|H_p(A_l, \omega_k)\right| = g(A_l)\left|H(\omega_k)\right| \tag{7.2}$$

$$\angle H_p(A_l, \omega_k) = \Phi(A_l) + \angle H(\omega_k) \tag{7.3}$$

where $g(A_l)$ is the AM/AM, and $\Phi(A_l)$ is the AM/PM conversion function of the polynomial model. Using Equations (7.2) and (7.3) the estimation problem defined by the error function in Equation (7.1) can be rewritten as two separate estimation problems where the objective is to minimize the error functions

$$E_g = \left|\left|H_{d,p}(A_l, \omega_k)\right| - g(A_l)\left|H(\omega_k)\right|\right|^2 \tag{7.4a}$$

$$E_\Phi = \left|\angle H_{d,p}(A_l, \omega_k) - \Phi(A_l) - \angle H(\omega_k)\right|^2 \tag{7.4b}$$

where E_g is the error function for the amplitude response estimation problem and E_Φ is the error function for the phase response estimation problem.

A simplified solution for the estimation problem defined by the error functions in Equation (7.4) can be found in [63] where $g(A_l)$, $\Phi(A_l)$, $|H(\omega_k)|$ and $\angle H(\omega_k)$ are approximated by polynomials. Unfortunately, the presented solution has some drawbacks and the authors only recommend it as a starting point for estimation of Hammerstein systems. First, the conversion of the nonlinear estimation problem into a linear estimation problem causes some excess error to the solution. Second, the solution is quite complex even though only linear estimation methods are used. Third, the FIR filter is merely described by the polynomials approximating the amplitude and phase response instead of being identified by its coefficients.

In the following a simplified estimation problem is formulated for determining the coefficients of both the polynomial model and the FIR filter of the Hammerstein model shown in Figure 7.1. The estimation problem defined by the error function in Equation (7.1) is simplified by assuming that the identification of the two blocks can be done separately. The static nonlinearity is assumed to be given by the

AM/AM and AM/PM measurements at the center frequency of the desired operating band. The linear dynamic part is assumed to be given by the small-signal frequency response of the modelled system. Mathematically, the estimation problem is to minimize the error functions

$$E_g = \left|A_{d,l} - g(A_l)\right|^2 \tag{7.5a}$$

$$E_\Phi = \left|\phi_{d_s,l} - \Phi(A_l)\right|^2 \tag{7.5b}$$

$$E_H = \left|H_{d,s_0}(\omega_k) - H(\omega_k)\right|^2 \tag{7.5c}$$

where $A_{d,l}$ are the desired discrete output amplitude values, $\phi_{d_s,l}$ are the desired scaled discrete output phase values and $H_{d,s_0}(\omega_k)$ is the desired scaled discrete small-signal response. The desired discrete output phase values must be scaled to zero degree at the small-signal input power level A_s at which $H(\omega_k)$ is fitted to or else the phase delay of the amplifier is included twice in the estimation. Similarly, the small-signal response $H_{d,s}(\omega_k)$ must be scaled to have unit gain at the center frequency ω_c at which $g(A)$ and $\Phi(A)$ are fitted to. Otherwise the gain of the amplifier is included twice in the estimation. Mathematically the required scaling operations can be written as

$$\phi_{d_s,l} = \phi_{d,l} - \phi_{d,s} \tag{7.6}$$

$$\left|H_{d,s_0}(\omega_k)\right| = \frac{\left|H_{d,s}(\omega_k)\right|}{|H_{d,s}(\omega_0)|}. \tag{7.7}$$

The estimation problem (minimization of the error functions in Equation (7.5)) can be solved in three steps. First, the output phase values $\phi_{d,l}$ and the small-signal frequency response $H_{d,s}(\omega)$ are scaled as described by Equations (7.6) and (7.7) to obtain $\phi_{d_s,l}$ and $H_{d,s_0}(\omega)$. Second, the coefficients of the polynomial model are estimated using the least-squares solution that was presented in Chapter 6.2. Finally, the coefficients of the FIR filter are estimated using weighted least-squares estimation that will be presented in Chapter 7.3. The proposed estimation technique is summarized in Table 7.1.

Table 7.1: Proposed technique for simplified parameter estimation of the Hammerstein model. The objective is to find the coefficients of the gain distortion function $g(A_l)$, the phase distortion function $\Phi(A_l)$ and the FIR filter $H(\omega)$.

Required input data	
A_l	A set of L discrete input amplitude values
A_s	Input amplitude level of the measured small-signal frequency response
ω_k	A set of K discrete angular frequencies contained in $[-\pi, \pi]$
ω_c	Center frequency of the desired frequency band
Required output data	
$A_{d,l}$	The desired discrete output amplitude values at ω_c
$\phi_{d,l}$	The desired discrete output phase values at ω_c
$H_{d,s}(\omega_k)$	The desired discrete complex-valued frequency response at A_s
Problem formulation	
The estimation problem is to choose the coefficients of $g(A_l)$, $\Phi(A_l)$ and $H(\omega_k)$ so that the least-squares error functions are minimized: $E_g = \left\|A_{d,l} - g(A_l)\right\|^2$, $E_\Phi = \left\|\phi_{d_s,l} - \Phi(A_l)\right\|^2$, $E_H = \left\|H_{d,s_0}(\omega_k) - H(\omega_k)\right\|^2$	
Solution	
Step 1:	Determine $\phi_{d_s,l}$ and $H_{d,s_0}(\omega_k)$ by scaling $\phi_{d,l}$ and $H_{d,s}(\omega_k)$: $\phi_{d_s,l} = \phi_{d,l} - \phi_{d,s}$, $\left\|H_{d,s_0}(\omega_k)\right\| = \left\|H_{d,s}(\omega_k)\right\| / \left\|H_{d,s}(\omega_0)\right\|$
Step 2:	Estimate coefficients of $g(A_l)$ and $\Phi(A_l)$ using the least-squares solution presented in Chapter 6.2
Step 3:	Estimate coefficients of $H_{d,s_0}(\omega_k)$ using the weighted least-squares solution presented in Chapter 7.3

The justification for this simplified estimation technique is that in a moderate to large-backoff condition the modelled amplifier performs almost linearly and the small-signal transfer function is what the signal can be expected to see. In saturated operation the signal can instead be expected to see the saturated transfer function. The difference between the estimation technique proposed here and the estimation technique defined by the error function in Equation (7.4) is that here the estimation of the blocks is assumed separable instead of assuming that the estimation of the amplitude and phase characteristics are separable.

It should be noted that the FIR filter is a baseband approximation of the measured frequency response. This means that the required sampling rate easily becomes very high. According to the *sampling theorem*[1], a bandlimited signal contained in $[f_1, f_2]$ can be uniquely determined by its samples, if and only if the sampling frequency f_s satisfies $f_s > 2f_2$ [64]. The highest frequency f_2 is usually called the *Nyquist frequency* since it determines the minimum sampling frequency $f_s = 2f_2$ called the *Nyquist rate*. The Nyquist rate for baseband FIR approximation is illustrated in Figure 7.2(a).

In practice only a relatively small subband of the whole frequency range of the amplifier is interesting. In such a case the sampling rate can be significantly reduced by first bandpass filtering the desired subband and then demodulating the filtered subband to baseband. An illustration of the filtering and demodulation process is shown in Figure 7.2. As an example let us consider that we are only interested in modelling the frequency band from 5 GHz to 7 Ghz, i.e., we have $f_1 = 1.5$ Ghz, $f_2 = 8.5$ GHz, $f_{d,1} = 5$ GHz and $f_{d,2} = 7$ GHz in Figure 7.2(a). Baseband approximation of the desired band requires a minimum sampling rate $f_{s,1} = 17$ GHz, since the Nyquist frequency is 8.5 GHz (see Fig. 7.2(a)). On the other hand, the Nyquist rate for the filtered and demodulated band is only $f_{s,2} = 2$ GHz, since we now have $f_{d_0,1} = -1$ GHz and $f_{d_0,2} = 1$ GHz (see Fig. 7.2(b)).

[1] Also called either the *Nyquist sampling theorem* or the *Shannon sampling theorem*.

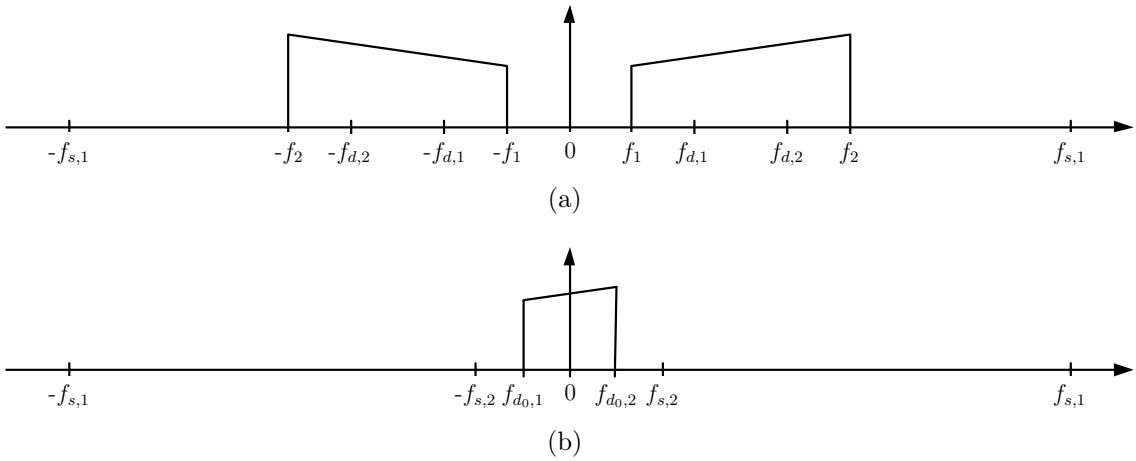

Figure 7.2: Illustration of the minimum sampling rate for the FIR filter design. (a) Baseband approximation of the signal contained in the range $[f_1, f_2]$, where the minimum sampling rate is $f_{s,1} = f_2$. (b) Desired subband contained in the range $[f_{d_0,1}, f_{d_0,2}]$ after bandpass filtering and demodulation to baseband. The required sampling rate is now only $f_{s,2} = f_{d_0,2}$.

7.3 Weighted Least-Squares FIR Approximation

Weighted least-squares approximation can be used to design FIR filters with desired arbitrary shape amplitude and phase response [62]. A solution for the continuous frequency case can be found in [65]. In this chapter the derivation presented in [65] is modified for use on a discrete frequency grid.

The frequency response of a Mth-order ($M + 1$ coefficients) causal FIR filter is defined as

$$H\left(e^{j\omega_k}\right) = \sum_{m=0}^{M} h_m e^{-j\omega_k m} \tag{7.8}$$

where the filter coefficients $h_0, h_1, \ldots, h_m$ are assumed to be real valued and ω_k is a set of discrete angular frequencies where the response is evaluated. The computational complexity of the filter described by Equation (7.8) can be reduced by adding a delay element with a constant delay of D samples before the filter. This is equivalent to setting the first D coefficients of the filter to zeroes. The frequency

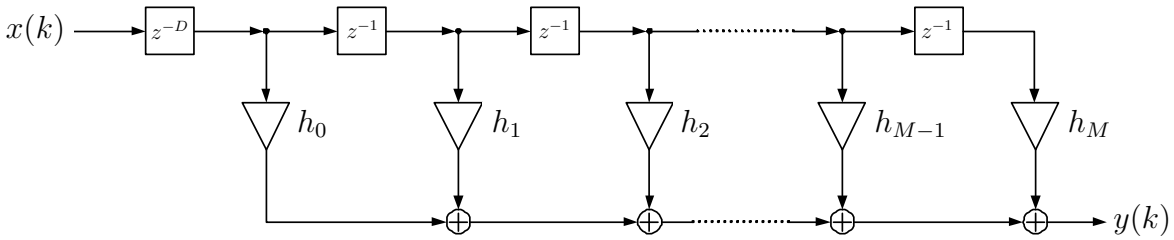

Figure 7.3: A Direct Form I realization of a causal Mth-order FIR filter. The FIR filter is preceded by a delay element with a constant delay of D samples.

response of the cascade of the delay element and the FIR filter is

$$H\left(e^{j\omega_k}\right) = \sum_{m=0}^{M} h_m e^{-j\omega_k(m+D)}. \tag{7.9}$$

An implementation of the system described by Equation (7.9) is shown in Figure 7.3 where the FIR filter has been realized using the *Direct Form I* structure [51].

The filter design problem is to choose the filter coefficients $h_0, h_1, \ldots, h_M$ so that the weighted least-squares error is minimized:

$$E = \sum_{k=0}^{K-1} W(\omega_k) \left| H_d\left(e^{j\omega_k}\right) - \sum_{m=0}^{M} h_m e^{-j\omega_k(m+D)} \right|^2 \tag{7.10}$$

where ω_k is a set of K discrete angular frequencies in the range $[-\pi, \pi]$, $H_d\left(e^{j\omega_k}\right)$ is the desired complex-valued frequency response, $W(\omega_k)$ is a real-valued nonnegative weight function, M is the desired order of the filter and D is the desired length of the constant delay element.

In order for the design problem described by Equation (7.10) to have a solution it is required that $K \geq M$. Obviously, the error is only minimized at the K sample points and hence a small enough frequency grid should be used in order to make the frequency response of the filter well behaved between the sample points. In other words, a large ratio of K/M indicates a more constrained error between the sample points. On the other hand choosing $K > M$ results in more equations than

unknowns and hence only approximate solutions are possible.

For $K = M$ the design problem can also be solved using the *frequency sampling* technique in which the filter coefficients are directly calculated from the desired frequency response using the Inverse Discrete Fourier Transform (IDFT). Naturally the use of IDFT requires that the sample points are equally spaced. Another drawback of the frequency sampling technique is that the frequency response is unconstrained between the sample points which might lead to large errors between the sample points if the desired phase response is in some way inconsistent with the amplitude response or the filter length [62]. Due to the possibility of large errors in the frequency response, the frequency sampling technique is not useful for the Hammerstein model.

To present the solution of Equation (7.10) in a clear and compact form, the problem is first rewritten in vector notation. Denoting the real-valued filter coefficient vector $\mathbf{h}$ and the complex-valued discrete-time Fourier transform vector $\mathbf{e}$ as

$$\mathbf{h} = \begin{bmatrix} h_0 & h_1 & \cdots & h_M \end{bmatrix}^{\mathrm{T}} \tag{7.11}$$

$$\mathbf{e}\left(\omega_k\right) = \begin{bmatrix} e^{-j\omega_k D} & e^{-j\omega_k (D+1)} & \cdots & e^{-j\omega_k (D+M)} \end{bmatrix}^{\mathrm{T}} \tag{7.12}$$

the error function defined in Equation (7.10) can be rewritten in vector notation as

$$E = \sum_{k=0}^{K-1} W\left(\omega_k\right) \left| H_d\left(e^{j\omega_k}\right) - \mathbf{h}^{\mathrm{T}} \mathbf{e}\left(\omega_k\right) \right|^2 . \tag{7.13}$$

Equation (7.13) can be written more compactly as (see Appendix A for details)

$$E = \mathbf{h}^{\mathrm{T}} \mathbf{P} \mathbf{h} - 2\mathbf{h}^{\mathrm{T}} \mathbf{p}_1 + p_0 \tag{7.14}$$

where

$$\mathbf{P} = \sum_{k=0}^{K-1} W(\omega_k)\mathbf{C}\left(\omega_k\right) \tag{7.15}$$

$$\mathbf{p}_1 = \sum_{k=0}^{K-1} W(\omega_k)\left[\mathrm{Re}\Big\{H_d\left(e^{j\omega_k}\right)\Big\}\mathbf{c}\left(\omega_k\right) - \mathrm{Im}\Big\{H_d\left(e^{j\omega_k}\right)\Big\}\mathbf{s}\left(\omega_k\right)\right] \tag{7.16}$$

$$p_0 = \sum_{k=0}^{K-1} W(\omega_k)\left|H_d\left(e^{j\omega_k}\right)\right|^2 \tag{7.17}$$

and

$$\mathbf{c}\left(\omega_k\right) = \begin{bmatrix}\cos D\omega_k & \cos(D+1)\omega_k & \cdots & \cos(D+M)\omega_k\end{bmatrix}^{\mathrm{T}} \tag{7.18}$$

$$\mathbf{s}\left(\omega_k\right) = \begin{bmatrix}\sin D\omega_k & \sin(D+1)\omega_k & \cdots & \sin(D+M)\omega_k\end{bmatrix}^{\mathrm{T}} \tag{7.19}$$

$$\mathbf{C}\left(\omega_k\right) = \begin{bmatrix} 1 & \cos\left(\omega_k\right) & \cdots & \cos\left(M\omega_k\right) \\ \cos\left(\omega_k\right) & 1 & \cdots & \cos\left[\left(M-1\right)\omega_k\right] \\ \vdots & \vdots & \ddots & \vdots \\ \cos\left(M\omega_k\right) & \cos\left[\left(M-1\right)\omega_k\right] & \cdots & 1 \end{bmatrix}. \tag{7.20}$$

The solution to Equation (7.14) (see Appendix A for details) is given by

$$\mathbf{h} = \mathbf{P}^{-1}\mathbf{p}_1. \tag{7.21}$$

A MATLAB implementation of the proposed design technique can be found in Appendix B. The computational complexity can be reduced by utilizing the Toeplitz structure of $\mathbf{P}$. The Levinson algorithm requires $4M^2$ floating-point operations to solve the problem [61].

7.4 Estimation Results

This section presents the estimation results obtained using the Hammerstein model. It seems justified to assume that in practice an amplifier is fed by signals that have a relatively large bandwidth, but that the bandwidth is still considerably smaller than the bandwidth of the amplifier. Therefore, it is reasonable to choose a subband of the amplifier's operating band and try to make the estimation as accurate as possible on the chosen subband.

As earlier mentioned in Section 7.1, the static nonlinearity is implemented using the polynomial model discussed in Chapter 4.1 and the linear dynamic system as an FIR filter. The estimation results obtained using the polynomial model were presented in Chapter 6.3. As can be seen from Figure 6.7, a 5th-order polynomial model fitted to the 6 GHz measurements estimates the characteristics of the amplifier quite well between 5 GHz and 7 GHz. Therefore, it is reasonable to choose the frequency band from 5 GHz and 7 GHz as the desired estimation range.

A brief outline of this section follows. First, the weighted least-squares FIR approximation discussed in Section 7.3 is verified by MATLAB simulations. The following subsection presents the FIR approximation of the measured small-signal response of the Mini-Circuit ZVE-8G power amplifier. Finally, the estimation results using the Hammerstein model are presented.

7.4.1 Verification of the Weighted Least-Squares FIR Approximation

Before trying to estimate the small-signal frequency-response of the Mini-Circuits ZVE-8G power amplifier, the weighted least-squares FIR approximation presented in Section 7.3 is first verified by approximating a 5th-order lowpass Butterworth filter. The cutoff frequency of the filter was set to $f_s/4$ where f_s is the sampling frequency. Butterworth filters are of IIR-type and are characterized by a magnitude

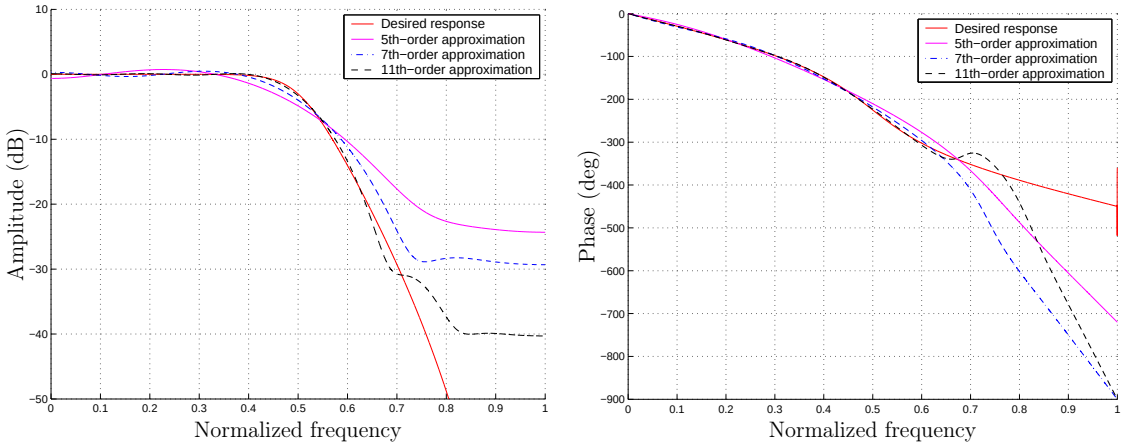

(a) Amplitude response (b) Phase response

Figure 7.4: Frequency response of FIR filters designed using weighted least-squares FIR approximation. The desired response of the FIR filters is a fifth-order lowpass Butterworth filter with cutoff frequency $f_s/4$ (normalized frequency 0.5).

response that is maximally flat in the passband and monotonic overall [62]. It should be noted that Butterworth filters do not have linear phase response.

Using the frequency response of the Butterworth filter as the desired response, FIR filters of selected orders were designed using the weighted least-squares FIR approximation presented in Section 7.3. The obtained estimations of the desired frequency response are shown in Figure 7.4. As can be seen from Figure 7.4(a), the FIR approximations are not flat in the passband as the desired response and the attained stopband attenuation is significantly smaller. Nevertheless, the passband approximation is quite good and an 11th-order FIR filter can be considered to approximate the desired amplitude response quite well.

The obtained estimates of the phase response are plotted in Figure 7.4(b). As in the amplitude estimation, the passband approximation is again much better than the stopband approximation. The high ripple of the desired response at half the sampling frequency is caused by numerical problems since the values of the complex frequency response approach the working precision of the computer. Generally, the FIR approximation can be considered accurate and to produce filters with good characteristics as can be seen from Figure 7.5. The pole-zero plot of the 11th-order

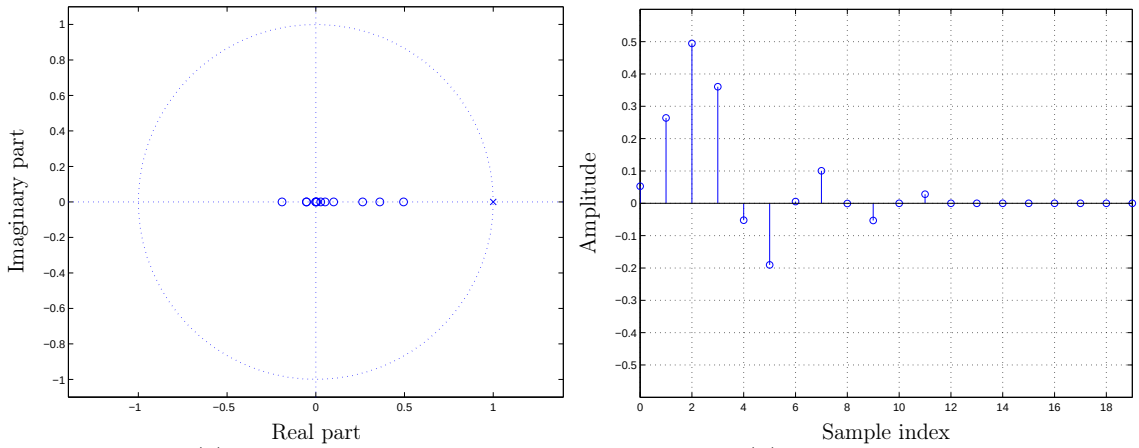

(a) Pole-zero plot (b) Impulse response

Figure 7.5: Illustration of the filter characteristics obtained using weighted least-squares FIR approximation. (a) Pole-zero plot and (b) impulse response of the 11th-order FIR approximation of the desired 5th-order Butterworth filter response.

approximation plotted in Figure 7.5(a) shows that the designed filter has *minimum-phase*[2] characteristics which indicates that the filter has a small phase delay.

Obviously it is not possible to find an FIR filter that has exactly the same response as an IIR filter. However, the approximation error should approach zero as the order of the filter approaches infinity. Figure 7.6 shows that derived weighted least-squares design technique fulfils this requirement. As can be seen from Figure 7.6, the estimation error is decreasing monotonously until the working precision of the computer is reached.

7.4.2 Results of the FIR Approximation

The accuracy of the weighted least-squares FIR approximation discussed in Section 7.3 is affected by two factors. The principal factor is the order M of the FIR filter. Increasing the order of the filter improves the estimation accuracy, however, the computational complexity and the processing delay of the filter is increased. The

[2] A causal stable filter that has all its zeros and poles inside or on the unit circle is called a *minimum-phase* filter.

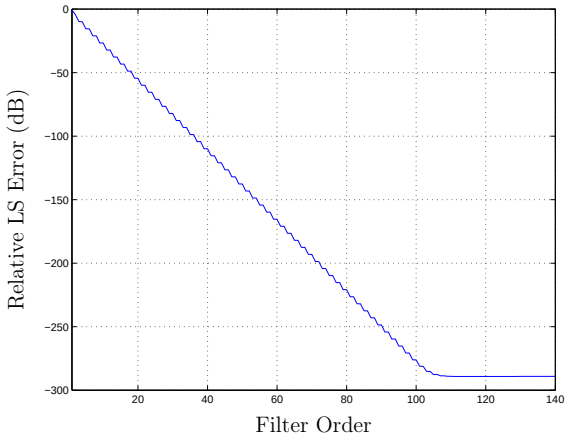

Figure 7.6: Relative least-squares error of the weighted least-squares FIR approximation as a function of the filter order. The desired response is a fifth-order lowpass Butterworth filter with cutoff frequency $f_s/4$.

computational complexity can be reduced by adding a delay element with a constant delay D before the filter. This is equivalent to setting the first D coefficients of the filter to zero. In other words, the delay element estimates the natural delay of the modelled system. The second factor that affects the estimation accuracy is the weight function $W(\omega_k)$ that can be used to emphasize a desired subband of the modelled system.

The simplest approach is to use a rectangular weighting function defined as

$$W(\omega_k) = \begin{cases} W_{desired}, & \omega_{d,min} \leq \omega_k \leq \omega_{d,max} \\ W_{other}, & otherwise \end{cases} \tag{7.22}$$

where $W_{desired}$ and W_{other} are constants (obviously $W_{other} < W_{desired}$), $\omega_{d,min}$ is the lower bound and $\omega_{d,max}$ is the upper bound of the desired band. The rectangular weight function is described by the *weighting factor* W_f defined as

$$W_f = \frac{W_{desired}}{W_{other}}. \tag{7.23}$$

A higher weighting factor yields more accurate results within the desired frequency band. On the other hand, a small weighting factor constrains the error outside the

desired band more. Therefore, the weighting factor should be chosen small enough to make the filter response well behaved while still being accurate.

As stated in Table 7.1, the FIR filter that implements the linear dynamic block of the Hammerstein model should be designed to have equal response as the scaled small-signal response of the modelled power amplifier. Figure 7.7 shows different order approximations of the scaled small-signal response of the Mini-Circuits ZVE-8G power amplifier. The length of the constant delay of each filter is chosen so that the estimation error is minimized. All filters have been weighted using a rectangular weight function with a weighting factor of 10^3.

As can be seen from Figure 7.7(a), a 7th-order filter is not yet able to completely model the response, an 8th-order filter already performs quite well and increasing the order above 13 does not significantly improve the estimation accuracy within the desired frequency band due to the noise in the measurement data. Nevertheless a higher-order filter results in a more well-behaved error outside the desired band. Figure 7.7(b) shows that the phase estimation is less sensitive to the order of the filter since the phase response is almost linear and good accuracy within the desired band is obtained with all filters.

The effect of the weighting factor W_f is studied in Figure 7.8. The figure shows a 13th-order filter with a 17 sample constant delay fitted to the measured frequency response with weighting factors 10, 10^3, 10^5 and 10^7. As can be seen from Figure 7.8(a), choosing the weighting factor as 10 results in too much ripple within the desired frequency band. On the other hand, using a weighting factor of 10^7, the error outside the desired band grows too high. In this case, choosing the weighting factor between 10^3 and 10^5 gives good performance. Again, the phase estimation is not as sensitive to the weighting factor as the amplitude estimation (see Fig. 7.8(b)).

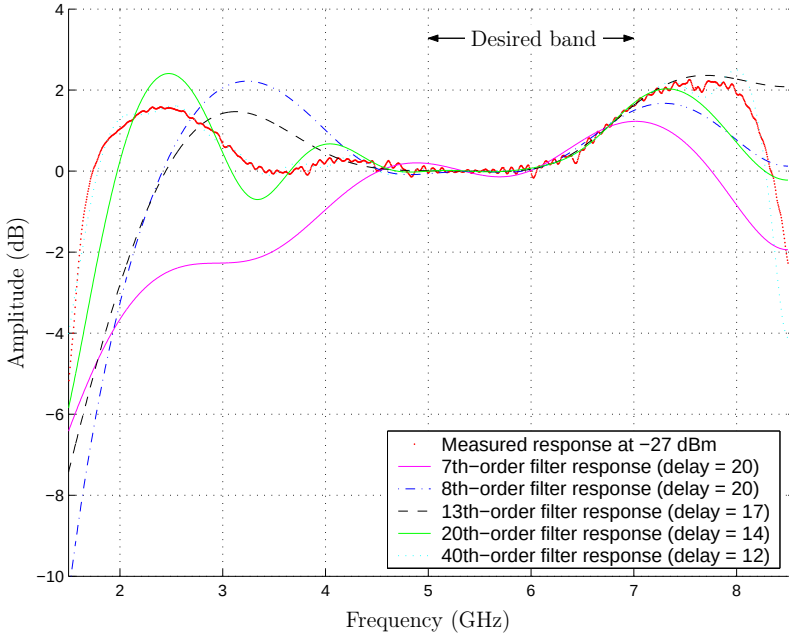

(a) Amplitude response

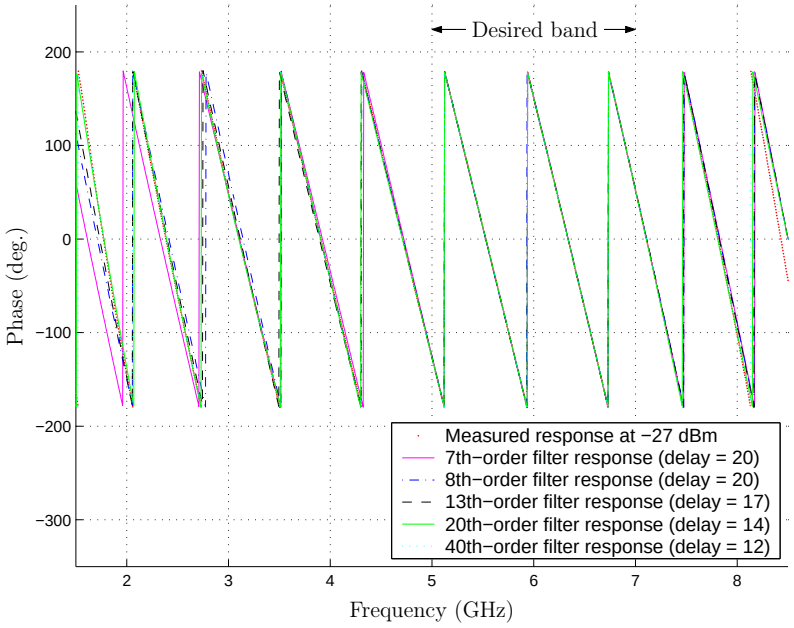

(b) Phase response

Figure 7.7: FIR filters of selected orders fitted to the measured small-signal amplitude and phase response of the Mini-Circuits ZVE-8G power amplifier. The weighted frequency band is 5-7 GHz with a weighting factor of 10^3.

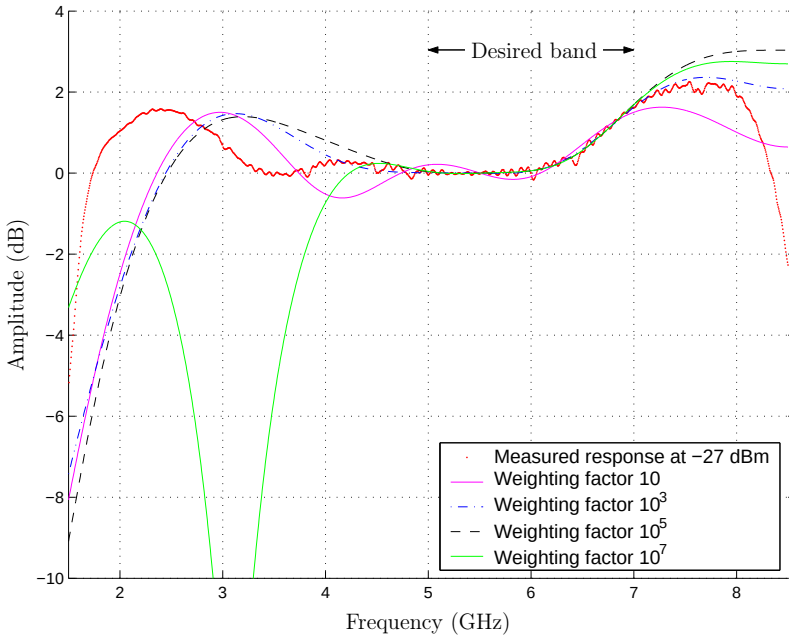

(a) Amplitude response

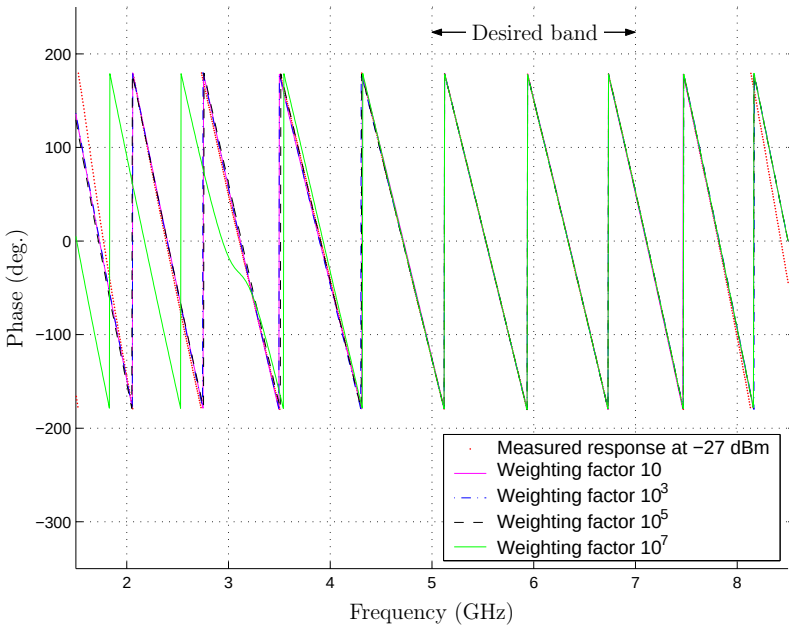

(b) Phase response

Figure 7.8: Illustration of the effect of the weighting factor on the estimation accuracy. The order of the filter is 13 and the length of the constant delay is 17 samples.

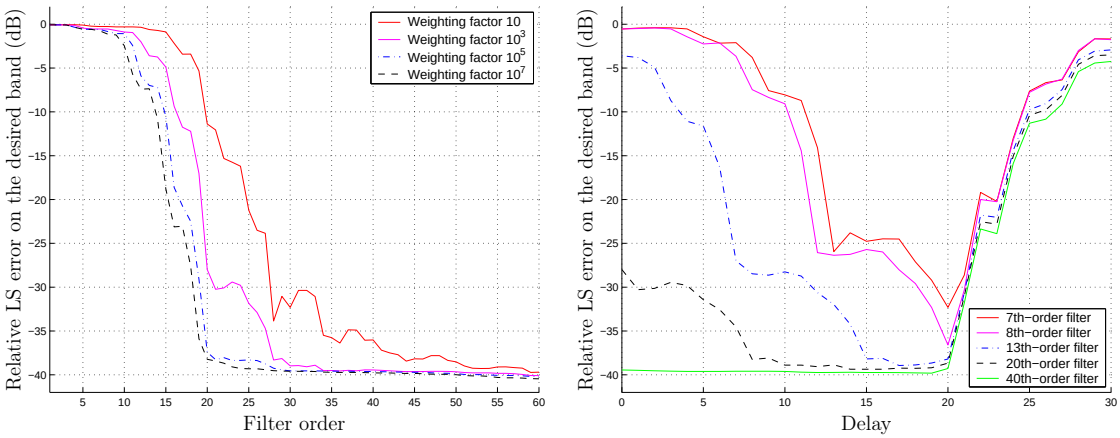

Figure 7.9: Estimation accuracy of the weighted least-squares FIR approximation. (a) Effect of the filter order on the estimation accuracy for selected weighting factors. The length of the constant delay is zero samples. (b) Effect of the length of the constant delay on the estimation accuracy for selected filter orders with a weighting factor of 10^3.

The estimation accuracy is evaluated using the relative least-squares error defined as

$$E_{LS,relative} = 20 \lg \frac{\|H_d(\omega_k) - H(\omega_k)\|}{\|H_d(\omega_k)\|} \tag{7.24}$$

where $H_d(\omega_k)$ is the desired complex-valued frequency response and $H(\omega_k)$ is the complex-valued frequency response of the designed filter. The effect of the filter order on the estimation accuracy is shown in Figure 7.9(a) where the relative least-squares error on the desired band is plotted as a function of the filter order. In order to make the results comparable, the constant delay element was omitted. It should be noted that the error is not monotonically decreasing, since only the error of the desired band is considered. Figure 7.9(a) shows that increasing the order above 20 does not improve the estimation significantly if the weighting factor is chosen properly. Using a weighting factor of 10 requires a very high-order filter in order to produce accurate results. Sufficiently good estimation is obtained by choosing a weighting factor of 10^3, and increasing it above 10^5 gives very little improvement in the accuracy.

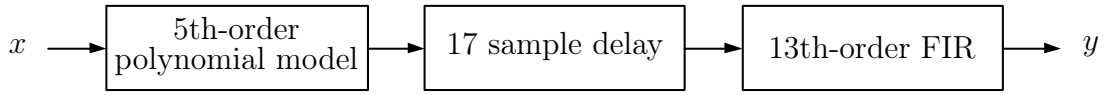

Figure 7.10: Implementation of the Hammerstein model.

Figure 7.9(b) shows the relative least-squares error on the desired band as a function of the delay. Clearly, the filter order can be significantly reduced by using a constant delay before the filter. This lowers the computational complexity of the filter. However, it comes with the cost of a higher processing delay, since the delay of the constant delay and the filter is greater than the delay of a higher-order filter without a constant delay for a given error level. The figure also shows that delay should be chosen carefully, since a too long delay increases the error rapidly.

7.4.3 Results of the Hammerstein Model Estimation

Now that the estimation results of both the polynomial model and the filter design have been presented, the estimation results of the Hammerstein model can be presented. The nonlinear static block is implemented as 5th-order polynomial model and the linear dynamic block as a 13th-order FIR filter with a constant delay of 17 samples and a weighting factor of 10^3. Figure 7.10 illustrates the chosen implementation of the Hammerstein model.

Figure 7.11 shows the estimated amplitude response at the boundaries of the dynamic range of the amplifier, i.e. at both –27 dBm and 0 dBm. As can be seen from Figure 7.11(b), the estimation is very accurate within the desired frequency band at both power levels. Improving the accuracy further is difficult due to the noise in the measurement data. The estimated phase response is shown in Figure 7.12 at power levels –27 dBm and 0 dBm. The figure shows that the phase estimation is even better than the amplitude estimation on the desired band.

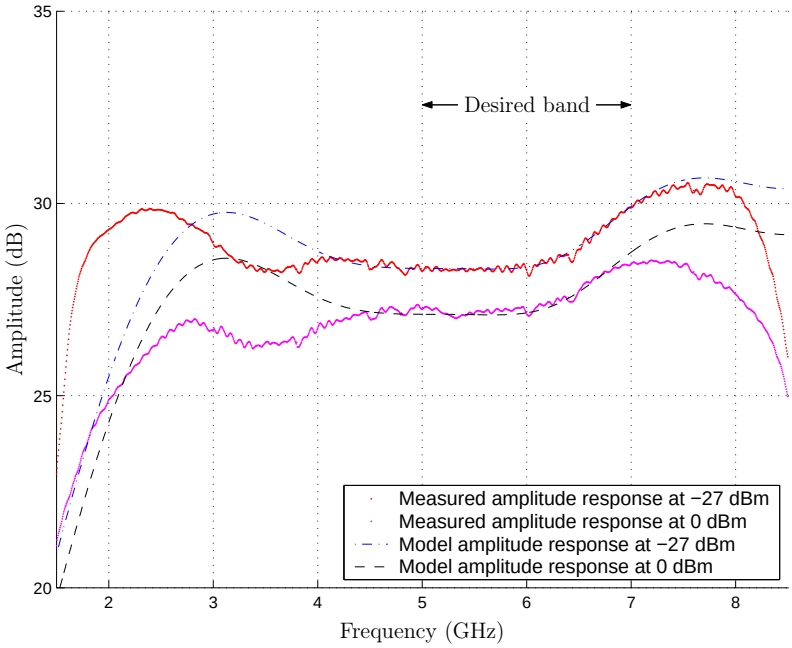

(a) Amplitude response

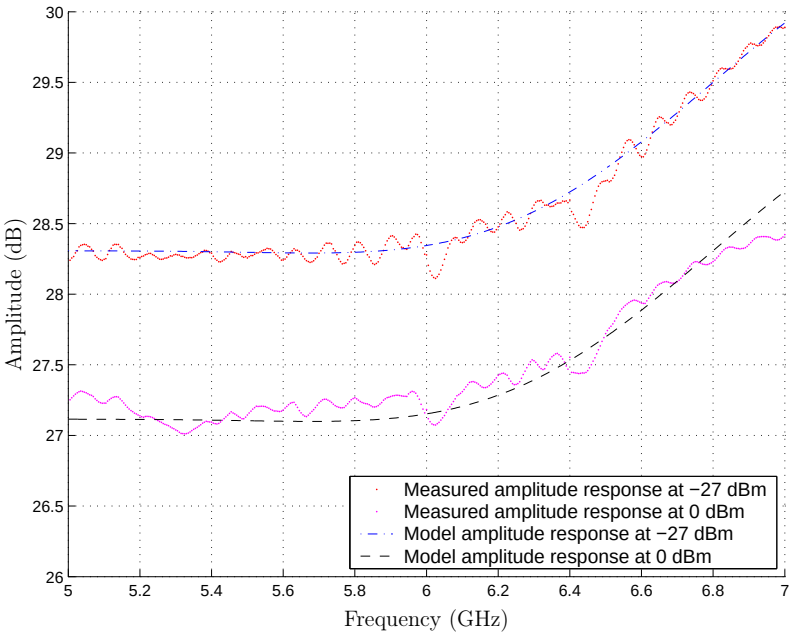

(b) Amplitude response on the desired band

Figure 7.11: A comparison between the measured and estimated amplitude response at –27 dBm and 0 dBm input power levels. The order of the polynomial model is 5 and the order of the FIR filter is 13 with a constant delay of 17 samples and a weighting factor of 10^3.

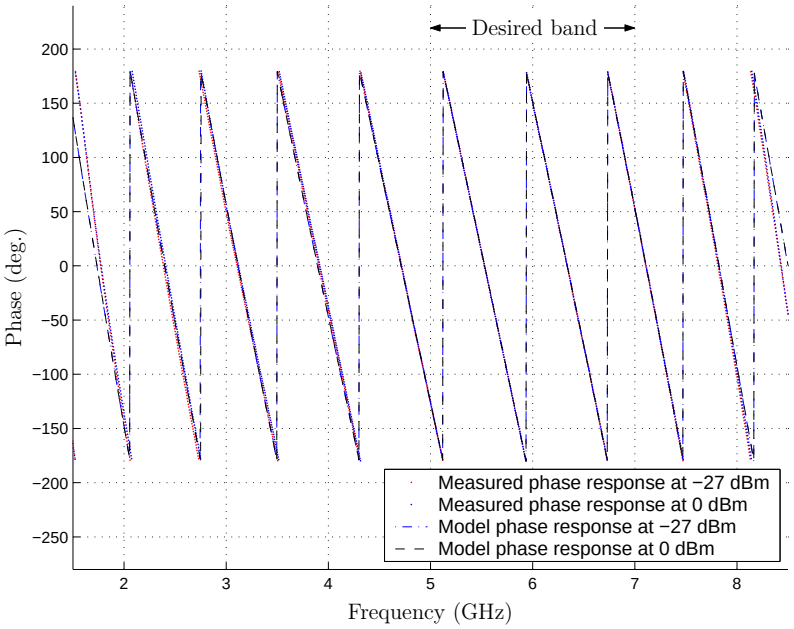

(a) AM/AM characteristics

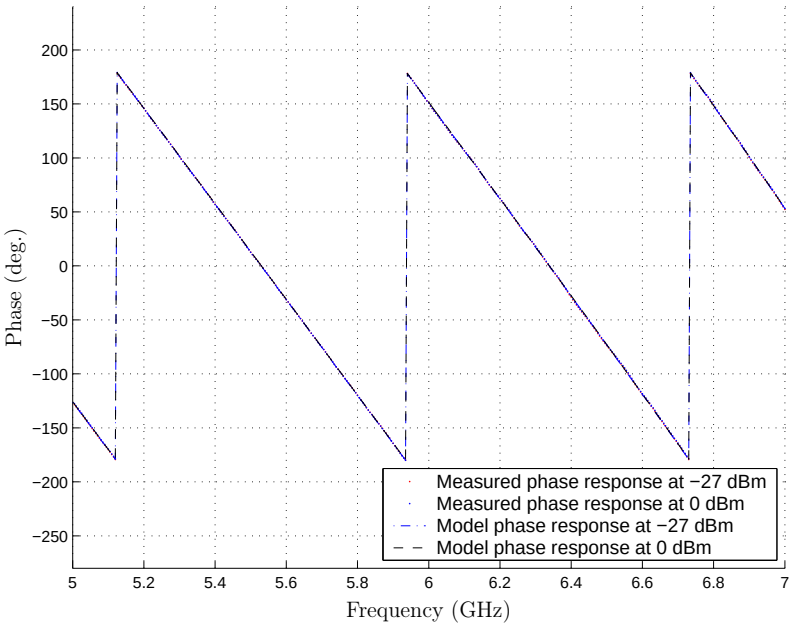

(b) AM/AM characteristics at selected frequencies on the desired band

Figure 7.12: A comparison between the measured and estimated phase response at –27 dBm and 0 dBm input power levels. The order of the polynomial model is 5 and the order of the FIR filter is 13 with a constant delay of 17 samples and a weighting factor of 10^3.

The estimated AM/AM characteristics at selected frequencies on the operating band of the amplifier are shown in Figure 7.13(a). The poor estimation result at 2 and 8 GHz is a consequence of the amplitude response of the FIR filter as can be seen from Figure 7.11(a). However, the estimation result is very good on the desired band as shown in Figure 7.13(b). Only the 7 GHz estimation is somewhat inaccurate at the power range from 0 to 5 dBm, which is not very crucial since the 1-dB compression point of the amplifier is at 0 dBm and hence it is not likely that the amplifier will be used at such high input power levels.

Figure 7.14(a) shows the estimated AM/PM characteristics at selected frequencies on the operating band. The figure shows that the estimation error outside the desired band is approximately 5 to 10 degrees. Again the estimation result on the desired band is very good as can be seen from Figure 7.14(b). The estimation seems to be equally good on the whole desired band.

The estimation error of the Hammerstein model was defined in Equation (7.1) as

$$E = \left| H_{d,p}(A_l, \omega_k) - H_p(A_l, \omega_k) \right|^2$$

where $H_{d,p}(A_l, \omega_k)$ is the desired power-dependent frequency response and $H_p(A_l, \omega_k)$ is the power-dependent frequency response of the model. The relative least-squares error of the Hammerstein model can be written as

$$E_{A,\omega}(A_l, \omega_k) = 20 \lg \left(\frac{\left| H_{d,p}(A_l, \omega_k) - H_p(A_l, \omega_k) \right|^2}{\left| H_{d,p}(A_l, \omega_k) \right|^2} \right). \tag{7.25}$$

The error surface generated by Equation (7.25) is plotted in Figure 7.15(a) where the desired band can be seen as a deep valley. Figure 7.15(b) shows the error surface directly from above. From this figure it can be seen that the estimation is equally good on the desired band for all power levels up to the 1-dB compression point.

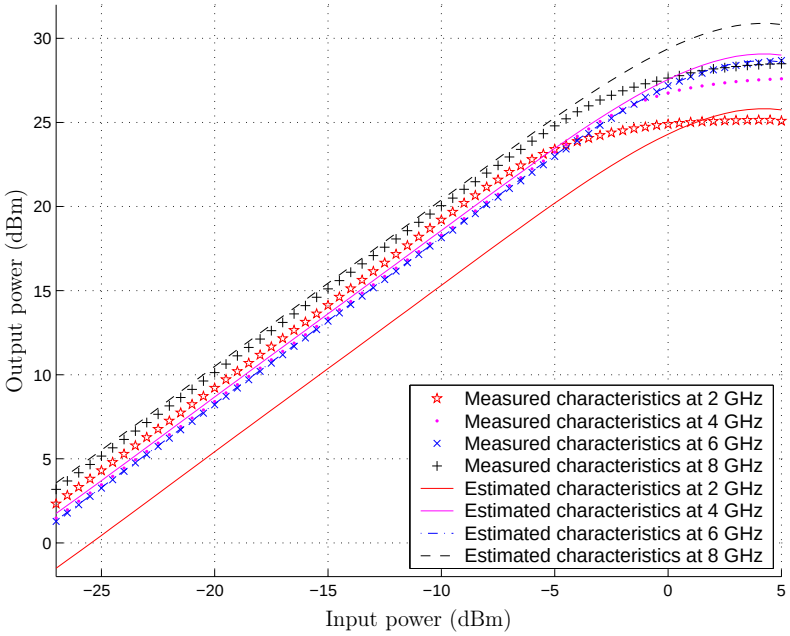

(a) AM/AM characteristics

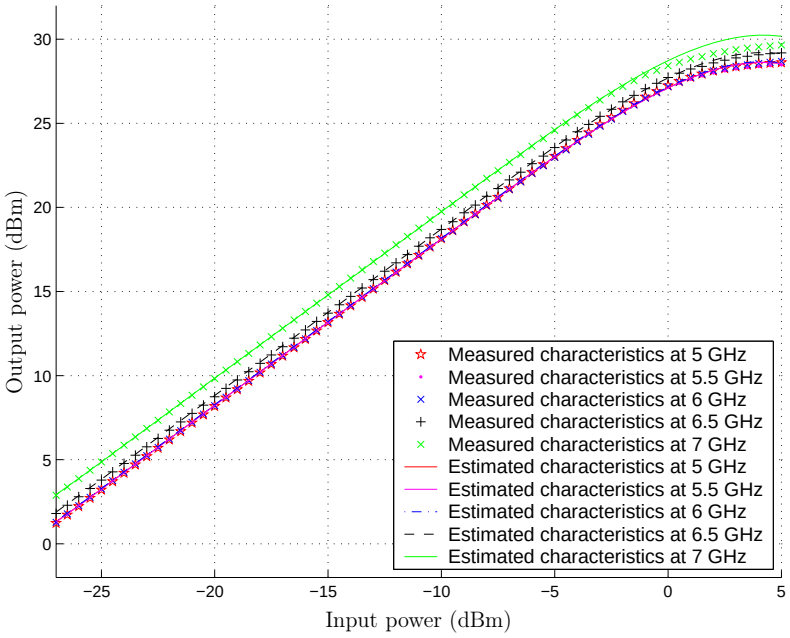

(b) AM/AM characteristics at selected frequencies on the desired band

Figure 7.13: A comparison between the measured and estimated AM/AM characteristics at selected frequencies. The order of the polynomial model is 5 and the order of the FIR filter is 13 with a constant delay of 17 samples and a weighting factor of 10^3.

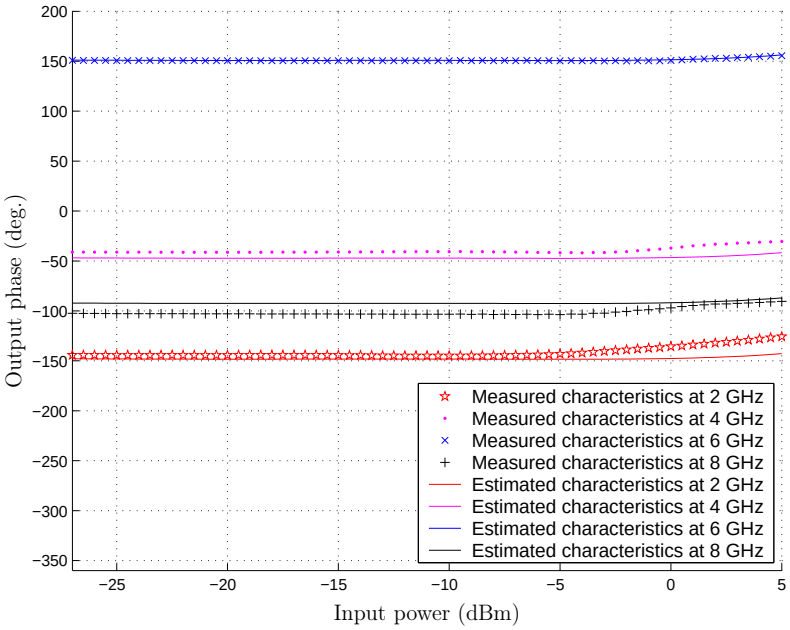

(a) AM/PM characteristics

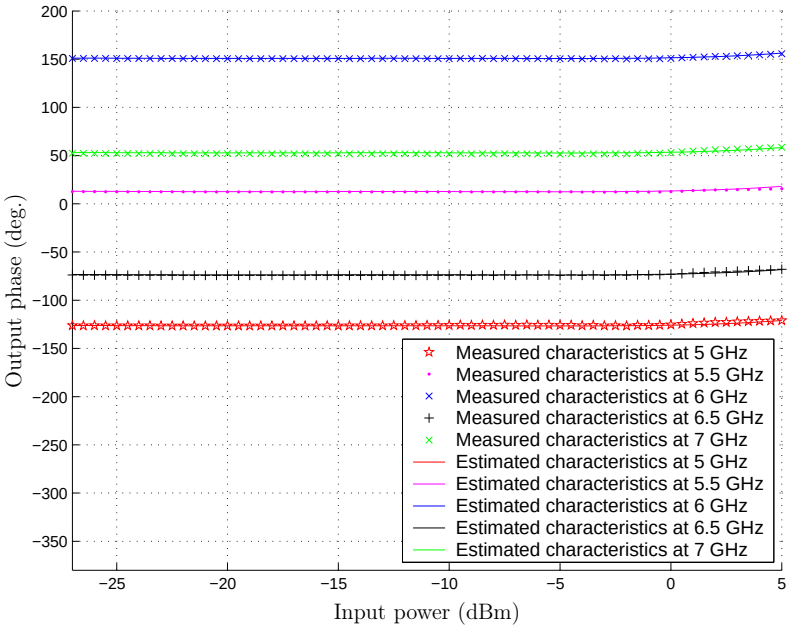

(b) AM/PM characteristics at selected frequencies on the desired band

Figure 7.14: A comparison between the measured and estimated AM/PM characteristics at selected frequencies. The order of the polynomial model is 5 and the order of the FIR filter is 13 with a constant delay of 17 samples and a weighting factor of 10^3.

The estimation error is further analyzed by calculating the average relative least-squares error for a given frequency

$$E_\omega(\omega_k) = 20\lg\left(\frac{\sum_{l=0}^{L-1}\left|H_{d,p}(A_l,\omega_k) - H_p(A_l,\omega_k)\right|^2}{\sum_{l=0}^{L-1}\left|H_{d,p}(A_l,\omega_k)\right|^2}\right) \tag{7.26}$$

and the average relative least-squares error for a given input power level

$$E_A(A_l) = 20\lg\left(\frac{\sum_{k=0}^{K-1}\left|H_{d,p}(A_l,\omega_k) - H_p(A_l,\omega_k)\right|^2}{\sum_{k=0}^{K-1}\left|H_{d,p}(A_l,\omega_k)\right|^2}\right). \tag{7.27}$$

The error measures defined by Equations (7.26) and (7.27) are plotted in Figures 7.15(c) and 7.15(d) respectively. Figure 7.15(c) can be thought of as a cross-section of Figure 7.15(a) at a given input power level. In the figure the estimation error has been averaged over all power levels, and for power levels up to the 1-dB compression point. There is almost no difference in the curves since all power levels are equally weighted. The figure shows that the estimation accuracy is very good on the desired band and that the estimation error is constrained outside the desired band. Therefore the estimation results can be considered very good.

Similarly, Figure 7.15(d) can be thought of as a cross-section of Figure 7.15(a) at a given frequency. This figure shows that estimation accuracy is almost constant at power levels up to the 1-dB compression point. At higher input power levels the nonlinearity of the power amplifier increases which naturally implies reduced estimation accuracy. This is not crucial since it is not likely that the amplifier will be driven at input power levels above the 1-dB compression point.

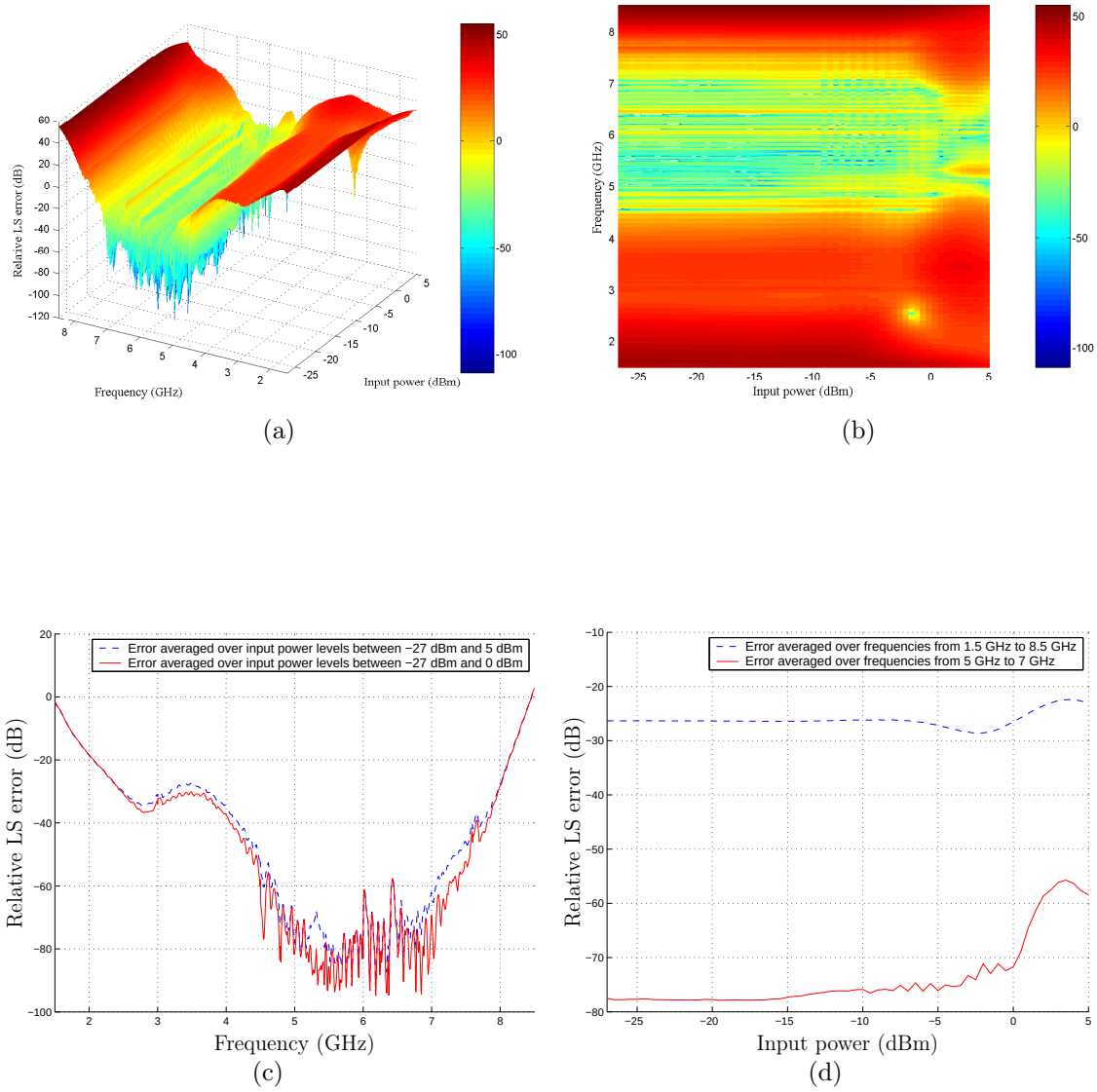

Figure 7.15: Illustration of the Hammerstein model estimation error. a) Error surface. b) Error surface viewed directly from above. c) Average error as a function of the frequency. d) Average error as a function of the input power.

7.5 Summary

In this chapter the Hammerstein model discussed in Chapter 5.2 was applied for frequency-dependent estimation of the Mini-Circuits ZVE-8G power amplifier. First, the implementation of the Hammerstein model was discussed. After that a simplified estimation technique for determining the parameters of the two blocks separately was proposed. Next, a weighted least-squares FIR approximation technique for designing filters with arbitrary amplitude and phase response was derived. Finally estimation results were presented and the estimation error was analyzed.

The nonlinear static block was implemented as a polynomial model and the linear dynamic block was implemented as an FIR filter. The parameters of the blocks were determined using the simplified estimation technique proposed in Section 7.2. The estimation results of the polynomial model were earlier presented and analyzed in Chapter 6. Therefore only the FIR approximation and the cascade of the two blocks was analyzed in this chapter.

The FIR filter was shown to model the dynamics of the amplifier very well even with filters of low order. The relative least-squares error on the desired band for the 13th-order filter was -38.12 dB. Increasing the order of the filter above 13 does not significantly improve the estimation accuracy due to the noise in the measurement data. Nevertheless a higher-order filter gives a more well-behaved error outside the desired band.

The estimation results of the Hammerstein model implemented as a 5th-order polynomial model and a 13th-order FIR filter with a constant delay of 17 samples and a weighting factor of 10^3 were shown to be very good. The obtained model is very accurate for single-tone inputs over the desired band at all power levels from the noise floor to the 1-dB compression point. The average relative least-squares error at a given frequency was less than –70 dB for all power levels below the 1-dB compression point.

Chapter 8

Conclusions and Future Work

The objective of this thesis was to find both a frequency-independent and a frequency-dependent model of different types of amplifiers. In order to achieve the objective, the distortion characteristics of a power amplifier were first discussed. Next, parameter estimation theory required for determining the unknown coefficients of the models were discussed. After that, a literature survey of existing models was conducted, and finally based on the literature study, two models were chosen for more detailed evaluation.

The distortion characteristics of a power amplifier can be examined in both time-domain and frequency-domain. In time domain the distortion can be seen as a transformation of the transmitted waveform and in frequency domain the distortion can be seen as generation of new frequency components. The generated frequency components are either harmonics or intermodulation components of the original signal components. Spectral spreading of the transmitted signal and deformation of the signal constellation are the most severe effects of the distortion on modulated signals.

In this thesis, a polynomial model was applied for frequency-independent modelling of a Mini-Circuits ZVE-8G power amplifier. The coefficients of the polynomials were determined using the derived Least-Squares Estimator (LSE). Even though the op-

timality of the LSE cannot be guaranteed, it was shown that the derived estimator converges rapidly. It was concluded that even low-order polynomials estimate the characteristics of the power amplifier at a given frequency very well. Sufficiently accurate results were obtained already with a fifth-order model. However, it was shown that a frequency-dependent model is required if the amplifier is fed by wide-band signals and its frequency response is not flat.

The frequency-dependent behavior of the power amplifier was modelled using a Hammerstein model, where the nonlinear static block was implemented using a polynomial model and the linear dynamic block as an FIR filter. The parameters of the Hammerstein model were determined using the proposed simplified parameter estimation technique in which the parameters of the blocks are estimated separately. The coefficients of the polynomials were obtained exactly as in the frequency-independent case and the filter coefficients were determined using the derived weighted least-squares FIR approximation filter design technique. It should be noted that the filter design technique is not restricted to amplifier modelling but also applicable for designing FIR filters with arbitrary amplitude and phase response. The obtained model was shown to be very accurate within the desired band at all power levels from the noise floor to the 1-dB compression point. Furthermore, the estimation error outside the desired band was well behaved.

The results and the applied techniques show that the objective of the thesis is met quite well. However, it should be noted that the models are based on single-tone measurements, and therefore their applicability to other input signals, e.g. Orthogonal Frequency Division Multiplexed (OFDM) signals, should be verified in future research. Time-domain analysis of the Hammerstein model using sampled input-output sequences is probably the most interesting topic of future research work. The objective would be to find the parameters of the Hammerstein model by comparing the input and output samples of an OFDM signal. In addition to the time-domain analysis it would be interesting to compare the proposed simplified parameter estimation technique to results obtained by joint parameter estimation of the two blocks of the Hammerstein model.

Appendix A

Weighted Least-Squares FIR Approximation

Weighted least-squares approximation can be used to design FIR filters with desired amplitude and phase response [62]. The desired amplitude and phase response can have arbitrary shape. A solution for the continuous frequency case can be found in [65]. In this appendix the derivation presented in [65] is modified for use on a discrete frequency grid.

The frequency response of a Mth-order ($M + 1$ coefficients) causal FIR filter is defined as

$$H\left(e^{j\omega_k}\right) = \sum_{m=0}^{M} h_m e^{-j\omega_k m} \tag{A.1}$$

where the filter coefficients $h_0, h_1, \ldots, h_M$ are real valued and ω_k is a set of discrete angular frequencies where the response is evaluated. The computational complexity of the filter described by Equation (A.1) can be reduced by adding a delay element with a delay of D samples before the filter. The frequency response of the cascade

of the constant delay element and the FIR filter is

$$H\left(e^{j\omega}\right) = \sum_{m=0}^{M} h_m e^{-j\omega_k(m+D)}. \tag{A.2}$$

The filter design problem is to choose the filter coefficients $h_0, h_1, \ldots, h_M$ so that the weighted least-squares error is minimized:

$$E = \sum_{k=0}^{K-1} W(\omega_k) \left| H_d\left(e^{j\omega_k}\right) - \sum_{m=0}^{M} h_m e^{-j\omega_k(m+D)} \right|^2 \tag{A.3}$$

where ω_k is a set of K discrete angular frequencies in the range $[-\pi, \pi]$, $H_d\left(e^{-j\omega_k}\right)$ is the desired complex-valued frequency response, $W(\omega_k)$ is a real-valued nonnegative weight function, M is the desired order of the filter and D is the desired length of the constant delay element. Obviously, it is required that $K > M$.

Denoting the real-valued filter coefficient vector $\mathbf{h}$ and the complex-valued discrete-time Fourier transform vector $\mathbf{e}$ as

$$\mathbf{h} = \begin{bmatrix} h_0 & h_1 & \cdots & h_M \end{bmatrix}^{\mathrm{T}} \tag{A.4}$$

$$\mathbf{e} = \begin{bmatrix} e^{-j\omega_k D} & e^{-j\omega_k(D+1)} & \cdots & e^{-j\omega_k(D+M)} \end{bmatrix}^{\mathrm{T}} \tag{A.5}$$

the error function defined in Equation (A.3) can be rewritten in vector notation as

$$E = \sum_{k=0}^{K-1} W(\omega_k) \left| H_d\left(e^{j\omega_k}\right) - \mathbf{h}^{\mathrm{T}}\mathbf{e} \right|^2 \tag{A.6a}$$

$$= \sum_{k=0}^{K-1} W(\omega_k) \left[H_d\left(e^{j\omega_k}\right) - \mathbf{h}^{\mathrm{T}}\mathbf{e} \right] \left[H_d\left(e^{j\omega_k}\right) - \mathbf{h}^{\mathrm{T}}\mathbf{e} \right]^* \tag{A.6b}$$

$$= \sum_{k=0}^{K-1} W(\omega_k) \left[\left| H_d\left(e^{j\omega_k}\right) \right|^2 - \mathbf{h}^{\mathrm{T}} \left[H_d\left(e^{j\omega_k}\right) \mathbf{e}^* - H_d^*\left(e^{j\omega_k}\right) \mathbf{e} \right] + \mathbf{h}^{\mathrm{T}}\mathbf{e}\mathbf{e}^{\mathrm{H}}\mathbf{h} \right] \tag{A.6c}$$

$$= \sum_{k=0}^{K-1} W(\omega_k) \left[\left| H_d\left(e^{j\omega_k}\right) \right|^2 - \mathbf{h}^{\mathrm{T}} 2\mathrm{Re}\left[H_d\left(e^{j\omega_k}\right) \mathbf{e}^* \right] + \mathbf{h}^{\mathrm{T}}\mathbf{e}\mathbf{e}^{\mathrm{H}}\mathbf{h} \right] \tag{A.6d}$$

where * denotes complex conjugation and H denotes Hermitian operation, i.e., transposition with conjugation.

The second and last term of the sum in Equation (A.6d) can be simplified by splitting the discrete-time Fourier transform vector $\mathbf{e}$ into its real and imaginary part

$$\mathbf{e} = \mathbf{c} + j\mathbf{s} \tag{A.7}$$

where

$$\begin{aligned} \mathbf{c} &= \mathrm{Re}\{\mathbf{e}\} \\ &= \begin{bmatrix} \cos D\omega_k & \cos(D+1)\omega_k & \cdots & \cos(D+M)\omega_k \end{bmatrix}^{\mathrm{T}} \end{aligned} \tag{A.8}$$

and

$$\begin{aligned} \mathbf{s} &= \mathrm{Im}\{\mathbf{e}\} \\ &= \begin{bmatrix} \sin D\omega_k & \sin(D+1)\omega_k & \cdots & \sin(D+M)\omega_k \end{bmatrix}^{\mathrm{T}}. \end{aligned} \tag{A.9}$$

The second term can be simplified by first splitting $\mathbf{e}^*$ into its real and imaginary part and then splitting $H_d\left(e^{j\omega_k}\right)$ into its real and imaginary part

$$\mathrm{Re}\Big\{ H_d\left(e^{j\omega_k}\right)\mathbf{e}^* \Big\} \tag{A.10a}$$

$$= \mathrm{Re}\Big\{ H_d\left(e^{j\omega_k}\right)\mathbf{c} - jH_d\left(e^{j\omega_k}\right)\mathbf{s} \Big\} \tag{A.10b}$$

$$= \mathrm{Re}\Big\{ H_d\left(e^{j\omega_k}\right) \Big\}\mathbf{c} - \mathrm{Re}\Big\{ \mathrm{Im}\left\{ H_d\left(e^{j\omega_k}\right) \right\}\mathbf{s} - j\mathrm{Re}\left\{ H_d\left(e^{j\omega_k}\right) \right\} \Big\}\mathbf{s} \tag{A.10c}$$

$$= \mathrm{Re}\Big\{ H_d\left(e^{j\omega_k}\right) \Big\}\mathbf{c} - \mathrm{Im}\Big\{ H_d\left(e^{j\omega_k}\right) \Big\}\mathbf{s}. \tag{A.10d}$$

Similarly, the third term can be simplified by splitting $\mathbf{e}\mathbf{e}^{\mathrm{H}}$ into its real and imaginary part

$$\mathbf{e}\mathbf{e}^{\mathrm{H}} = \left(\mathbf{c} + j\mathbf{s}\right)\left(\mathbf{c}^{\mathrm{T}} - j\mathbf{s}^{\mathrm{T}}\right) \tag{A.11a}$$

$$= \mathbf{c}\mathbf{c}^{\mathrm{T}} + \mathbf{s}\mathbf{s}^{\mathrm{T}} + \underbrace{j\left(\mathbf{s}\mathbf{c}^{\mathrm{T}} - \mathbf{c}\mathbf{s}^{\mathrm{T}}\right)}_{=0} \tag{A.11b}$$

$$= \mathbf{C} \tag{A.11c}$$

where $\mathbf{C}$ has the special form of a Toeplitz matrix [61]

$$\mathbf{C} = \begin{bmatrix} 1 & \cos\left(\omega_k\right) & \cdots & \cos\left(M\omega_k\right) \\ \cos\left(\omega_k\right) & 1 & \cdots & \cos\left[\left(M-1\right)\omega_k\right] \\ \vdots & \vdots & \ddots & \vdots \\ \cos\left(M\omega_k\right) & \cos\left[\left(M-1\right)\omega_k\right] & \cdots & 1 \end{bmatrix}. \tag{A.12}$$

Substituting Equations (A.10d) and (A.11c) back into Equation (A.6d) and rearranging the terms yields

$$E = \mathbf{h}^{\mathrm{T}} \sum_{k=0}^{K-1} \Big[W(\omega_k)\mathbf{C}\Big]\mathbf{h} \tag{A.13a}$$

$$- 2\mathbf{h}^{\mathrm{T}} \sum_{k=0}^{K-1} W(\omega_k) \left[\mathrm{Re}\Big\{H_d\left(e^{j\omega_k}\right)\Big\}\mathbf{c} - \mathrm{Im}\Big\{H_d\left(e^{j\omega_k}\right)\Big\}\mathbf{s}\right] \tag{A.13b}$$

$$+ \sum_{k=0}^{K-1} W(\omega_k) \left|H_d\left(e^{j\omega_k}\right)\right|^2. \tag{A.13c}$$

which can be written more compactly as

$$E = \mathbf{h}^{\mathrm{T}}\mathbf{P}\mathbf{h} - 2\mathbf{h}^{\mathrm{T}}\mathbf{p}_1 + p_0 \tag{A.14}$$

where

$$\mathbf{P} = \sum_{k=0}^{K-1} \Big[W(\omega_k)\mathbf{C} \Big] \tag{A.15}$$

$$\mathbf{p}_1 = \sum_{k=0}^{K-1} W(\omega_k) \Big[\mathrm{Re}\Big\{ H_d\left(e^{j\omega_k}\right) \Big\}\mathbf{c} - \mathrm{Im}\Big\{ H_d\left(e^{j\omega_k}\right) \Big\}\mathbf{s} \Big] \tag{A.16}$$

$$p_0 = \sum_{k=0}^{K-1} W(\omega_k) \left| H_d\left(e^{j\omega_k}\right) \right|^2 . \tag{A.17}$$

The error function in Equation (A.14) is quadratic and thus has a unique minimum at the zero of the gradient if and only if $\mathbf{P}$ is symmetric, nonsingular and positive definite [2]. The gradient is

$$\frac{\partial E}{\partial \mathbf{h}} = 2\mathbf{P}\mathbf{h} - 2\mathbf{p}_1. \tag{A.18}$$

Setting the gradient to zero and solving for $\mathbf{h}$ yields

$$\mathbf{h} = \mathbf{P}^{-1}\mathbf{p}_1 \tag{A.19}$$

which is the desired weighted least-squares solution for the filter design problem.

Appendix B

MATLAB implementation of the Weighted Least-Squares FIR Approximation

```
function [B,E] = LSCPLXFIR(M, W, w, Hd, D)
%LSCPLXFIR
%
%   [B,E]=LSCPLXFIR(M, W, w, Hd, D) designs an Mth-order FIR filter using
%   weighted least-squares approximation.
%
%   Input arguments:
%       - M is the desired filter order (M+1 coefficients)
%       - W is a real-valued nonnegative vector of weights
%       - w is an angular frequency vector scaled between -pi and pi
%       - Hd is the desired complex-valued frequency response
%       - D is the desired constant delay of the delay preceding the filter
%         (optional, default value is zero)
%
%   Output values:
%       - B is the filter coefficients [h0 h1 ... hM]
%       - E is the least-squares error of the filter design
%
%   Author: Peter Jantunen
%   Date: 11.11.2003
```

```
%   Version: 1.0
%

% Set delay to zero if not given as input
if (nargin < 5)
    D = 0;
end

% Number of frequency samples
L = length(w);

% Initialize and evaluate p and p1 vectors
p = zeros(1,M+1);
p1 = zeros(M+1,1);
for m=0:M
    p(m+1) = sum(W.*cos(m*w));
    p1(m+1) = sum(W.*(real(Hd).*cos((D+m)*w) - imag(Hd).*sin((D+m)*w)));
end

% Construct the Toeplitz form matrix P
P = toeplitz(p);

% Solve filter coefficients
B = P\p1;

% Evaluate least-squares error of the design if necessary
if (nargout > 1)
    p0 = sum(W.*abs(Hd).^2);
    E = B'*P*B - 2*B'*p1 + p0;
end
```

Bibliography

[1] W. Mohr, R. Lüder, and K.-H. Möhrmann, "Data rate estimates, range calculations and spectrum demand for new elements of systems beyond IMT-2000," in *Proc. Int. Symp. on Wireless Personal Multimedia Communications*, vol. 1, Oct. 2002, pp. 37–46.

[2] S. Friedberg, A. Insel, and L. Spence, *Linear Algebra*, 3rd ed. Upper Saddle River, New Jersey, USA: Prentice-Hall, 1997.

[3] A. Sedra and K. Smith, *Microelectronic Circuits*, 4th ed. New York, USA: Oxford University Press, 1998.

[4] L. Råde and B. Westergren, *Mathematics Handbook for Science and Engineering*, 4th ed. Lund, Sweden: Studentlitteratur, 1998.

[5] P. Kenington, *High-Linearity RF Amplifier Design*. Boston, USA: Artech House, 2000.

[6] M. Jeruchim, P. Balaban, and K. Shanmugan, *Simulation of Communication Systems: Modeling, Methodology and Techniques*, 2nd ed. New York, USA: Kluwer Academic/Plenum Publishers, 2000.

[7] J. Vuolevi and T. Rahkonen, *Distortion in RF Power Amplifiers*. Boston, USA: Artech House, 2003.

[8] S. Maas, *Nonlinear Microwave Circuits*. Norwood, USA: Artech House, 1988.

[9] C. Rapp, "Effects of HPA-nonlinearity on a 4-DPSK/OFDM-signal for a digital sound broadcasting system," in *Proc. of the Second European Conference on Satellite Communications*, Liège, Belgium, Oct. 1991.

[10] E. Costa, M. Midrio, and S. Pupolin, "Impact of amplifier nonlinearities on OFDM transmission system performance," *IEEE Communications Letters*, vol. 2, no. 2, pp. 37–39, Feb. 1999.

[11] A. D'Andrea, V. Lottici, and R. Reggiannini, "RF power amplifier linearization through amplitude and phase predistortion," *IEEE Trans. Commun.*, vol. 44, no. 11, pp. 1477–1484, Nov. 1996.

[12] S. Kay, *Fundamentals of Statistical Signal Processing: Estimation Theory.* Englewood Cliffs, USA: Prentice Hall, 1993.

[13] E. Barankin, "Locally best unbiased estimates," *Ann. Math. Stat.*, vol. 20, pp. 477–501, 1949.

[14] R. McAulay and E. Hofstetter, "Barankin bounds on parameter estimation," *IEEE Trans. Inform. Theory*, vol. 17, no. 6, pp. 669–676, Nov. 1971.

[15] J. Ziv and M. Zakai, "Some lower bounds on signal parameter estimation," *IEEE Trans. Inform. Theory*, vol. 15, no. 3, pp. 386–391, May 1969.

[16] S. Bellini and G. Tartara, "Bounds on error in signal parameter estimation," *IEEE Trans. Commun.*, vol. 22, no. 3, pp. 340–342, Mar. 1974.

[17] ——, "Correction to: Bounds on error in signal parameter estimation," *IEEE Trans. Commun.*, vol. 23, no. 4, p. 486, Apr. 1975.

[18] K. Bell, Y. Steinberg, Y. Ephraim, and H. V. Trees, "Extended Ziv-Zakai lower bound for vector parameter estimation," *IEEE Trans. Inform. Theory*, vol. 43, no. 2, pp. 624–637, Mar. 1997.

[19] E. Weinstein and A. Weiss, "A general class of lower bounds in parameter estimation," *IEEE Trans. Inform. Theory*, vol. 34, no. 2, pp. 338–342, Mar. 1988.

[20] C. Meyer, *Matrix Analysis and Applied Linear Algebra*. Philadelphia, USA: SIAM, 2000.

[21] C. F. Gauss, "Theoria motus corporum coelestium in sectionibus conicis solem ambientium," in *Werke*. Göttingen, Germany: Dieterich, 1863, vol. 7, pp. 1–288.

[22] Y. Guo and J. Cavallaro, "A novel adaptive pre-distorter using LS estimation of SSPA non-linearity in mobile OFDM systems," in *Proc. Int. Symp. on Circuits and Systems*, vol. 3, May 2002, pp. 453–456.

[23] A. Nordsjö, "An algorithm for adaptive predistortion of certain time-varying nonlinear high-power amplifiers," in *RADAR 2002*, Oct. 2002, pp. 469–473.

[24] H. Gutierrez, K. Gard, and M. Steer, "Spectral regrowth in microwave amplifiers using transformation of signal statistics," in *IEEE Int. Microwave Symposium Digest*, vol. 3, June 1999, pp. 985–988.

[25] J. Vörös, "Modeling and identification of wiener systems with two-segment nonlinearities," *IEEE Trans. Control Syst. Tech.*, vol. 11, no. 2, pp. 253–257, Mar. 2003.

[26] A. Saleh, "Frequency-independent and frequency-dependent nonlinear models of TWT amplifiers," *IEEE Trans. Commun.*, vol. 29, no. 11, pp. 1715–1720, Nov. 1981.

[27] E. Aschbacher and M. Rupp, "Modelling and identification of a nonlinear power-amplifier with memory for nonlinear digital adaptive pre-distortion," in *Proc. Workshop on Signal Processing Advances in Wireless Communications*, June 2003, pp. 555–559.

[28] J. Tellado, L. Hoo, and J. Cioffi, "Maximum-likelihood detection of nonlinearly distorted multicarrier symbols by iterative decoding," *IEEE Trans. Commun.*, vol. 51, no. 2, pp. 218–228, Feb. 2003.

[29] D.-S. Han and T. Hwang, "An adaptive pre-distorter for the compensation of HPA nonlinearity," *IEEE Trans. Broadcasting*, vol. 46, no. 2, pp. 152–157, June 2000.

[30] D. Dardari, V. Tralli, and A. Vaccari, "A theoretical characterization of nonlinear distortion effects in OFDM systems," *IEEE Trans. Commun.*, vol. 48, no. 10, pp. 1755–1764, Oct. 2000.

[31] G. Sante and F. Mazzenga, "A hybrid analytical-simulation procedure for performance evaluation in M-QAM-OFDM schemes in presence of nonlinear distortions," *IEEE Trans. Vehicular Technol.*, vol. 47, no. 1, pp. 142–151, Feb. 1998.

[32] A. Ghorbani and M. Sheikhan, "The effect of solid state power amplifiers (SSPAs) nonlinearities on MPSK and M-QAM signal transmission," in *Proc. Int. Conf. on Digital Processing of Signals in Communications*, Sept. 1991, pp. 193–197.

[33] M. Honkanen and S.-G. Häggman, "New aspects on nonlinear power amplifier modeling in radio communication system simulations," in *Proc. Int. Symp. on Personal, Indoor and Mobile Radio Communications*, vol. 3, Sept. 1997, pp. 844–848.

[34] M. Honkanen, O. Pöllänen, J. Tanskanen, E. Järvinen, and S.-G. Häggman, "Comparison of measured and simulated $\pi/4$-DQPSK adjacent channel power using a functional high power amplifier model," in *Proc. IEEE Vehicular Technology Conference*, vol. 3, May 1998, pp. 2459–2463.

[35] G. White, A. Burr, and T. Javornik, "Modelling of nonlinear distortion in broadband fixed wireless access systems," *IEEE Electronics Letters.*, vol. 39, no. 8, pp. 686–687, Apr. 2003.

[36] J. Mathews and G. Sicuranza, *Polynomial Signal Processing*. New York, USA: John Wiley & Sons, 2000.

[37] J. Mathews, "Adaptive polynomial filters," *IEEE Trans. Signal Processing*, vol. 8, no. 3, pp. 10–26, July 1991.

[38] C. Lesiak and A. Krener, "The existence and uniqueness of Volterra series for nonlinear systems," *IEEE Trans. Automatic Control*, vol. 23, no. 6, pp. 1090–1095, Dec. 1978.

[39] I. Sandberg, "The mathematical foundations of associated expansions for mildly nonlinear systems," *IEEE Trans. Circuits, Syst.*, vol. 30, no. 7, pp. 441–455, July 1983.

[40] S. Boyd and L. Chua, "Fading memory and the problem of approximating nonlinear operators with Volterra series," *IEEE Trans. Circuits, Syst.*, vol. 32, no. 11, pp. 1150–1161, Nov. 1985.

[41] G. Giannakis and E. Serpedin, "Linear multichannel blind equalizers of nonlinear FIR Volterra channels," *IEEE Trans. Signal Processing*, vol. 45, no. 1, pp. 67–81, Jan. 1997.

[42] G. Karam and H. Sari, "Analysis of predistortion, equalization, and ISI cancellation techniques in digital radio systems with nonlinear transmit amplifiers," *IEEE Trans. Commun.*, vol. 37, no. 12, pp. 1245–1253, Dec. 1989.

[43] S. Pupolin, A. Sarti, and H. Fu, "Performance analysis of digital radio links with nonlinear transmit amplifier and data predistorter with memory," in *Proc. Int. Conf. on Communications*, vol. 1, Boston, USA, June 1989, pp. 292–296.

[44] C. Eun and E. Powers, "A new Volterra predistorter based on the indirect learning architecture," *IEEE Trans. Signal Processing*, vol. 45, no. 1, pp. 223–227, Jan. 1997.

[45] M. Tummla, M. Donovan, B. Watkins, and R. North, "Volterra series based modeling and compensation of nonlinearities in high power amplifiers," in *Proc. Int. Conf. on Acoustics, Speech, and Signal Proc.*, vol. 3, Apr. 1997, pp. 2417–2420.

[46] T. Wang and T. Brazil, "The estimation of Volterra transfer functions with applications to RF power amplifier behavior evaluation for CDMA digital communication," in *IEEE Int. Microwave Symposium Digest*, vol. 1, June 2000, pp. 425–428.

[47] S. Chang and E. Powers, "A simplified predistorter for compensation of nonlinear distortion in OFDM systems," in *Proc. IEEE GLOBECOM*, vol. 5, Nov. 2001, pp. 25–29.

[48] A. Heiskanen, J. Aikio, and T. Rahkonen, "A 5th order Volterra study of a 30W LDMOS power amplifier," in *Proc. Int. Symp. on Circuits and Systems*, vol. 4, May 2003, pp. 616–619.

[49] A. Zhu, M. Wren, and T. Brazil, "An efficient Volterra-based behavioral model for wideband RF power amplifiers," in *IEEE Int. Microwave Symposium Digest*, vol. 2, June 2003, pp. 787–790.

[50] O. Nelles, *Nonlinear System Identification: From Classical Approaches to Neural Network and Fuzzy Models*. Berlin, Germany: Springer–Verlag, 2001.

[51] S. Mitra, *Digital Signal Processing: A Computer Based Approach*. New York, USA: McGraw-Hill, 1998.

[52] E.-W. Bai, "Frequency domain identification of Hammerstein models," *IEEE Trans. Automatic Control*, vol. 48, no. 4, pp. 530–542, Apr. 2003.

[53] H. Kang, Y. Cho, and D. Youn, "An efficient adaptive predistorter for nonlinear high power amplifier in satellite communication," in *Proc. Int. Symp. on Circuits and Systems*, June 1997, pp. 2288–2291.

[54] ——, "Adaptive precompensation of Wiener systems," *IEEE Trans. Signal Processing*, vol. 46, no. 10, pp. 2825–2829, Oct. 1998.

[55] ——, "On compensating nonlinear distortions of an OFDM system using an efficient adaptive predistorter," *IEEE Trans. Commun.*, vol. 47, no. 4, pp. 522–526, Apr. 1999.

[56] L. Ding, R. Raich, and G. Zhou, "A Hammerstein predistortion linearization design based on the indirect learning architecture," in *Proc. Int. Conf. on Acoustics, Speech, and Signal Proc.*, vol. 3, May 2002, pp. 2689–2692.

[57] M. Sano and L. Sun, "Identification of Hammerstein-Wiener system with application to compensation for nonlinear distortion," in *Proc. SICE Ann. Conf.*, vol. 3, Aug. 2002, pp. 1521–1526.

[58] W. Greblicki, "Nonparametric approach to Wiener system identification," *IEEE Trans. Circuits, Syst. I: Fundamental Theory and Applications*, vol. 44, no. 6, pp. 538–545, June 1997.

[59] M. Kozek and N. Javanovic, "Identification of Hammerstein/Wiener nonlinear systems with extended Kalman filters," in *Proc. of the American Control Conf.*, May 2002, pp. 969–974.

[60] G. Gámez, "Measurement and analysis of power amplifier nonlinearities for wireless communications," Master's thesis manuscript, Helsinki University of Technology, Helsinki, Finland, 2004.

[61] G. Golub and C. V. Loan, *Matrix Computations*, 3rd ed. Baltimore, Maryland, USA: The Johns Hopkins University Press, 1996.

[62] T. Parks and C. Burrus, *Digital Filter Design*. New York, USA: John Wiley & Sons, 1987.

[63] X. Vuong and A. Guibord, "Modelling of nonlinear elements exhibiting frequency-dependent AM/AM and AM/PM transfer characteristics," *Can. Elec. Eng. J.*, vol. 9, no. 3, pp. 112–116, 1984.

[64] P. Diniz, E. da Silva, and S. Netto, *Digital Signal Processing: System Analysis and Design*. Cambridge, United Kingdom: Cambridge University Press, 2002.

[65] T. Laakso, V. Välimäki, M. Karjalainen, and U. Laine, "Splitting the unit delay," *IEEE Signal Processing Mag.*, vol. 13, no. 1, pp. 30–60, Jan. 1996.